AN EXPERIMENTAL INVESTIGATION OF CATALYSIS IN THE COMBUSTION OF COMPOSITE SOLID PROPELLANTS

A THESIS

Presented to

The Faculty of the Division of Graduate Studies

by

John Charles Handley

In Partial Fulfillment

of the Requirements for the Degree

Doctor of Philosophy

in the School of Aerospace Engineering

Georgia Institute of Technology

March, 1976

U-264

AN EXPERIMENTAL INVESTIGATION OF CATALYSIS IN THE COMBUSTION OF COMPOSITE SOLID PROPELLANTS

Approved:

Warren C. Strahle, Chairman

Ben T. Zinn

Edward W. Price

Date approved by Chairman: 3/2/76

ACKNOWLEDGMENTS

I would like to express my appreciation to Dr. Warren C. Strahle for his suggestion of the dissertation topic. His guidance and assistance have made the experimental work and writing of this manuscript possible. I would also like to thank Dr. Ben T. Zinn and Professor Edward W. Price for their careful examination and constructive criticism of the manuscript.

I am grateful for the encouragement of Dr. James C. Wu to continue my graduate studies and the opportunity to continue these studies with the help of Dr. Arnold L. Ducoffe. The assistance of Mr. Thomas T. Milkie and Mr. Narendra Kumar in the preparation of test samples is also acknowledged.

I appreciate the financial assistance provided by the School of Aerospace Engineering and the Office of Naval Research under contract numbers N0014-67-A-0159-0016 and N0014-75-C-0332.

I am grateful for the assistance and support of my family. I wish to express my sincere appreciation to my wife, Phyllis, whose patience and encouragement have been of greatest personal help. Her aid in the preparation of this dissertation has been invaluable.

Finally to my children, Deborah, John, Stephen, Melinda and Daniel, I extend my thanks for their understanding and their acceptance of the sacrifices that have been made during my graduate work.

I wish to thank Mrs. Lydia Geeslin for her excellent typing of the manuscript.

TABLE OF CONTENTS

TABLE OF CONTENTS (Concluded)

LIST OF TABLES

LIST OF ILLUSTRATIONS

LIST OF ILLUSTRATIONS (Continued)

LIST OF ILLUSTRATIONS (Concluded)

SUMMARY

Experiments were conducted to provide data on the effectiveness and mechanism of action of four burn rate modifiers in the catalysis of the combustion of composite solid propellants. In addition, combinations of these modifiers were studied to determine if interaction effects on propellant burn rate exist. The four modifiers that have been investigated were Harshaw catalyst Cu 0202 P, ferric oxide, iron blue and ferrocene. The combustion pressure was varied from 600 to 2000 psia.

Two-dimensional solid propellant sandwiches of layers of ammonium perchlorate and hydroxyl terminated polybutadiene were used extensively in the initial phases of this investigation. The modifiers were restricted to either the binder, oxidizer or a thin layer at the binder-oxidizer interface. The site of action and the effect on sample burn rate of these modifiers were determined by using cinephotomacrography of burning samples and examination of partially burned samples with the scanning electron microscope. The sample burn rate and burning surface profiles were obtained from the high speed motion pictures. The surface details of the oxidizer, residual material on the oxidizer surface, binder melt flow and residual binder material were observed in electron micrographs of partially burned two-dimensional sandwiches.

Pairs of modifiers were added uniformly to two-dimensional solid propellant sandwiches to determine if there was a catalytic synergistic effect on sample burn rate. All combinations of the four modifiers were

tested at 600 psia. The two most promising pairs of modifiers were tested over the 300 to 2000 psia range.

Synergistic catalytic effects on sample burn rate were obtained for the Harshaw catalyst Cu 0202 P - ferric oxide and iron blue - ferric oxide systems for the two-dimensional samples. These two combinations were added to a cured composite propellant to see if this synergistic effect would carry over to the real propellant.

The extent of the binder melt flow observed on the two-dimensional sandwiches was reduced by all catalysts at all pressures for the three types of catalyst loading. The catalysts were most effective in catalyzing the binder-oxidizer reactions when introduced hot into the gas phase for the sandwich configuration.

The ammonium perchlorate deflagration rate was either augmented or suppressed depending upon the catalyst type and pressure level.

The positive synergistic effect of the two catalysts on the burn rate of a solid propellant was discovered using the two-dimensional composite solid propellant sandwich. All combinations of the four catalysts exhibited either a positive or a possible synergistic effect on both the sandwich vertical burn rate and the oxidizer normal regression rate when tested at 600 psia. The results for the cast composite propellant samples were not as conclusive as for the two-dimensional sandwich samples.

There were two conclusions of this investigation that remain unresolved. The oxidizer surface slope and its pressure dependence for the two-dimensional sandwiches obtained from the scanning electron microscopy investigation did not always agree with the high speed motion pictures. The sandwich vertical burn rate for the uniformly loaded samples was greater than the oxidizer, binder or binder-oxidizer interface loaded samples.

CHAPTER I

INTRODUCTION

This dissertation summarizes an experimental investigation of catalysis in the combustion of composite solid propellants. In particular this investigation was undertaken to study the effectiveness and mechanism of action of several burn rate catalysts. In addition, combinations of these catalysts were studied to determine if interaction effects on propellant burn rate exist. The experimental facilities for carrying out this study were previously developed and are described in Refs. 1-3.

A composite solid propellant is a heterogeneous mixture of oxidizer, metal fuel and burn rate modifier dispersed in a matrix of polymeric binder. The oxidizer is often ammonium perchlorate (AP). Sufficient binder material is used to wet and bond all solid particles into a propellant grain. The solid propellant burns by the propagation of a combustion wave into the unreacted propellant. This process is maintained by the transfer of heat from the exothermic reactions in diffusion or premixed flames near the surface. There can also be heat generation at the propellant surface by exothermic surface reactions. When there is steady burning of the propellant, the solid surface regresses at a rate defined as the burn rate.

Chemical additives are used extensively to modify the burn rate of composite solid propellants. Compounds and additives that increase the burn rate of propellants and only slightly modify the free energy change

of the process are referred to as catalysts.[4] Additives are either suspended or dissolved in the binder around the oxidizer particles in a composite solid propellant.

The action of catalysts is not well understood. Some catalysts enhance the thermal decomposition while inhibiting the deflagration of the oxidizer.[5] Others enhance the ignition process of gaseous oxidizer products in the presence of fuels.[6,7] Some catalysts are effective cracking agents for hydrocarbons,[8] but the corresponding action of these catalysts on hydrocarbon binders has not been demonstrated. The heat transfer from the flame to the solid propellant due to radiation has been investigated for additives that alter the propellant emissivity.[9,10,11] Chemical additives can behave as catalysts in pure oxidizer deflagration experiments and inhibit the combustion process when added to a composite solid propellant. While attempts have been made to develop consistent theories of catalysis for solid propellant additives,[12-15] none have been successful. The site of the catalysis process, the reaction that is catalyzed and the interaction of various catalysts have not been determined.

It has not been found possible to observe the microscopic interaction of oxidizer, catalyst and binder in combustion of a real propellant because of the small scale heterogeneity and the hostile environment. As a consequence, two-dimensional solid propellant sandwiches have been used as a test vehicle for observation of the interaction of layers of oxidizer and binder. The binder-oxidizer interface simulates the interface of an oxidizer particle burning in a binder matrix of a cast propellant, but yields a more definable microgeometry. True simulation is not

possible however because the size scale of the sandwich layers is generally much larger than size scales found in a real propellant. Both the oxidizer and binder layers behave as semi-infinite slabs of material which interact in the vicinity of their common interface. The sandwich configuration also fails to demonstrate the intermittency of conditions caused in propellant combustion by the particulate nature of the oxidizer and the associated combustion effects must be studied by other means. It is the relative ease of observation of these interface phenomena that gives the sandwich its usefulness.

The laboratory burn rates of these two-dimensional samples are unique and reproducible. Characteristic oxidizer deflagration rates are obtained far from the binder-oxidizer interface. The sandwich regresses at its maximum rate normal to the surface near the interface.

The two-dimensional sandwich is a convenient test geometry for the observation of the region of action of various burn rate catalysts. The normal mode of catalyst addition would be simulated by adding the material to the binder layer. This can be accomplished with a sandwich. Another method of catalyst addition can be obtained by restricting the catalyst to a thin layer at the binder-oxidizer interface. This might simulate a coated oxidizer particle burning in a binder matrix. Another obvious mode of catalyst loading would be oxidizer loading. This is accomplished by pressing the catalyst in the polycrystalline oxidizer slab. This does not simulate any current cast propellant techniques but it allows the effect of the catalyst on the oxidizer reactions to be insulated and studied independently of catalyzed binder-oxidizer reactions.

If a chemical compound operates effectively on one intermediate

reaction and another compound operates on another intermediate reaction, then combinations of these compounds can produce resultant effects that are additive if the intermediate reactions are independent. If the compounds accelerate the production of reaction intermediates at a faster rate earlier in the reaction scheme, then combinations of compounds can yield effects much greater than additive processes would produce. The inhibition of ammonium perchlorate deflagration by combinations of two compounds has been investigated by Glaskova.[16-18] She denoted the combined effect as a synergistic effect on the inhibition of the deflagration rate when the effect exceeded the sum of the separate effects. The two-dimensional sandwich could be used to effectively test combinations of catalysts for catalytic synergistic effects on sample burn rates.

Following the lines suggested above, four proven catalysts of cast propellant burn rate were chosen for investigation in this study. They are Harshaw catalyst Cu 0202 P, which is specified as a mixture of 82 percent cupric oxide (CuO) and 17 percent chromium oxide (Cr_2O_3); ferric oxide (Fe_2O_3); iron blue ($Fe(NH_4)Fe(CN)_6$); and ferrocene ($(C_5H_5)_2Fe$).

The site of action and the effect on sample burn rate of these catalysts were investigated by several experimental methods using the two-dimensional solid propellant sandwich. The catalysts were restricted to either the binder, oxidizer or a thin layer at the binder-oxidizer interface. High speed motion pictures of burning samples were obtained at 600 to 2000 psia. The sandwich vertical burn rate and the burn rate normal to the oxidizer surface were obtained from these motion pictures. The pressure range was chosen to eliminate possible anomalous results near the low pressure deflagration limit of ammonium perchlorate and

anomalous deflagration phenomena above 2000 psia.[19]

The surface details of partially burned two-dimensional samples were examined with a scanning electron microscope. These samples were obtained by terminating the combustion process by rapid depressurization of the combustion chamber. Comparative binder melt flows and residual binder heights were obtained from electron micrographs of the partially burned samples. Surface details of the oxidizer and residual surface structure for various catalysts were observed. The possibility of using an electron probe x-ray micro analysis technique to identify the chemical composition of these residual particles was also explored.

Pairs of catalysts were added to two-dimensional solid propellant sandwiches to determine if there was a catalytic synergistic effect on sample burn rate. All combinations of the above mentioned catalysts were tested at 600 psia. The two most promising pairs of catalysts and their base line samples with single catalysts present were tested over the 300 to 2000 psia pressure range.

Synergistic catalytic effects on sample burn rate were obtained for the Harshaw catalyst Cu 0202 P - ferric oxide and iron blue - ferric oxide systems for the two-dimensional samples. These two combinations were added to a cured composite propellant to see if this synergistic effect would carry over to the real propellant.

CHAPTER II

PREPARATION AND TESTING OF SANDWICHES

Catalysts

In this study several experimental methods were used to investigate the combustion mechanisms of composite solid propellants when catalysts were present. The four catalysts which have been investigated in previous studies[2,20-22] at Georgia Tech have been used again in all phases of this investigation. They are Harshaw catalyst Cu 0202 P (CC), ferric oxide (IO), iron blue (IB) and ferrocene (F). These chemical compounds have been investigated in other studies, as is evident from Table 8 in Appendix A. They were supplied by the Thiokol Chemical Corporation.

Harshaw catalyst Cu 0202 P is a commercially available, finely powdered catalyst. It is a copper chromite catalyst and is also available in a tablet form. It is capable of selectivity to hydrogenate or dehydrogenate functional groups in organic compounds without changing the unsaturation or saturation in aromatic rings or alkyl chains.[23] It has been one of the most investigated chemical compounds in solid propellant combustion, because of its significant catalysis of ammonium perchlorate decomposition, deflagration and ignition. Copper chromite catalysts are prepared by the thermal decomposition of ammonium copper chromate. This may or may not be followed by an acetic acid leach[8] and various heat treating cycles. Some contain barium as a stabilizer. Harshaw specifies Cu 0202 P as being a mixture of 82 percent cupric oxide (CuO) and 17

percent chromium oxide (Cr_2O_3). Copper chromite catalysts are used to accelerate both oxidation and reduction processes.

Ferric oxide, Fe_2O_3, exhibits as do most transition element compounds, a high degree of catalytic activity. It is used primarily for oxidation processes. It has been used as a major catalyst in the synthesis of ammonia from nitrogen and hydrogen and as a hydro cracking catalyst in converting coal to oil. It was used in a finely powdered form.

Iron blue is also known as Prussian, Chinese or Milori blue. It is used commercially as a pigment. It is a complex ammonium iron hexacyanoferrate with the chemical formula, $Fe(NH_4)Fe(CN)_6$. It has a cubic crystalline structure. The iron is present as both ferric and ferrous ions in the lattice. It was used in a finely powdered form.

Ferrocene is an organometallic compound with the chemical name, biscyclopentadienyl iron, $(C_5H_5)_2Fe$. It is a yellow crystalline solid with relatively high thermal stability for an organometallic compound. It is used in: 1) oxidation processes, 2) reactions involving destruction of iron-carbon bonds, and 3) substitution of hydrogen in the cyclopentadienyl rings. It was supplied in a relatively coarse crystalline form. It was ground to a fine powder form for use.

Available Facilities

Combustion Apparatus

This investigation was conducted in the Propulsion Laboratory of the School of Aerospace Engineering, Georgia Institute of Technology. A high pressure combustion apparatus with a variable flow, variable pressure nitrogen purge system was used for all phases of this investigation.

This basic apparatus was designed by Varney[1] and was used when the combustion process was quenched by rapid depressurization of the test chamber. The central section of the test chamber was replaced by a three window section for observation of the sample using cinephotomacrography techniques. This window section was designed by Jones.[2] A high intensity light source and high speed motion picture camera were used for the cinephotomacrography investigation. The experimental equipment arrangement is shown in Figure 1.

The maximum working pressure of the nitrogen flow system shown in Figure 2 is 3500 psia. The maximum working pressure of the combustion bomb section is 6000 psia. All tests, for this investigation were in the 600 to 2000 psia pressure range. This range was selected to avoid anomalous results near the low pressure deflagration limit of ammonium perchlorate and the unexplained deflagration phenomena above 2000 psia.[19]

A nitrogen flow of one ft/sec in the window section was used for smoke control while taking high speed motion pictures. This flow rate was determined experimentally by Jones.[2] There was no apparent edge cooling due to the low velocity of the nitrogen flow.

A small amount of nitrogen was bled from the combustion apparatus during quench testing of the propellants. This prevented a build up of the combustion chamber pressure as the sample burned.

Cinephotomacrography

The high speed motion pictures were obtained by using a Hycam 16 mm camera with a frame rate of 10 to 11,000 frames per second. All results in this investigation were obtained at approximately 1600 frames per second. The exact camera speed was obtained at the section of film

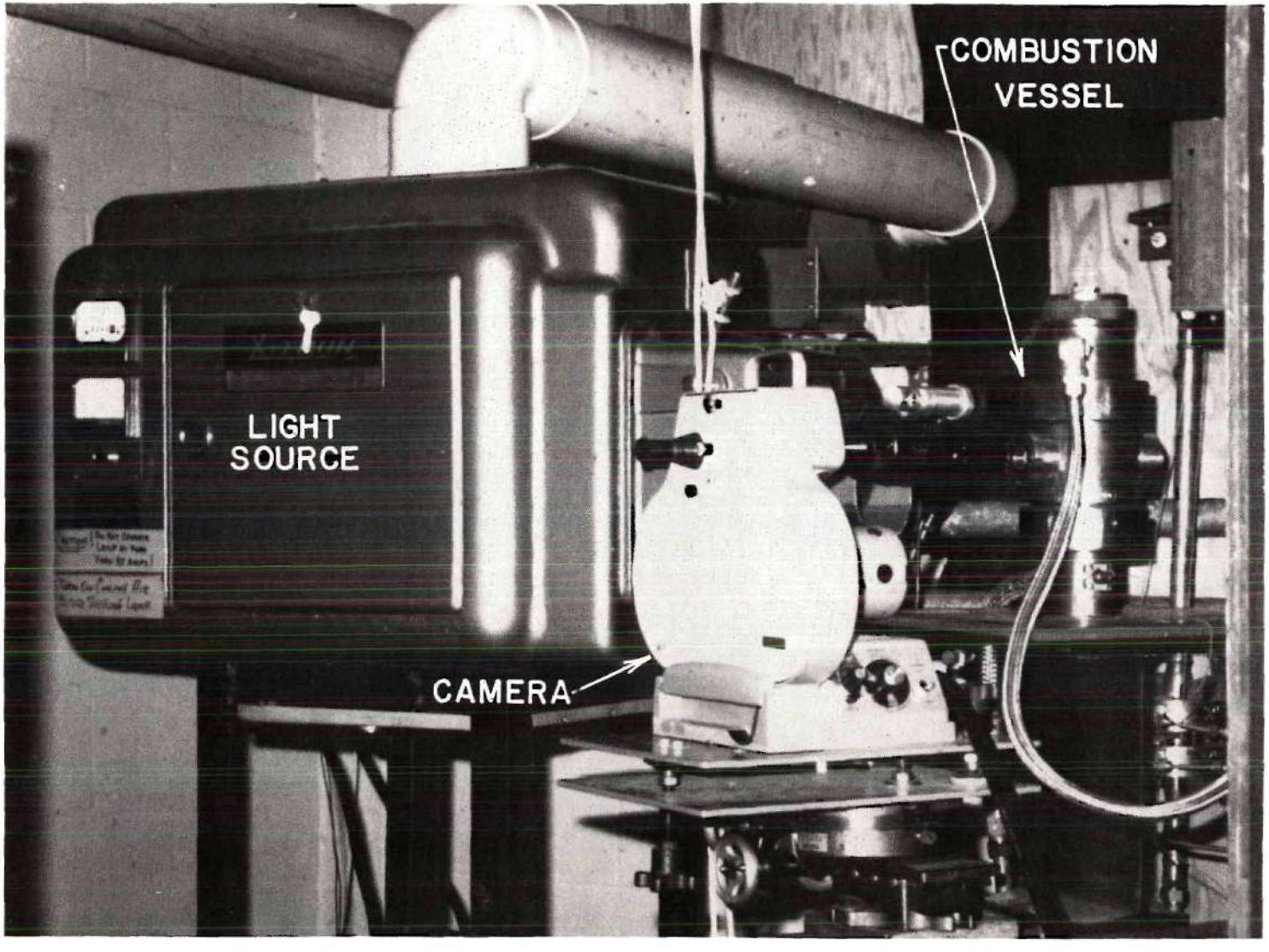

Figure 1. Combustion Apparatus and Cinephotomacrography Equipment

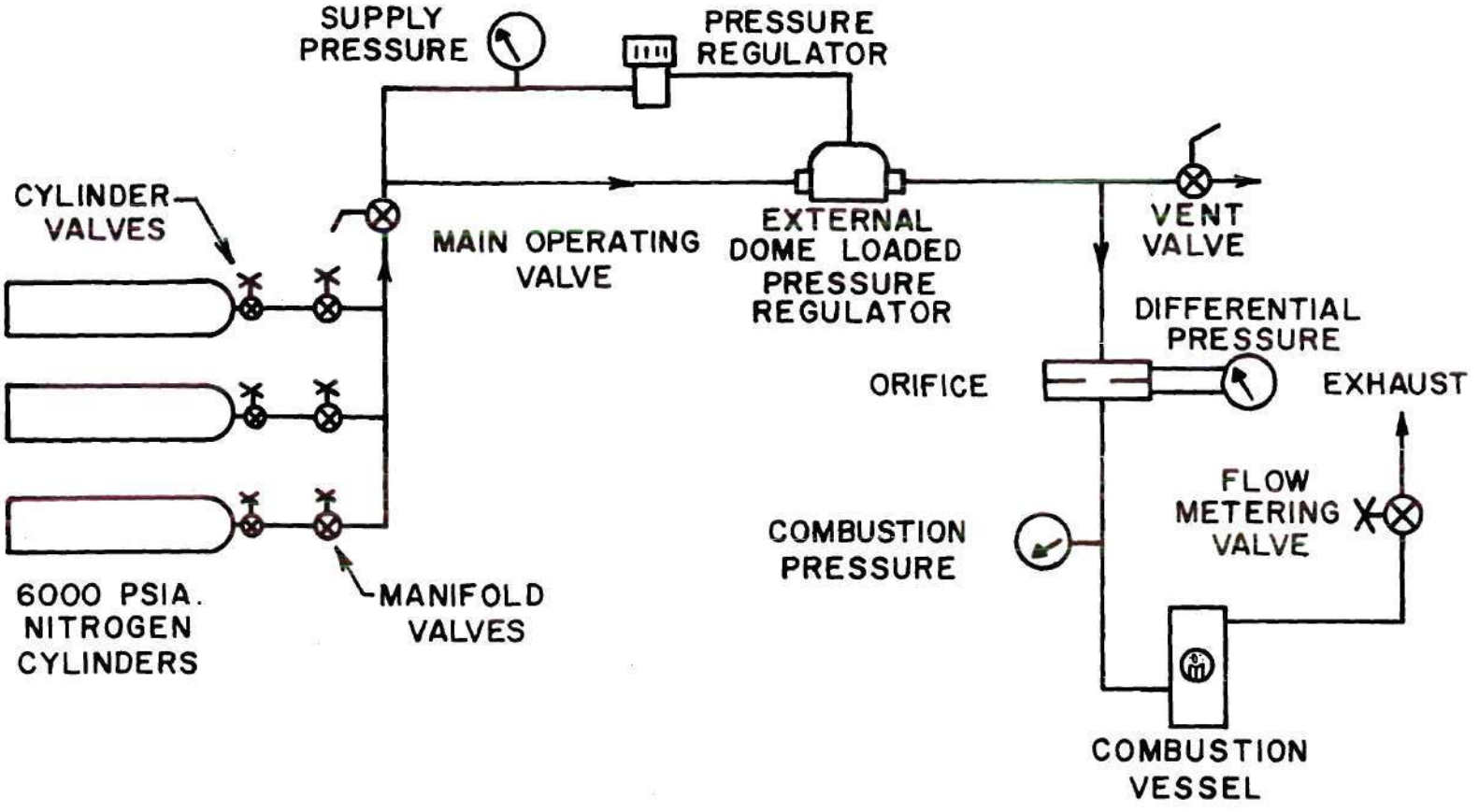

Figure 2. Nitrogen Flow System

that was used for the burning rate determination. A signal generator supplies a voltage to a neon light at a measurable rate which in turn exposed the edge of the film. The frequency of this light flash was measured to five significant figures. It was adjusted to give approximately 1000 marks per second. A Vivitar Preset, 85 mm focal length lens was used for this investigation. This lens had a maximum aperture of f-1.8. A combination of appropriate extension tubes and lens adapter was used to give a latent image magnification, the ratio of film image to actual sample size, of four to one. A 2500 watt xenon light source was used for sample illumination. The motion pictures are viewed using a L-W Model 900 Motion Analyzer.

Quenched Combustion Testing

The samples for the scanning electron microscope investigation were obtained by quenching the combustion process by rapid depressurization of the combustion bomb. A rapid change of pressure causes the extinction of the combustion process when ammonium perchlorate propellants were involved. This depressurization was accomplished by using the burst diaphragm method developed by Varney.[1] An experimentally determined number of Mylar disks was used to contain the pressure in the combustion bomb. A .010 inch nichrome wire was inserted between the outer Mylar disks. This wire was used to heat and melt a sufficient number of disks to cause the remaining disks to rupture and depressurize the combustion bomb. The sample observation was carried out in the Physical Science Division of the Engineering Experiment Station, Georgia Institute of Technology. A Cambridge Stereoscan Scanning Electron Microscope, Mark II a, was used for all observations. Magnifications from 18 to 50,000

were available.

Sample Preparation

The two-dimensional composite solid propellant sandwiches were prepared from compacted, polycrystalline disks of ammonium perchlorate and layers of hydroxyl terminated polybutadiene binder which was prepared following the procedure outlined in Appendix B. The ammonium perchlorate for this phase of the investigation was obtained from the Fisher Scientific Company as certified to have less than .004 percent total impurities. This was later down graded to less than .018 percent total impurities by Fisher. The ammonium perchlorate was analyzed by the Naval Weapons Center and as reported by Boggs et al.[15] contained an impurity level of .03 weight percent of potassium ion.

The polycrystalline disks were prepared from this ammonium perchlorate. Approximately 1.3 grams of ammonium perchlorate was ground by hand in a pyrex mortar and pestle for ten minutes. This produced a particle distribution suitable for pressing into a polycrystalline disk. This ground material was transferred to a mold assembly designed by Varney.[1] The diameter of the pressed disk was one inch. The mold assembly was placed in a Carver Laboratory Hydraulic Press capable of exerting 24,000 pounds of force, which was equivalent to 30,500 psia. The disk was subjected to the maximum pressure for one hour. No measurable change of burning rate was noted if the pressure was maintained for longer intervals of 8 or 24 hours. These disks were approximately .050 inch thick. All disks and prepared samples were stored in a desiccator until tested.

Multilayered sandwiches were prepared from these polycrystalline disks by bonding them together in layers, using hydroxyl terminated

polybutadiene. The thickness of the binder was maintained uniform by a Teflon shim of .005 inch thickness. This yielded a binder thickness of .005 - .006 inch (120-150 μm). The uncured samples were clamped between two 1/16 inch sheets of Teflon using a number of alligator clips and placed in the curing oven for seven days at 60°C.

For dispersal of the burning rate modifiers in the oxidizer, two percent by weight was added to the ammonium perchlorate prior to the grinding and pressing into polycrystalline disks. For loading in the binder, the same volumetric loading as occurred in the ammonium perchlorate was mixed into the binder prior to curing. For hydroxyl terminated polybutadiene this was 4.37 percent by weight.

Two methods of sample preparation were used in tests in which this burning rate modifier was to be concentrated at the binder-oxidizer interface. Initially the material was suspended in methyl alcohol and painted on one surface of an oxidizer disk.[2,20] The amount of material adhering to the oxidizer surface could not be controlled. It was impossible to obtain a uniform coating with the iron blue and ferrocene using this method. Therefore these samples were prepared by pressing a thin layer of the catalyst mixed with an equal amount of ammonium perchlorate onto the surface of a lightly pressed ammonium perchlorate disk. This composite disk of burning rate modifier and ammonium perchlorate was then processed as a normal polycrystalline oxidizer disk. The result was a narrow-band "interface" burning rate modifier layer that adhered well to the oxidizer and binder. This layer of high concentration of burning rate modifier (50 percent by weight) was approximately .002 inch thick.

CHAPTER III

BURNING RATES OF SANDWICHES

A cinephotomacrographic investigation of the four catalysts has been conducted using the oxidizer, binder and interface loading of the catalysts as described above. Tests were conducted at 600, 1000, 1500 and 2000 psia. High speed motion pictures with a latent magnification of two to one (image to actual) were taken at a rate of 1600 or 3200 frames per second.

These motion pictures were used to obtain an accurate value of the sample burning rate. Sample data reductions and sketches of actual burning samples are included in Appendix D. Burning rate data were taken only after a steady profile had been achieved and was clearly visible over a substantial portion of the run. Characteristic sandwich profiles are shown in Figure 3. Two burn rates were obtained for each sandwich. For a steady profile the sandwich vertical burn rate, r, is the same regardless of the perpendicular distance from the binder-oxidizer interface although it is measured at the point of maximum regression of the sample. The burn rate normal to the oxidizer surface, r_n, is indicative of the oxidizer deflagration rate, and is related to the sandwich vertical burn by the cosine of the surface slope angle. That is

$$r_n = r \cos\theta \ .$$

The slope of the oxidizer surface must be determined at a sufficient

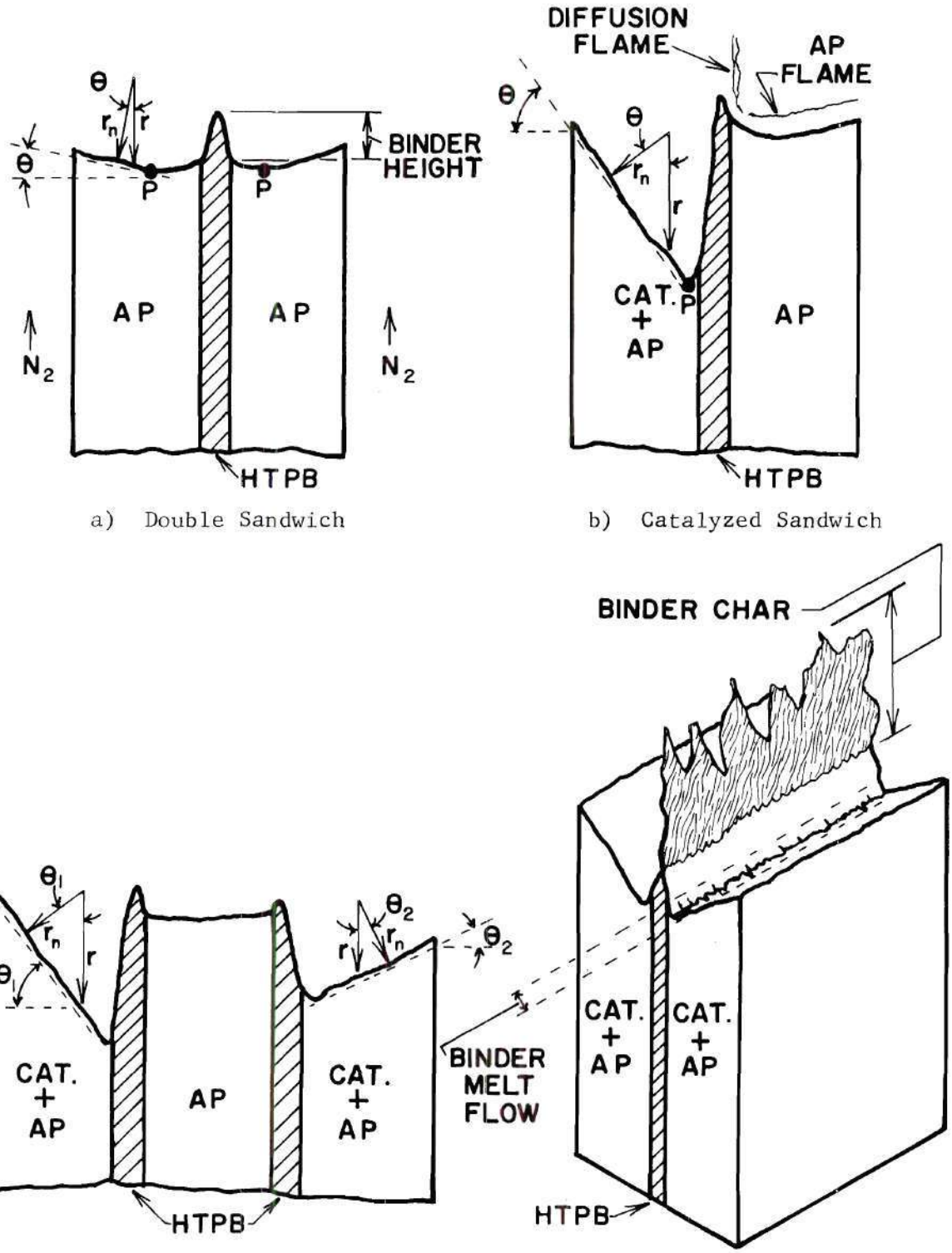

a) Double Sandwich

b) Catalyzed Sandwich

c) Triple Sandwich

d) Isometric View

Figure 3. Characteristic Sandwich Profiles and Details

distance from the binder-oxidizer interface for the oxidizer surface to have a definable constant slope.

The pure AP-HTPB double sandwich has been sketched in Figure 3a. The oxidizer surface slope is very small. The residual binder height has been indicated. This was the binder remaining on the quenched combustion samples. It was measured on the electron micrographs obtained from the scanning electron microscope investigation. As long as the sample was symmetrical, that is, the oxidizer layers were identical, and the binder layer thickness remained constant, the residual binder height measurement was a meaningful quantity.

The profile shown in Figure 3b was obtained when unsymmetrical double sandwiches were burned. One oxidizer layer has been loaded with an effective burn rate catalyst. The point of maximum sandwich regression, P, has moved closer to the binder-oxidizer interface for the oxidizer loaded with catalyst. The AP flame and the binder-AP diffusion flame are also shown in Figure 3b.

Triple sandwiches consisting of three oxidizer layers and two binder layers were used to reduce the total number of tests necessary for the evaluation of all four catalysts. A typical sandwich profile is shown in Figure 3c. A pure AP layer was always used to separate the catalysts. This type of sandwich was used when ferrocene and iron blue were loaded in the oxidizer and for all catalysts loaded in the binder.

An isometric drawing of a burning double sandwich is shown in Figure 3d. This would be for a symmetrical, oxidizer loaded sample. The binder char layer visible in the high speed motion pictures is shown. This was removed during the quench process leaving a residual binder

height. The extent of the binder melt flow from the binder-oxidizer interface out onto the oxidizer surface has been shown.

Almost all of the burn rate data presented in this dissertation have been normalized by dividing the burn rates of interest by the burn rate of the corresponding pure, uncatalyzed sample of AP-HTPB. The uncatalyzed two-dimensional sandwiches burned with a relatively flat profile; therefore, both the sandwich vertical burn rate and the burn rate normal to the oxidizer surface were the same. In the figures of burn rate ratio as a function of pressure, the solid curves are the ratio of the sandwich vertical burn rates. The dashed curves are the ratio of the burn rates normal to the oxidizer surface. These normal burn rates reflect any acceleration or inhibition of the burn rate of the ammonium perchlorate alone due to the modifiers and results should be compared systematically with those of other AP deflagration experiments (Friedman[24] and Boggs[5]).

Catalyst Added to Oxidizer

The burn rates for the four catalysts added to the oxidizer at two weight percent are shown in Figure 4. They have been normalized by dividing by the burn rates of uncatalyzed AP-HTPB sandwiches. Again it should be noted that the same ammonium perchlorate with the same impurity level and obtained from Fisher Scientific Company was used for all two-dimensional sandwiches. The data for Harshaw catalyst Cu 0202 P and ferric oxide were also reported in Ref. 21.

Harshaw catalyst Cu 0202 P augments the sandwich vertical burn rate and the burn rate normal to the oxidizer surface over the entire

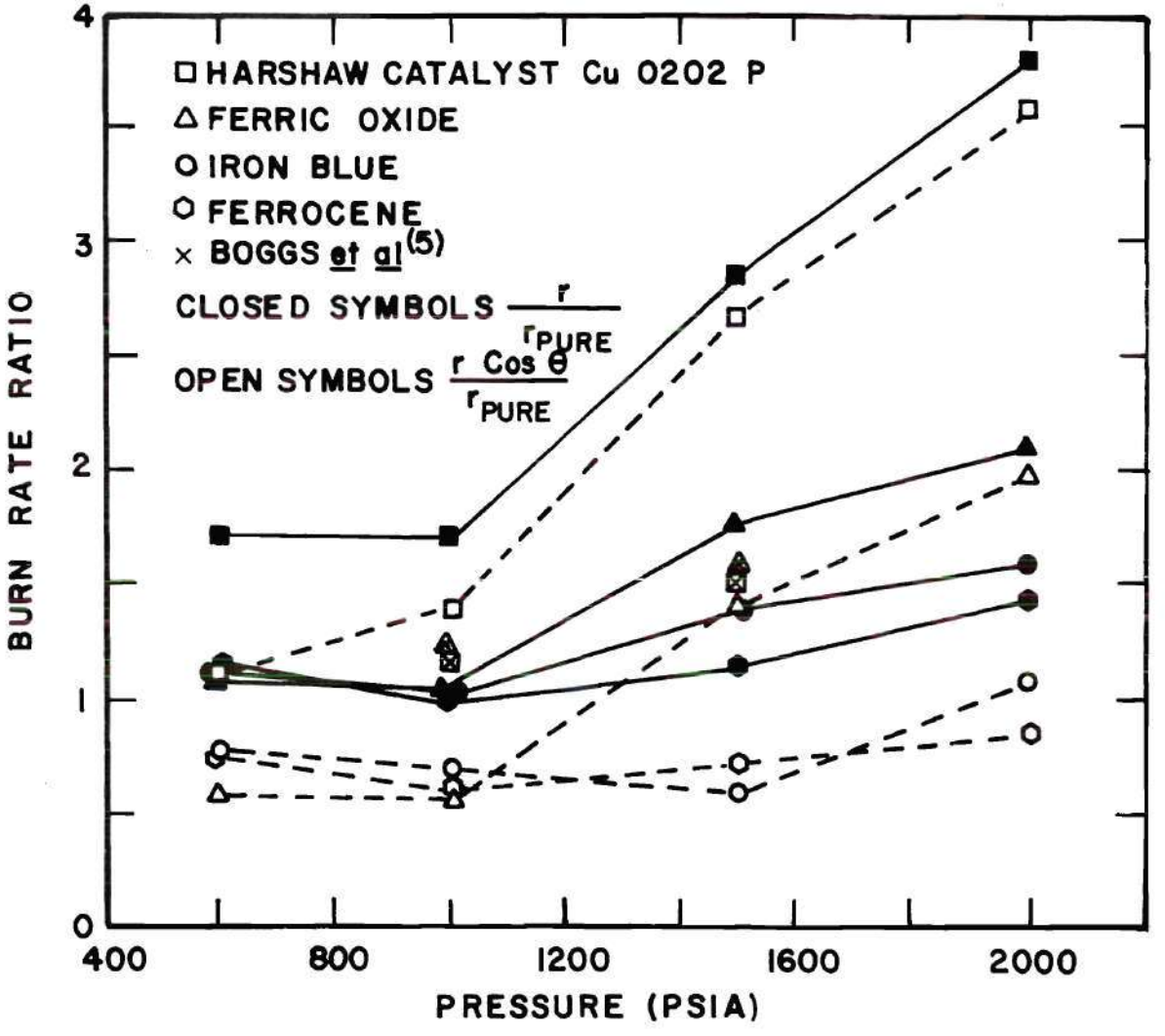

Figure 4. Burn Rate Ratio for Catalyst Added to the Oxidizer

pressure range. Iron blue and ferrocene retard the burn rate normal to the oxidizer surface for the entire pressure range. Ferric oxide retards this normal burn rate for pressures less than 1200 psia. Even though these three catalysts retard the burn rate normal to the oxidizer surface, they do augment the sandwich vertical burn rate to some degree over the entire pressure range.

The separation of the solid and dashed curves in Figure 4 for each catalyst is representative of the amount of catalytic activity taking place in the binder-oxidizer reactions. This separation is greatest for both iron blue and ferrocene and it decreases for both ferric oxide and Harshaw catalyst Cu 0202 P as the pressure increases. This indicates that both iron blue and ferrocene might be most effective if they are restrained to the binder-oxidizer interface.

Friedman et al.[24] have studied the effect of Harshaw catalyst Cu 0202 P and ferric oxide on the deflagration of ammonium perchlorate with no fuel present. Their tests were conducted with three weight percent of catalyst added to the ammonium perchlorate. In the pressure range they studied, their burn rates were above the burn rates normal to the oxidizer surface for this investigation for Harshaw catalyst Cu 0202 P and below for ferric oxide. Since the deflagration rate is a function of the concentration level, it was difficult to compare Friedman's results with the results of this investigation which were at concentrations of two weight percent.

Boggs et al.[5] have also studied Harshaw catalyst Cu 0202 P and ferric oxide at the same weight ratio, two weight percent, as in these tests, but in simple oxidizer deflagration, i.e. no binder present.

Their data at 1000 and 1500 psia are shown in Figure 4. Their results for Harshaw catalyst Cu 0202 P were considerably below the burn rates normal to the oxidizer surface (dashed curve) for this investigation. They did not maintain deflagration below 1000 psia. Their ferric oxide data are close to the sandwich vertical regression rate for this investigation but above the burn rates normal to the oxidizer surface (dashed curve). Boggs' data should agree with the dashed curves. The difference between the two results was unexplained. It did lead to further testing of the ammonium perchlorate.

The ammonium perchlorate disks used in the preparation of the two-dimensional sandwiches for this investigation were analyzed by Boggs. An impurity level of .03 weight percent of potassium ion was found.[20] The burn rates for two-dimensional sandwiches using the ammonium perchlorate with .03 weight percent of potassium ion impurity are shown as triangles in Figure 4. The deflagration rate data for ultra-pure ammonium perchlorate (99.99 percent pure) of Boggs and Zurn[25] are also shown. Again this is for simple oxidizer deflagration, i.e. no binder present. When they tested this same AP with .03 weight percent potassium ion impurity added, the dashed curve was obtained. The impurity increased the deflagration rate of the oxidizer at pressures below 1500 psia and decreased it from 1500 to 2000 psia.

Two-dimensional sandwiches were prepared from ultra-pure ammonium perchlorate supplied by Boggs. The burn rates for these sandwiches are included as squares in Figure 5. They were consistently below the sandwich burn rates for the samples made of impure ammonium perchlorate. This is consistent with the impurity effect on simple AP deflagration rate at

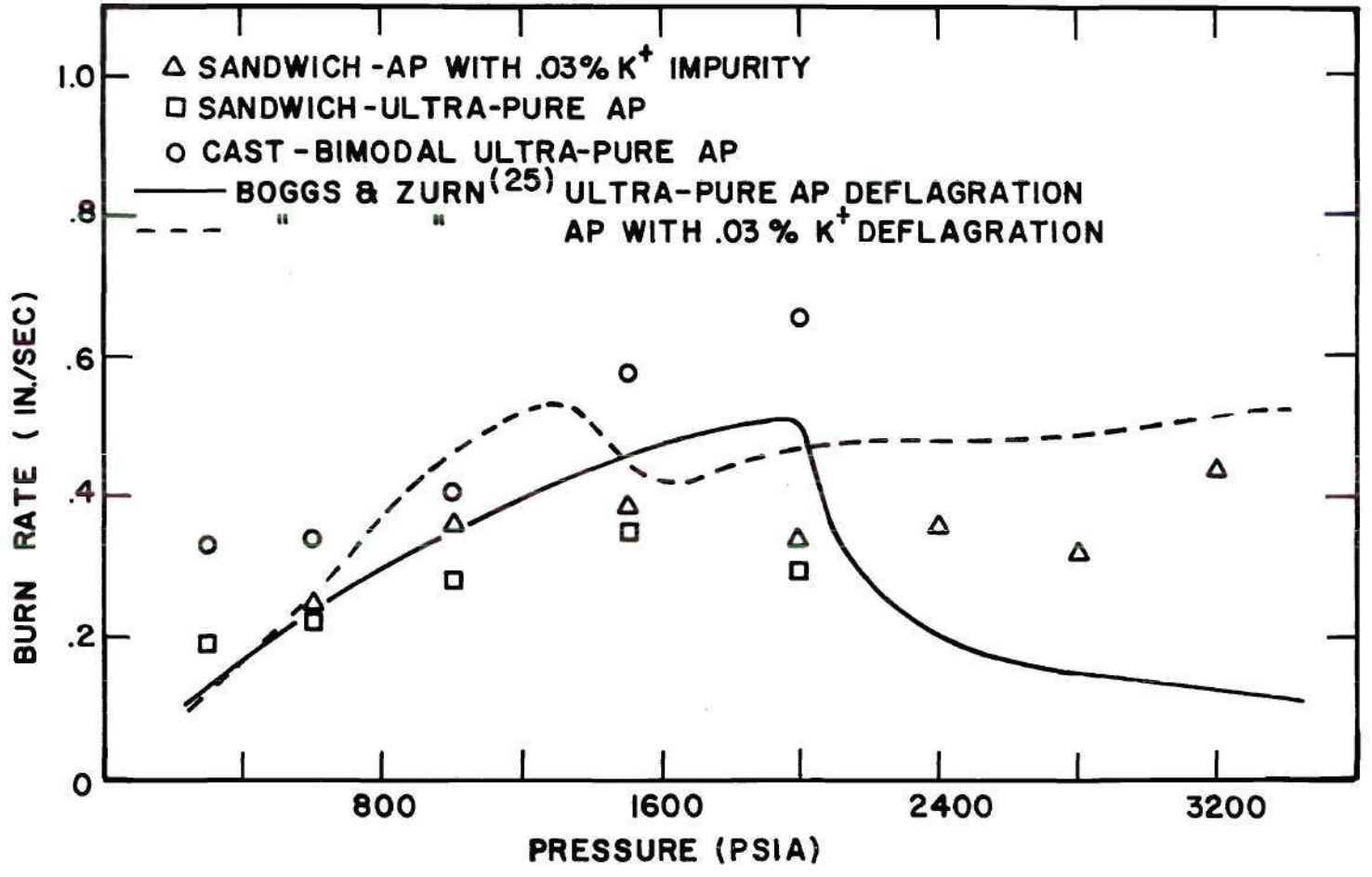

Figure 5. Burn Rates of Ammonium Perchlorate Used in This Investigation

pressures below 1500 psia, but does not follow the reversal of impurity effect observed at higher pressures.

The burn rates for the AP-HTPB sandwiches using the AP with .03 weight percent of potassium ion impurity were used to normalize all burn rates of catalyzed samples prepared from the impure ammonium perchlorate. At the conclusion of this phase of the cinephotomacrographic investigation of oxidizer, binder or binder-oxidizer interface catalytic loading, all subsequent propellant samples were fabricated using ultra-pure ammonium perchlorate supplied by Boggs. The burn rates described above for the samples prepared from ultra-pure ammonium perchlorate were used to normalize all burn rates of catalyzed samples prepared from the ultra-pure ammonium perchlorate. This included both the two-dimensional sandwich and the cast, bimodal propellant samples. All uncatalyzed sample burn rates are shown in Figure 5.

The purity of the ammonium perchlorate was initially investigated to determine if it could account for the difference between the results of this investigation for Harshaw catalyst Cu 0202 P and ferric oxide added to the oxidizer and the results of Boggs et al.[5] at 1000 and 1500 psia. The sandwich vertical burn rate did decrease as the purity of ammonium perchlorate increased. This could account for a slight lowering of the Harshaw catalyst Cu 0202 P results in Figure 4, but the burn rates would still not agree with Boggs et al.[5] For the ferric oxide samples the correction would be in the wrong direction.

Catalyst Added to the Binder

The burn rate ratios for the case of catalyst added to the binder

are shown in Figure 6. Within the accuracy of the experimental techniques there were no detectable angles from the horizontal present in the oxidizer. This indicates very little catalytic activity taking place in the vicinity of the binder-oxidizer interface. The scatter of the sandwich vertical burn rate ratios about a ratio of unity in the 1000 to 2000 psi range is indicative of the test to test accuracy of this sample configuration. There is no significant visible effect on the sandwich deflagration process with catalyst present compared to the pure AP-HTPB sandwich. At 600 psia, however, there is a catalytic effect indicated for ferrocene and iron blue but there was no inclination of the surface to the horizontal. This is an unexplained phenomenon, since an increase in vertical rate for a fixed oxidizer normal regression rate would require an inclination of the oxidizer to the horizontal.

Catalyst at the Binder-Oxidizer Interface

The burn rate ratios for the samples with catalyst restricted to the binder-oxidizer interface are shown in Figure 7. As was mentioned above, two methods of sample preparation were used for this type of catalyst loading. A measurable amount of iron blue and ferrocene (two weight percent of the disk) was located at the binder-oxidizer interface. Considerably less Harshaw catalyst Cu 0202 P and ferric oxide were deposited at the binder-oxidizer interface due to a painting procedure.

Iron blue consistently augmented the sandwich vertical burn rate over the entire pressure range. The separation between the solid and dashed curves increased as the pressure was increased. This was expected considering the indication of increased binder-oxidizer reactions in

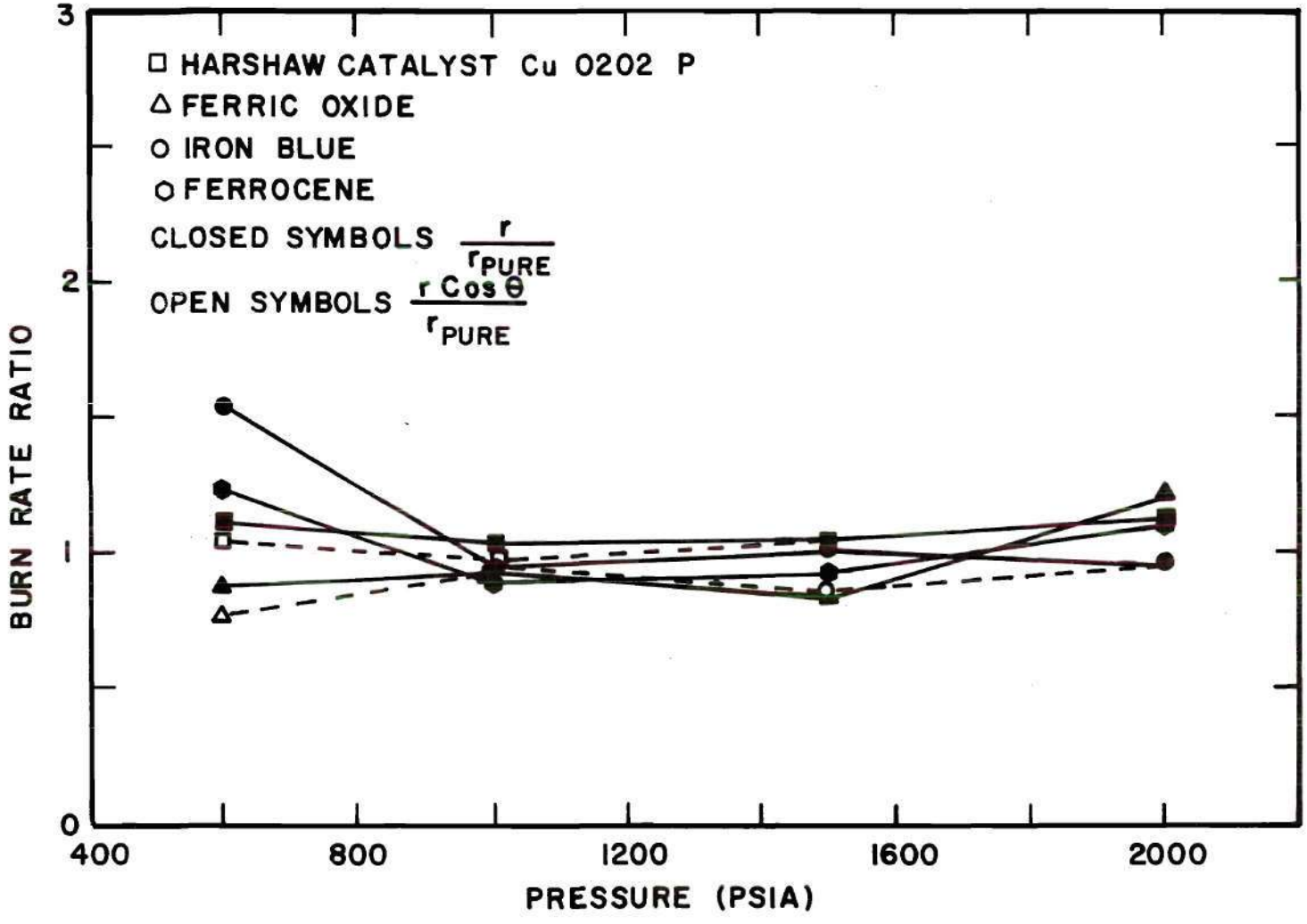

Figure 6. Burn Rate Ratio for Catalyst Added to the Binder

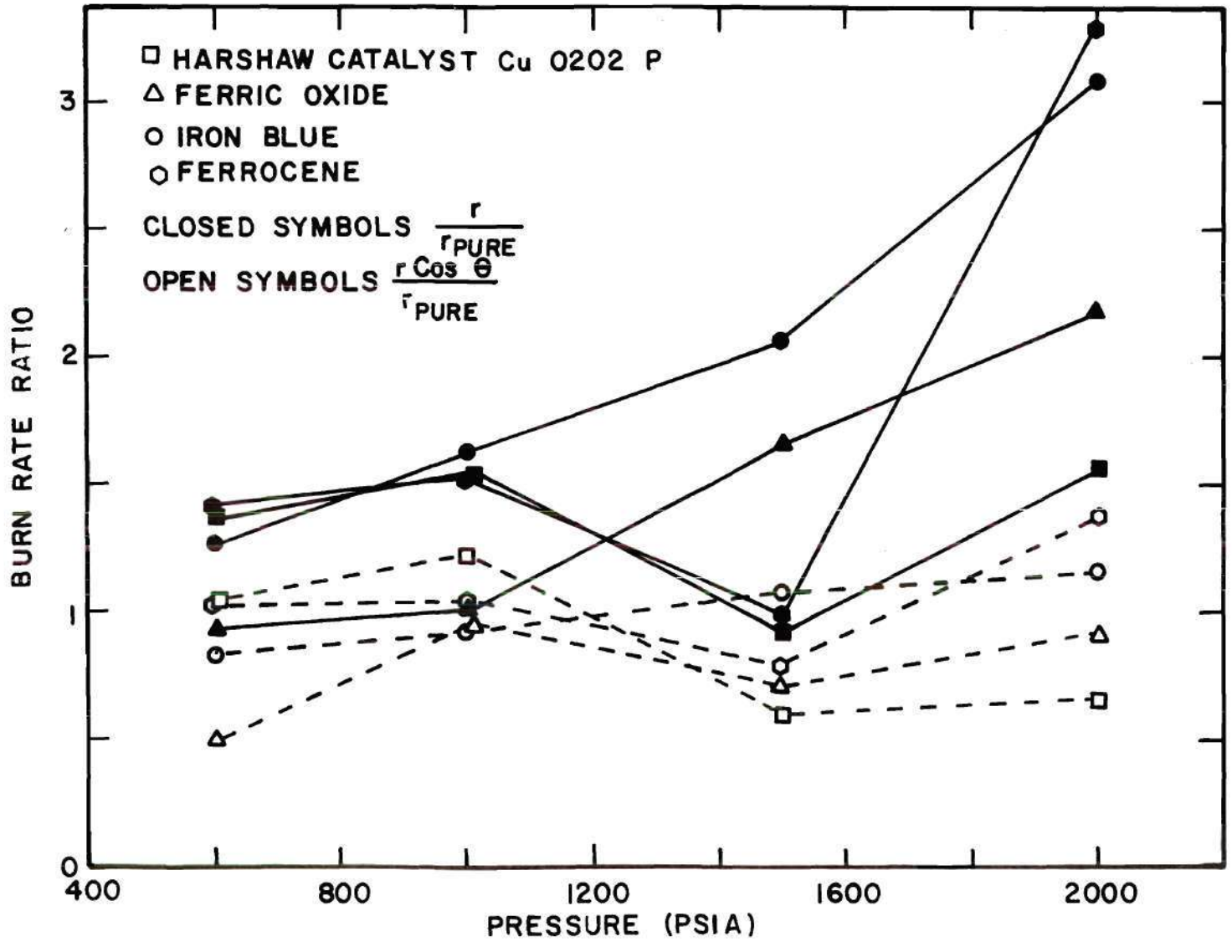

Figure 7. Burn Rate Ratio for Catalyst at the B-O Interface

Figure 4. Ferrocene was also an effective augmenter of the sandwich vertical burn rate over this pressure range, except at 1500 psia. Ferric oxide continuously increased the sandwich vertical burn rate from a retarded burn rate at 600 psia to an augmented burn rate for pressures greater than 1200 psia. Again this was indicated in Figure 4.

Harshaw catalyst Cu 0202 P was as effective as iron blue and ferrocene in augmenting the sandwich vertical burn rate at 600 and 1000 psia. It was considerably less effective at 1500 and 2000 psia. The burn rate normal to the oxidizer surface should not be affected by the presence of catalyst at the binder-oxidizer interface; therefore, the scatter of these burn rates may be considered to be an indication of the test to test fluctuation of data for these interface sandwiches. This experimental band of data fluctuation is larger than that for the catalyst loaded in the binder (see Figure 6). The interface samples were more difficult to prepare. The ingredients and disks required more handling.

The lower bounds of this region of burn rates normal to the oxidizer surface are determined by the ferric oxide and Harshaw catalyst Cu 0202 P tests. This may be due to the fact that less catalyst was present at the interface or it may be due to coating the disk with the catalyst suspended in a methyl alcohol solution. No further investigation of this type of sample preparation was attempted since the thin layer of catalyst pressed on the oxidizer disk resulted in a reproducible sample for all catalysts used.

Summary

The cinephotomacrography study of four catalysts loaded in the oxidizer, binder or at the binder-oxidizer interface resulted in several conclusions.

1. Harshaw catalyst Cu 0202 P is the most effective catalyst of the ammonium perchlorate deflagration process in the sandwich configuration (Figure 4). It also exhibits the greatest augmentation of the sandwich vertical burn rate.

2. Iron blue and ferrocene inhibit the ammonium perchlorate deflagration process over the entire pressure range studied (Figure 4).

3. Ferric oxide retards the ammonium perchlorate deflagration rate below 1200 psia (Figure 4).

4. Iron blue and ferrocene show a greater catalysis of binder-oxidizer reactions when loaded in the ammonium perchlorate (Figures 4 and 7).

5. There was no augmentation of the sandwich vertical burn rate when the catalyst was loaded in the binder (Figure 6).

6. All catalysts were effective in augmenting the sandwich vertical burn rate when restricted to the binder-oxidizer interface for pressures greater than 1500 psia (Figure 7).

CHAPTER IV

SURFACES OF QUENCHED SAMPLES

Experimental Program

The sample fabrication techniques for this phase of the investigation were perfected during the cinephotomacrography experiments. Ultra-pure AP (99.99 percent) was used to prepare the polycrystalline disks of oxidizer for this phase of the investigation and all work reported in later chapters. The four catalysts, Harshaw catalyst Cu 0202 P, ferric oxide, iron blue and ferrocene, were loaded in the oxidizer, binder and at the binder-oxidizer interface. Partially burned samples were obtained for scanning electron microscopy by terminating combustion by rapid depressurization using the burst diaphragm method.[1] An electronic timer circuit, Figure 8, was used to obtain accurate, reproducible time delays between the ignition of the sample and interruption of burning of the sample. The timer was modified to allow delays of from 22 milliseconds to three seconds. The initial estimates for the time delays were obtained from the cinephotomacrography burn rate data of Chapter III.

The sample observation was carried out in the Physical Science Division of the Engineering Experiment Station, Georgia Institute of Technology. A Cambridge Stereoscan Electron Microscope, Mark II a, was used for all observations in this chapter. Magnifications from 18 to 50,000 were available. A focused electron beam of .01 μm in diameter was used to scan the samples which were placed in the specimen holder under a

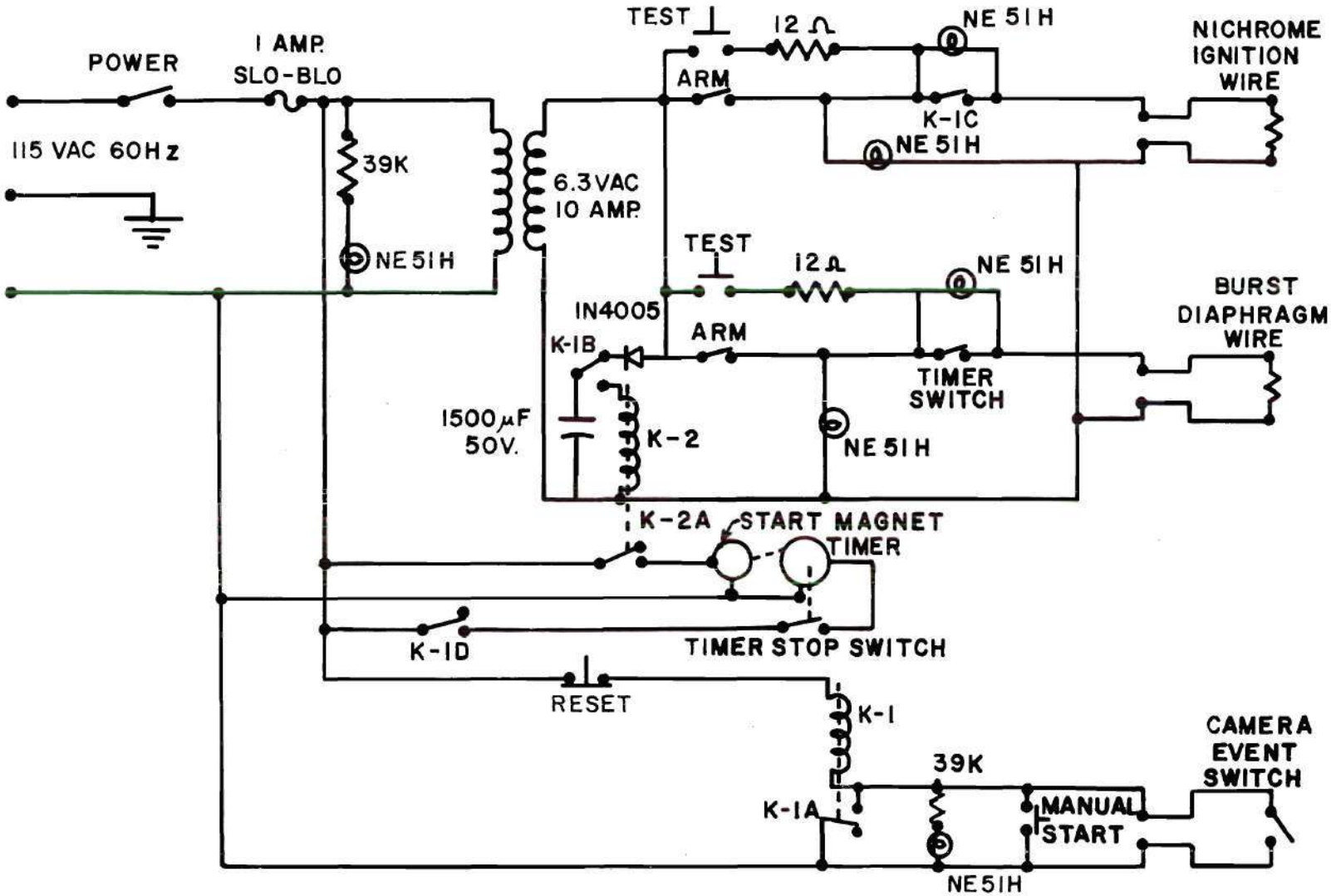

Figure 8. Ignition and Depressurization Circuit

high vacuum. The high energy beam stimulates the emission of the secondary electrons or backscattered electrons, x-rays and, sometimes, light photons from the sample surface. If the sample is electrically non-conducting, it will gradually accumulate an electrical charge and cause an additional scattering of the electron beam. Since the composite propellant samples were non-conducting, they had to be coated with a conducting coating before the surface could be examined with the scanning electron microscope. A combined coating of carbon and gold-palladium (60-40) was placed on the samples by vacuum deposition. This coating varied from 300 to 400 Å in thickness. It would not be detected unless magnifications in excess of 50,000 were used.

The electrical signal generated by the collected secondary or backscattered electrons is used to control the brightness of a cathode ray tube which is synchronized to the scan of the electron beam. The photograph of the cathode ray tube is referred to as the electron micrograph. The x-rays emitted by the sample are characteristic of the elements present in the sample and can be collected and analyzed. Both the chemical identify and spatial distribution of the elements in the region of the electron beam can be determined. Iron is always indicated due to its presence in the construction of the microscope. For non-conducting samples the coating materials are also detected. This analysis was used to determine the high iron content of particles visible in the AP-IO samples. The spatial resolution of this measurement is 10^4 times better than the electron microprobe investigation described in Chapter V, but the number of elements that can be detected is limited and the quantitative results are not as accurate as with the microprobe.

The entire compilation of the results of this investigation is available in Ref. 22. This consists of a series of 106 electron micrographs covering the surface details of 32 partially burned samples. These sampled were burned at 600, 1000, 1500 and 2000 psia in a dry nitrogen atmosphere. There were 13 electron micrographs of four pure AP-HTPB samples and 39 electron micrographs of 13 samples with catalyst added to the AP. Triple sandwiches of three AP disks and two layers of HTPB binder were prepared for the catalyst added to the binder and the catalyst located at the binder-oxidizer interface. There were 27 electron micrographs of eight triple sandwiches with catalyst added to the binder and 27 electron micrographs of seven triple sandwiches with catalyst located at the binder-oxidizer interface.

Partially burned samples were obtained for all four catalysts and loading in the oxidizer, binder or at the binder-oxidizer interface except for iron blue and ferrocene located at the binder-oxidizer interface at 1500 psia. Both of these catalysts were tested in the same triple sandwich.

The electron micrographs obtained from the scanning electron microscope have been studied carefully. The oxidizer surface has been observed and any unusual surface characteristics have been noted. The surface slope and its uniformity have been measured. The condition of the residual binder layer was observed. If the sandwich was symmetrical about the binder, then there was a residual binder height due to the excessive thickness of the binder layer. The extent of this binder height was measured. It would be impossible to extend this measurement to real propellants, because of different geometric ratios of oxidizer to binder thick-

nesses. It is known from the cinephotomacrography that there is a substantial binder char layer, which is apparently removed from the sandwich during the quench process. The less viscous binder is probably also ejected. This would also alter the residual binder height.

There is a binder melt that flows over the oxidizer surface as the sandwich burns. The extent of this flow has been measured for each sample. The oxidizer surface slope and the point of maximum sandwich regression were also measured. Because of qualitative similarity, electron micrographs of all samples are not shown here. They are presented in Ref. 22.

Uncatalyzed Sandwiches

A set of four AP-HTPB sandwiches was included in this study for comparison purposes. Two electron micrographs are shown in Figure 9a and b. The results for all four samples are summarized in Table 1.

Table 1. Summary of Results from Scanning Electron Microscopy of Pure AP-HTPB Composite Solid Propellant Sandwiches

Pressure psia	Figure No.	Binder Melt Flow μm	Binder Height μm
600		200-260	130-310
1000	9a	60-250	250-310
1500		50-270	260-430
2000	9b	90-370	340-650

These observations are in accord with the experiments of Boggs et al.[19, 26] over the 600 to 2000 psia pressure range.

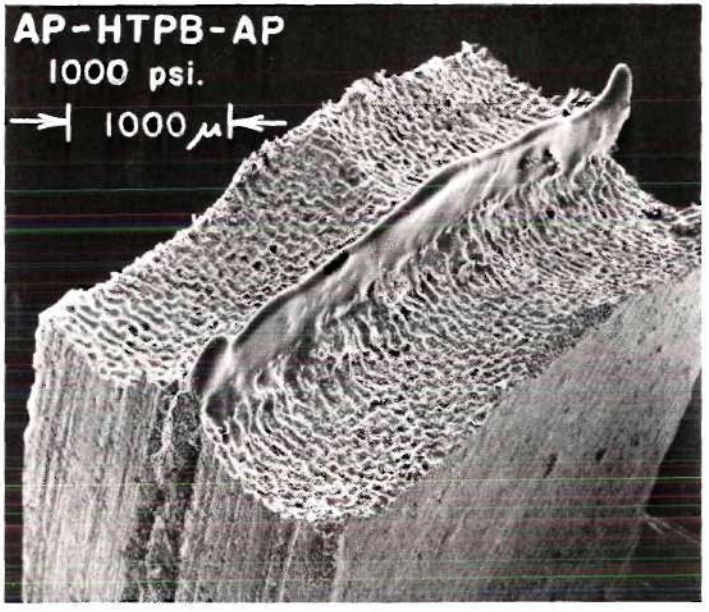

a) 1000 psia (x21.2)

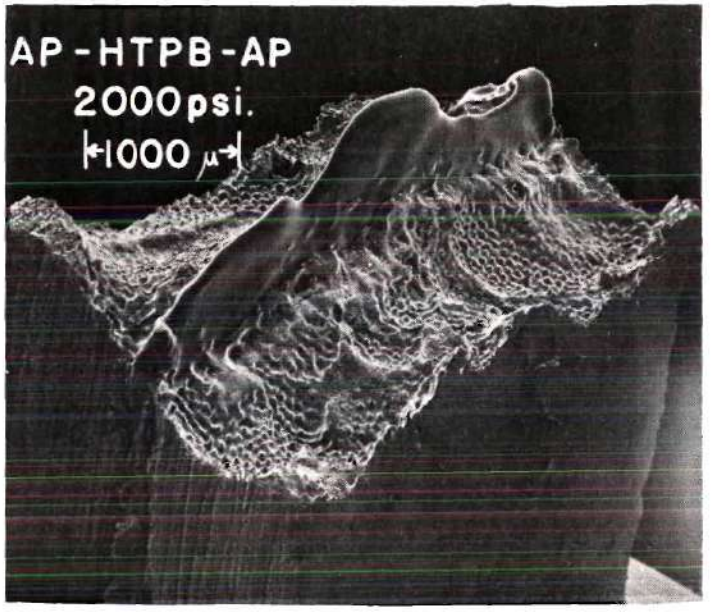

b) 2000 psia (20.4)

Figure 9. Uncatalyzed AP-HTPB-AP Sandwiches

600 psia

There is a visible binder melt flow out over the frothy oxidizer surface in the vicinity of the binder layer. It extends from 200 to 260 μm from the binder-oxidizer interface. This flow has retarded the oxidizer regression rate causing the point of regression of the sandwich to be at least 300 μm from the binder-oxidizer interface. The original layer of binder in the sandwich extends from 130 to 310 μm above the oxidizer surface. This residual binder layer has been tabulated as the binder height in Table 1. The surface slope of the sample is continuous in the vicinity of binder-oxidizer interface.

The entire oxidizer surface of the quenched combustion sandwich was covered with a frothy structure, similar to that shown in Figure 9a. This was first observed by Hightower and Price.[27] Boggs et al.[19] stated that the ammonium perchlorate surface was covered with a thin layer of reacting liquid and that gaseous decomposition products were generated at distinct sites. These gaseous bubbles expand up through this liquid layer as the gases are heated by feedback from the flame and possible exothermic reactions within the liquid layer.

The combustion quenching technique used to obtain these partially burned samples depends on the rapid depressurization of the combustion bomb, 10^6 psia per second, to interrupt the combustion process. This rapid decrease of pressure also causes these bubbles to expand, but this is compensated, in part, by the rapid cooling of the oxidizer surface. Cracks of a few microns in width appear in the solidified AP layer. These cracks are due to the thermal contraction of the surface layer as

it solidifies. This layer is approximately one μm thick in the vicinity of cracks and burst bubbles. There is no significant visible edge cooling effect shown by this sample. That is, the AP regression rate was not decreased near the free edges of the sample. This would show up as an increase of the surface slope at the free edges of the sample.

1000 psia (Figure 9a)

The binder melt flow varies from 60 to 250 μm from the binder-oxidizer interface. This variability has increased with the pressure increase. The residual binder height extends from 250 to 350 μm. There is a continuous surface slope of the sample. The point of maximum regression is at the midpoint of the oxidizer layer. This type of profile is similar to the "Christmas tree" profile obtained for AP-PBAA in Ref. 20. That is, the surface slope continuously increases from the free edge of the AP layer to the binder layer.

The frothy surface is still visible. A larger scale ridge and valley formation is starting to appear with the froth superimposed on it. There are cracks in the binder melt flow which reveal a porous AP structure. This flow is approximately one μm thick.

1500 psia

The binder melt flow extends from 50 to 270 μm over the oxidizer surface. The residual binder height is 260-430 μm high. There is a continuous slope at the binder-oxidizer interface and the point of maximum regression has been displaced further from the interface than at lower pressures.

The frothy surface is still visible. The density of the ridges and valleys has decreased but the height difference between the peaks and

the valleys has increased. The distribution of these ridges and valleys continues to be uniform over the entire AP surface.

2000 psia (Figure 9b)

The binder melt flow is more irregular. It extends up to 370 μm onto the AP in some areas and is almost nonexistent in other areas. The binder height ranges from 340 to 650 μm. The location of the point of maximum regression varies with the character of the binder melt flow. At one section it is located near the interface while at another section it has moved to the free edge of the oxidizer.

There is still a frothy nature to the surface and the ridges and valleys are also present. In several areas regions of hemispherical protrusions (mounds) with radii of approximately 50 μm were observed. There is some indication of an edge cooling effect at one free edge, but it is not uniform and none was observed with the previous three samples. Therefore, retardation of oxidizer burning rates near the free edges due to cooling effects has been considered unimportant.

Summary of AP-HTPB

As the pressure increases the mean surface irregularities increase for the pure AP-HTPB sandwiches. The binder melt flow exists and its extent increases. The residual binder height increases. The point of maximum regression is always in the oxidizer and tends to move away from the binder as the pressure increases. There is no substantial cooling effect noted. These observations are in accord with the results of Boggs et al.[19,26]

Catalysts in the Oxidizer

The following section is devoted to a discussion of the electron micrographs from the samples containing the catalyst in the ammonium perchlorate. The samples consisted of sandwiches with HTPB binder (150 μm thick) with pure AP (1270 μm thick) on one side and catalyst loaded (two weight percent) AP on the other side. Both double and triple sandwiches were used in this investigation. Ferrocene and iron blue were tested in triple sandwiches. That is, two catalyst loaded disks were separated by a pure AP disk. Each oxidizer layer was still separated by a layer of HTPB binder. Both of these catalysts had augmented sandwich vertical burn rates to the same degree in previous tests (Figure 4).

The electron micrographs of these partially burned samples were compared to each other and to the uncatalyzed sandwiches previously discussed. Ten micrographs will be given in the following figures. Thirteen samples were investigated with the scanning electron microscope to obtain the 16 data points included in Table 2.

There was no residual binder height extending above the oxidizer surface for these samples. The catalyzed oxidizer layers all burned faster than the pure AP-HTPB samples (Figure 4). Since all of these samples were not symmetrical, the excess binder was still bonded to the slowing burning AP layer.

AP and Cu 0202 P - HTPB

600 psia. Harshaw catalyst Cu 0202 P, when loaded in the AP oxidizer, catalyzes the sandwich vertical burn rate. There is a slight binder melt flow over the oxidizer surface of from 24-41 μm. The surface of the oxidizer loaded with catalyst has a slope of between 40 and 48 degrees.

Table 2. Summary of Results from Scanning Electron Microscopy of Composite Solid Propellant Sandwiches with Catalyst in the Oxidizer

Catalyst	Pressure psia	Figure No.	Binder Melt Flow, μm	Binder-Oxidizer Interface Slope
Cu 0202 P (CC)	600		24-41	continuous
	1000	10a	0-23	sections continuous
	1500	10b	11-58	sections continuous
	2000	10c	6-26	nearly discontinuous
Ferric Oxide (IO)	600	10d	49-77	nearly discontinuous
	1000	11a	0	discontinuous
	1500	11b	17-38	double dip
	2000	11c,d	0-23	double dip
Ferrocene (F)	600		28-44	continuous
	1000		15-55	continuous
	1500	12a	3-27	continuous
	2000		32-53	continuous
Iron Blue (IB)	600		24-34	continuous
	1000		22-32	continuous
	1500	12b	6-28	continuous
	2000		0	slight undercutting

The maximum regression of the oxidizer layer is at the edge of the binder melt flow.

The surface of the oxidizer is the same as the 1000 psia sample shown in Figure 9a. It is relatively smooth and uniform. There is a porous structure with holes of diameter less than four μm and cracks of approximately the same width occurring in this surface. This is representative of a gaseous decomposition beneath a liquid layer, similar to the pure AP, but with either a much thinner liquid layer or many more distinct decomposition sites. The hole diameter of the porous structure does not increase in size as the combustion pressure increases. Some particles of material have been deposited on the solidified binder during the quench process.

1000 psia (Figure 10a). Harshaw catalyst Cu 0202 P, when loaded in the AP oxidizer, catalyzes the sandwich vertical burn rate. The binder melt flow varies from zero to 23 μm. The slope of the oxidizer surface varies from 40 to 45 degrees. The maximum regression of the sandwich is at the edge of the binder melt flow. The surface slope is continuous as long as the binder melt flows over the oxidizer surface.

The surface of the oxidizer is relatively smooth and uniform with an indication of small scale porosity as seen at 600 psi. There was no indication that a ridge and valley formation was starting to form at this pressure as was indicated in the AP-HTPB samples.

The micrograph (Figure 10a) was taken to reveal as much of the profile of the binder-oxidizer interface as possible. From this angle it is impossible to realize just how much faster the catalyzed oxidizer has burned than the pure oxidizer (to the right of the binder). An additional

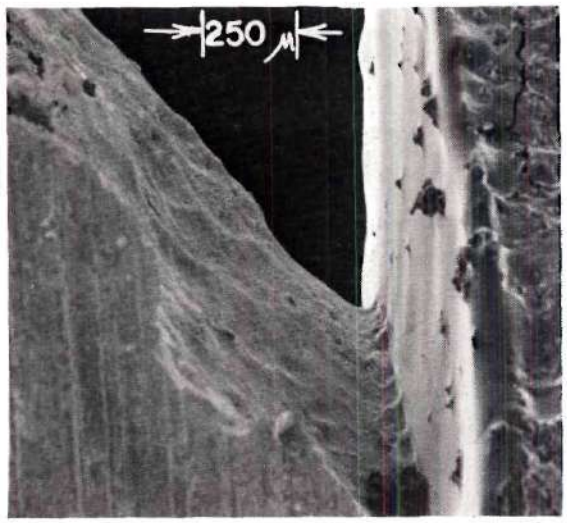

a) Harshaw Catalyst Cu 0202 P
1000 psia (x49.3)

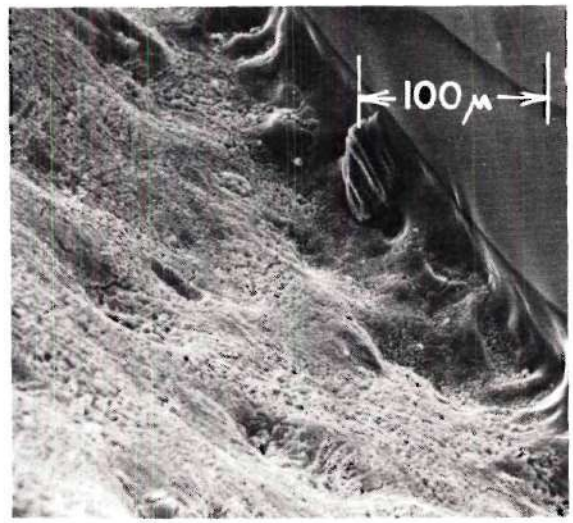

b) Harshaw Catalyst Cu 0202 P
1500 psia (x250)

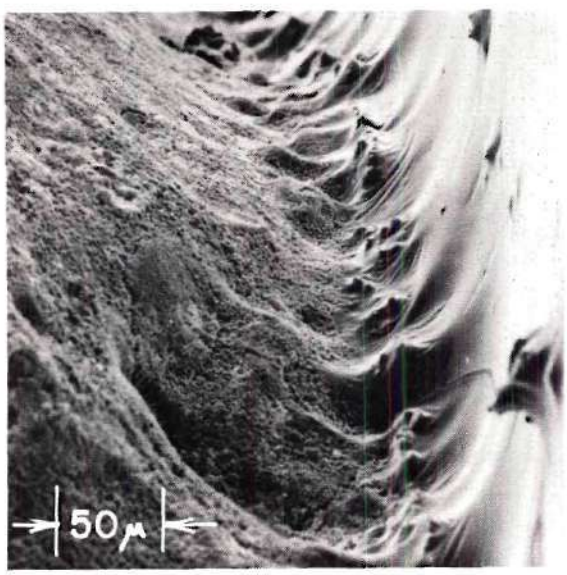

c) Harshaw Catalyst Cu 0202 P
2000 psia (x280)

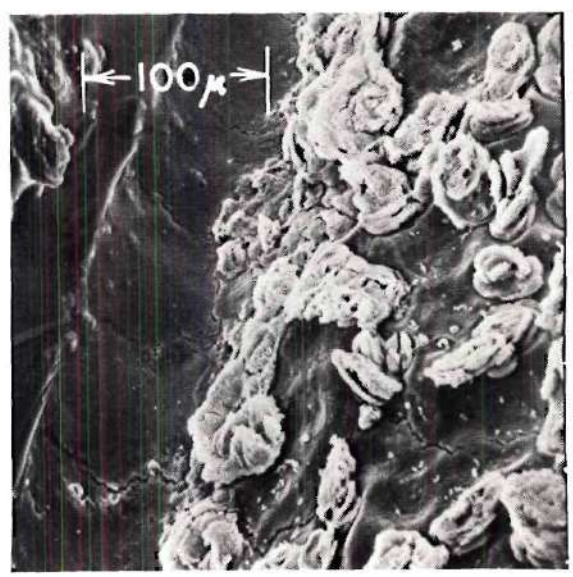

d) Ferric Oxide
600 psia (x260)

Figure 10. Catalysts Added to the Ammonium Perchlorate

micrograph[22] of this sample taken from above the burned surface showed that the variation in binder melt flow was a continuous variation from no flow to 23 μm.

1500 psia (Figure 10b). Harshaw catalyst Cu 0202 P, when loaded in the AP oxidizer, catalyzes the sandwich vertical burn rate. The binder melt flow has been reduced to between 11 and 58 μm. The slope of the oxidizer surface is approximately 49 degrees. Again the slope at the interface is continuous at specific locations where the binder melt is most extensive.

The surface of the oxidizer with catalyst continues to be relatively smooth with an indication of small scale porosity as seen above. The variation of the binder melt flow can be observed in this micrograph. The wrinkles in the solidified binder can cause the binder melt flow to be obscured if the sample is viewed from above. There is an indication of more unevenness in the catalyzed oxidizer surface in this micrograph but this was not uniformly distributed over the surface of the sample.

2000 psia (Figure 10c). Harshaw catalyst Cu 0202 P, when loaded in the AP oxidizer, continues to catalyze the sandwich vertical burn rate at this higher pressure. The binder melt flow appears to extend 6 to 25 μm from the binder oxidizer interface. The slope of the oxidizer surface has increased to 64 degrees. The maximum regression point occurs within 25 μm of the interface. The surface slope of the sample is not continuous at the binder-oxidizer interface. The oxidizer protrudes through the binder melt flow at the interface.

The surface of the oxidizer continues to be relatively smooth with an indication of small scale porosity as seen above.

Summary of Cu 0202 P

Harshaw catalyst Cu 0202 P, when loaded in the AP oxidizer at a concentration of two weight percent, catalyzed the sandwich vertical burn rate at all pressures. The oxidizer surface was relatively smooth for all samples. The slope of the surface of the oxidizer with catalyst increases as the pressure increases. This was inconsistent with the results obtained from the cinephotomacrography (Figure 4). As the pressure increased the difference between the two burn rates decreased. This indicates that the slope of the oxidizer surface was also decreasing. The surface slope was actually observed to decrease from 50 to 20 degrees as the pressure increased from 600 to 2000 psia. The leading edge of the sandwich regression is displaced outward from the binder-oxidizer interface into the oxidizer by the slight melt flow.

AP and Ferric Oxide - HTPB

600 psia (Figure 10d). Ferric oxide, when loaded in the AP oxidizer, did not catalyze the sandwich vertical burn rate. The binder melt flow varies from 49 to 77 μm. There is a mild slant of the oxidizer surface at the binder-oxidizer interface with evidence of retardation of the oxidizer regression at this interface due to the binder melt flow. The slope of the oxidizer surface is approximately 40 degrees. There is a slope discontinuity indicated at this interface.

The surface of the oxidizer, AP with two weight percent of ferric oxide, resembles that of the pure AP when viewed at low magnification (x27). At higher magnification (x260) the surface consists of smooth background with flakes of approximately 50 μm in diameter scattered over the entire surface. These flakes are probably the residue of larger scale

frothy growth which is noted in motion pictures. A majority of this material might be removed during the quench process.

These flakes are considerably larger than the pure ferric oxide particles that were added to the AP. The ferric oxide particle size was close to that of the small particles (one μm in diameter) observed in the solidified AP layer. There is an indication of a porous structure in the vicinity of cracks that appear in this smooth oxidizer surface. This indicates that there has been some decomposition below the liquid AP surface at discrete sites. It is only a slight indication of froth and not nearly as extensive as with either the pure AP-HTPB samples or those catalyzed by Harshaw catalyst Cu 0202 P.

It is known from Figure 4 that ferric oxide at this loading level and pressure does not catalyze the sandwich vertical burn rate and retards the burn rate normal to the oxidizer surface. Ferric oxide might restrict the formation of distinct decomposition sites by either poisoning them or reacting immediately with the decomposition products to form an easily agglomerated substance that forms this flaky structure.

1000 psia (Figure 11a). Ferric oxide, when loaded in the AP oxidizer, catalyzes the sandwich vertical burn rate. There is no obvious binder melt flow for this sample. The maximum regression appears to be at the binder-oxidizer interface where there is a definite discontinuity in slope. The slope of the oxidizer surface is 30 degree.

The flake structure is observed on the oxidizer surface. The size of individual particles has increased slightly to 60-100 μm. The structure of these flakes seems to be small petaloid structures with a center petal of approximately 10 μm in diameter. They appear to be formed in

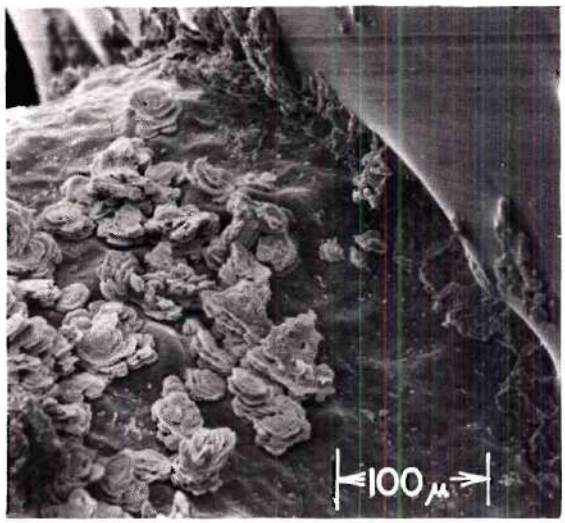

a) 1000 psia (x204)

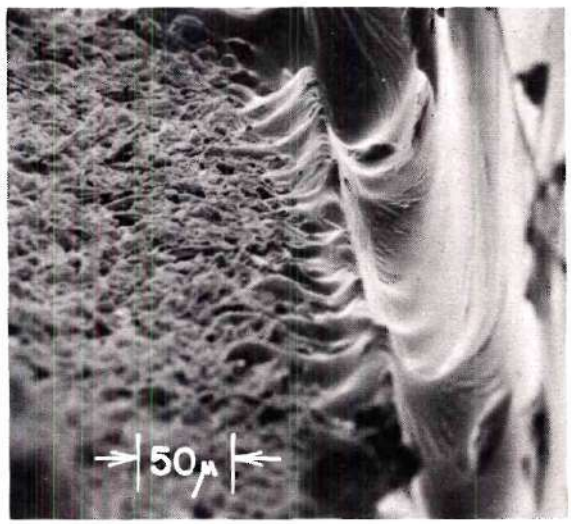

b) 1500 psia (x240)

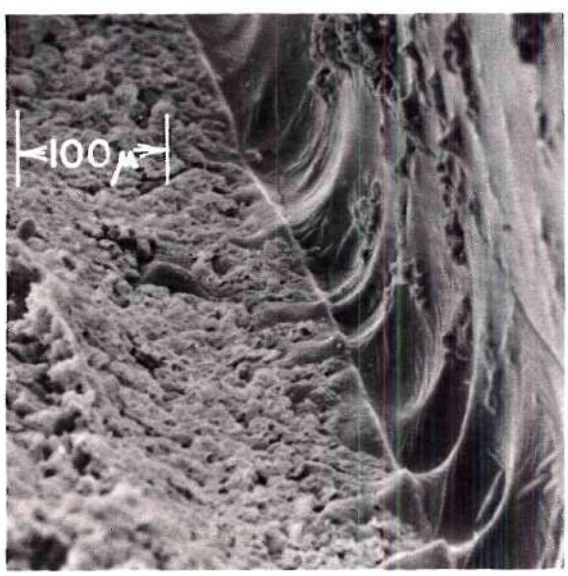

c) 2000 psia (x195)

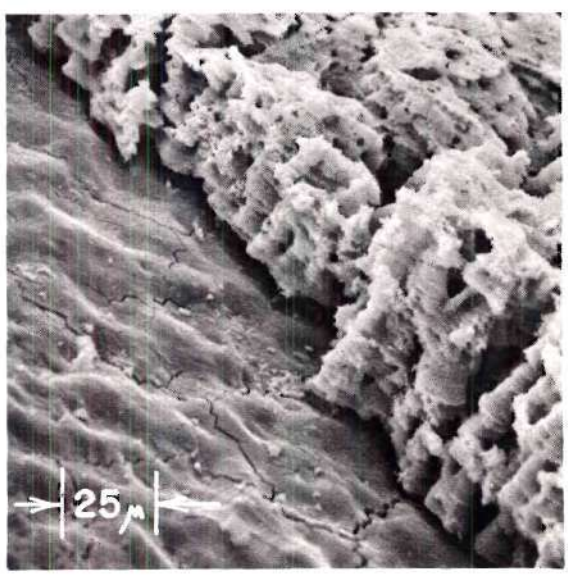

d) 2000 psia (x484)

Figure 11. Ferric Oxide Added to the Ammonium Perchlorate

layers parallel to the oxidizer surface. They could be formed with this layered structure, if the material that coalesces to form these flakes floats in the oxidizer liquid layer. There is still very little porosity in this liquid layer to indicate gaseous decomposition within the liquid layer of oxidizer.

1500 psia (Figure 11b). Ferric oxide, when loaded in the AP oxidizer, catalyzes the sandwich vertical burn rate. There is a binder melt flow of from 17 to 38 μm. The slope of the oxidizer surface is 30 degrees. There is a cusp or double dip of the binder and oxidizer surface visible in Figure 11b. The maximum regression of the oxidizer is displaced away from the binder-oxidizer interface by the melt flow. Considering the slope of the burning process the surface transition from binder to oxidizer was continuous. This cusp in the binder could be formed by the local ejection of molten binder during the quench process. The high speed motion pictures did not show any undercutting of the binder for these samples during normal burn. The entire oxidizer surface has been covered with a layer of particles either related to a further coalescing of the flake structure observed at lower pressures or an entirely different formation of a frothy surface. There are large cracks in this coating and sections missing, probably removed by the rapid depressurization. The oxidizer surface below this frothy structure is similar to the surface surrounding the flaky structure of the 600 and 1000 psia cases. There is a definite displacement of this frothy structure by a binder melt flow.

2000 psia (Figure 11c,d). Ferric oxide, when loaded in the AP oxidizer, continues to catalyze the sandwich vertical burn rate. The

binder melt flow is intermittent and less than 25 μm in extent when it occurs. The slope of the oxidizer surface is between 25 and 30 degrees. Again there is a relative maximum of the binder height giving the appearance of a cusp at the binder-oxidizer interface. The leading edge of regression appears to be located at the binder-oxidizer interface or slightly into the oxidizer. The molten binder has apparently been ejected during the quench process.

The entire oxidizer surface has been covered with a definite crust-like structure. This has no resemblance to the flakes observed at lower pressures. The difference is seen easily in Figure 11d. The surface where the crust has been removed is similar to the background surface observed at lower pressures for all ferric oxide-AP samples. Large sections of this crust have been removed, probably in the quench process.

Summary of Ferric Oxide

Ferric oxide, when loaded in the AP oxidizer at a concentration of two weight percent catalyzed the sandwich vertical burn rate for 1000, 1500 and 2000 psia. The subsurface of all of these samples was similar. There appears to be a liquid layer at all pressures with ferric oxide particles possibly suspended in it. There did not appear to be any large scale gaseous decomposition below or within this layer. Ferric oxide might retard the AP regression by eliminating this subsurface decomposition.

From the cinephotomacrography for this series of experiments, the formation of a large scale frothy structure was indicated. The formation of this froth increased as the pressure increased. Sections of this structure can be observed to break off as the sample continues to burn.

The flakes and the crust of the quenched samples are the only remnants of this frothy structure. As the pressure increased from 600 to 2000 psia the density of this auxiliary surface structure increased. This frothy structure has coalesced to a continuous structure over the same pressure interval (1000 to 1500 psia) that ferric oxide switches from a retarder to an augmenter of the normal oxidizer regression rate. This structure may act as a heterogeneous decomposition matrix for the oxidizer.

The slope of the surface of the sample is not continuous at the binder-oxidizer interface. The slope of the oxidizer surface far away from the interface varied from 40 degrees at 600 psia to 25-30 degrees at 200 psia. This was not consistent with the cinephotomacrography results. The sample slopes from approximately 60 degrees at 600 psia to 20 degrees at 2000 psia in the movies.

There was a definite undercutting of the binder layer of the quenched samples at 1500 and 2000 psia. This cusp in the binder was credited to the local ejection of molten binder during the quench process. This was not noted with any other samples. It could be caused by an interaction of the deflagration flame and the large scale frothy structure. This could cause a concentration of the heat feedback from the flame to the propellant surface in the binder-oxidizer interface region.

AP and Ferrocene - HTPB

600 psia. Ferrocene, when loaded in the AP oxidizer, catalyzed the sandwich vertical burn rate. The oxidizer surface slope far from the binder-oxidizer interface was 45 degrees. There was a definite binder melt flow of from 28 to 44 μm from the binder-oxidizer interface. The

maximum regression of the sample occurred at the edge of this binder melt flow. The surface slope of the sample was continuous across the binder-oxidizer interface.

The surface of the oxidizer was uneven and frothy. There was a resemblance to that of the pure AP. There appeared to be a scattering of additional particles of approximately 28 μm diameter on the surface of the oxidizer. These particles appeared to accumulate at the edge of the binder melt flow, but are dispersed over the entire oxidizer surface. The binder appeared to sag more than in previous samples, that is, there were more wrinkles showing in the solidified binder.

1000 psia. Ferrocene, when loaded in the AP oxidizer, catalyzed the sandwich vertical burn rate. The oxidizer surface slope far from the binder-oxidizer interface was 45 degrees. The binder melt flow extended from 15 to 55 μm from the binder-oxidizer interface out over the oxidizer. The maximum regression of the sample occurred at the edge of this binder melt flow. The surface slope of the sample was continuous across the binder-oxidizer interface.

The oxidizer surface resembled that of pure AP with additional particles of approximately 18 μm diameter scattered on the uneven surface. An optical microscopic investigation showed that these particles were red and black. There was no accumulation of these particles at the edge of the binder melt flow.

1500 psia (Figure 12a). Ferrocene, when loaded in the AP oxidizer, catalyzed the sandwich vertical burn rate. The oxidizer surface slope far from the binder-oxidizer interface had decreased to 30 degrees. The binder melt flow was less than 27 μm in extent. This retarded the AP

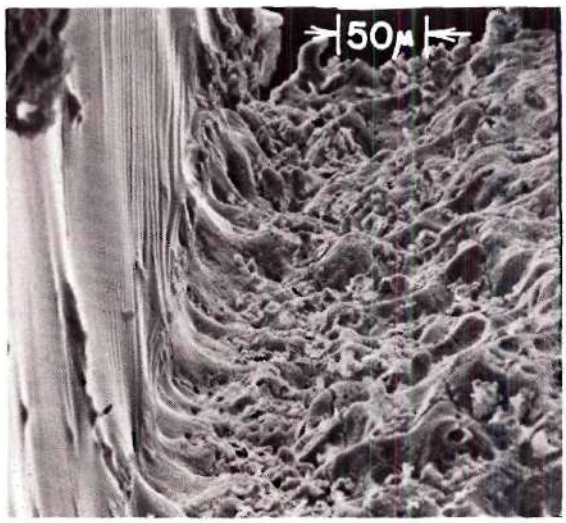

a) Ferrocene Added to AP
1500 psia (x240)

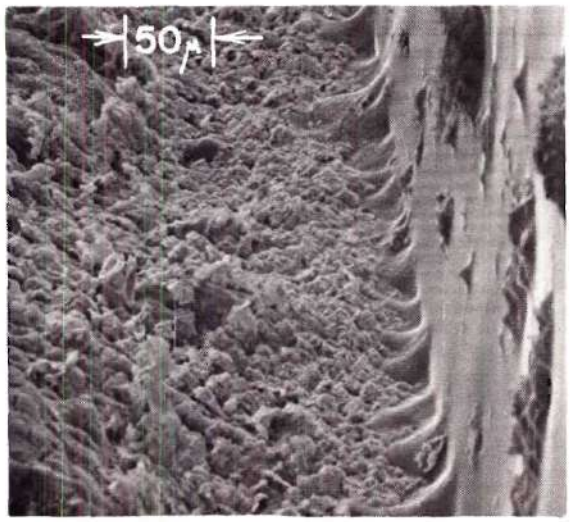

b) Iron Blue Added to AP
1500 psia (x230)

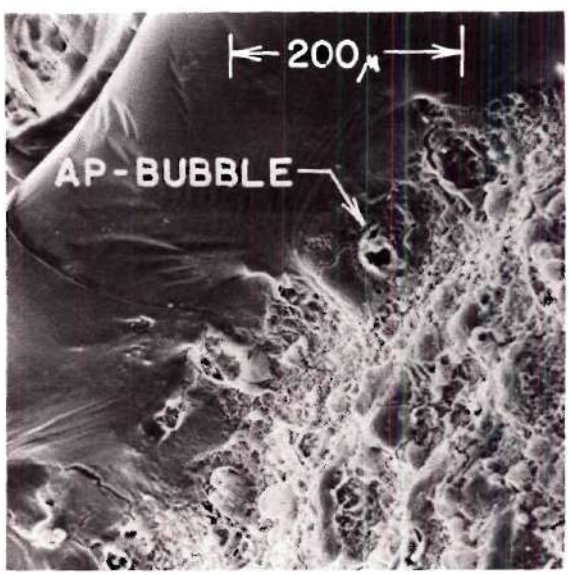

c) Iron Blue Added to HTPB
600 psia (x155)

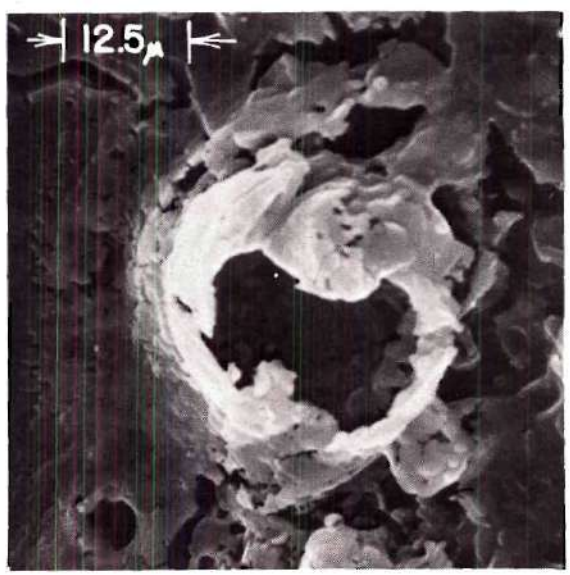

d) AP Bubble in Binder Melt Flow
600 psia (x1300)

Figure 12. Catalyst Added to the AP-HTPB Sandwiches

regression at the binder-oxidizer interface and displaced the point of maximum regression slightly into the oxidizer.

The appearance of the entire surface of the oxidizer was slightly smoother than for the pure AP of Figure 9b, when viewed at low magnification (x28.7). The ridges and valleys structure was apparent, but the extremes were closer together; because of this there were more ridges and valleys. Red and black particles of approximately 16 μm diameter, were visible on the oxidizer surface. The surface had to be observed from above to distinguish the size and shape of these additional particles. Considerably more debris was stuck on the vertical binder surface than on previous samples. These particles could be ejected from the oxidizer surface during the quench process.

2000 psia. Ferrocene, when loaded in the AP oxidizer, catalyzed the sandwich vertical burn rate. The oxidizer surface slope far from the binder-oxidizer interface was approximately 30 degrees. The binder melt flow extended from 32 to 53 μm from the binder-oxidizer interface. The maximum regression of the sample occurred at the edge of the binder melt flow. The surface slope of the sample was continuous across the binder-oxidizer interface.

The oxidizer surface did not resemble the pure AP case. The surface when viewed at low magnification (x24.3) was much more uniform and regressed uniformly. Upon closer examination it was seen that the size of the pore structure, up to eight μm diameter, was much larger than for the pure AP case. There was definite indication of a liquid layer with burst bubbles yielding views of porous materials and cracks occurring during the cooling process. Particles were visible on the oxidizer surface

but their diameters had decreased to approximately 11 μm. Fewer particles have adhered to the solidified binder.

Summary of Ferrocene

Ferrocene, when loaded in the AP oxidizer at a concentration of two weight percent, catalyzed the sandwich vertical burn rate at all pressures. There was a definite change in the surface structure as the combustion pressure increased. Initially there was little effect. The surface resembled that of pure AP. At the highest pressures the surface was completely different. The surface slope far from the binder-oxidizer interface remained essentially constant varying from 30 to 45 degrees. This was in agreement with the cinephotomacrography results. The binder melt flow decreased as the pressure increased. This allowed the point of maximum regression of the sandwich to be located very close to the binder-oxidizer interface at high pressures.

AP and Iron Blue - HTPB

600 psia. Iron blue, when loaded in the AP oxidizer, catalyzed the sandwich vertical burn rate. The binder melt flow extends 24 to 34 μm from the binder-oxidizer interface. The surface slope is between 30 and 45 degrees. The maximum regression of the sample occurs at the edge of the binder melt flow. The surface slope of the sample surface is continuous across the binder-oxidizer interface. The binder-oxidizer interface was visible through the binder melt flow. The surface of the oxidizer appears to be very porous for this case. Again, particles of 20 μm diameter are visible on the surface. These appear red when viewed with the optical microscope.

1000 psia. Iron blue, when loaded in the AP oxidizer, catalyzed

the sandwich vertical burn rate. The binder melt flow is less than 10 μm in extent from the binder-oxidizer interface to the point of maximum sandwich regression. The surface slope is approximately 10 degrees. The surface slope of the sample surface is continuous at the binder-oxidizer interface. The radius of curvature of the surface at this point is small. The surface in this case closely resembles that of AP with ferrocene; the particles appear to be about 20 μm in diameter. The porous structure is reduced over that of pure AP. The particle density has increased considerably over the AP with ferrocene. These particles appear as a definite red residue on this sample, visible to the eye.

1500 psia (Figure 12b). Iron blue, when loaded in the AP oxidizer, catalyzed the sandwich vertical burn rate. The binder melt flow extends up to 28 μm from the binder-oxidizer interface in sections, but is nonexistent in others. The surface slope is approximately 45 degrees. The maximum regression of the sandwich occurs at the edge of the binder melt flow or at the binder-oxidizer interface if there is no flow.

The surface of the oxidizer is covered with a red residue. The slope of this surface has decreased as the pressure increased. The porous structure beneath this red residue is similar to the AP with ferrocene surface.

There are no indications of cooling sags in the solidified binder layer, but there is a considerable residue of particles adhering to it.

2000 psia. Iron blue, when loaded in the AP oxidizer, catalyzed the sandwich vertical burn rate. There is no binder melt flow. The surface slope of the oxidizer has decreased to 30 degrees. There is a considerable binder sag with a possible indication of maximum regression

in the residual binder layer. The surface appears very porous with the indication of a crust coating which has been removed in sections due to the depressurization process. This coating is probably an agglomeration of the red particles observed at lower pressures. The surface is more uniform than in the pure AP case. There is no small particle residue adhering to the binder layer.

Summary of Iron Blue

Iron blue, when loaded in the AP oxidizer at a concentration of two weight percent catalyzed the sandwich vertical burn at all pressures.

The surface of the AP and iron blue becomes smoother as the pressure increases. A surface coating of particles also increases. The slope of the surface increases as the pressure increases and this was contrary to the cinephotomacrography results. A maximum slope of 64 degrees was reached at 1500 psia with the movie experiments.

The AP and iron blue samples at all pressures exhibited edge burning of the same magnitude as the sandwich vertical regression. That is, the combustion proceeded down the sandwich vertical edge faster than the sample burned in the center.

A comparison of the extent of the binder melt flows is shown in Figure 13. The mean of the maximum and minimum extent of the binder melt flow has been plotted, with an indication of the variation where possible. All of the catalysts reduce the binder melt flow by almost an order of magnitude when they are loaded into the oxidizer. Ferric oxide exhibits the most variation. It has the maximum binder melt flow at 600 psia, none at 1000 psia and double dips with the flow at 1500 and 2000 psia. Iron blue seems to behave the most consistently in reducing the

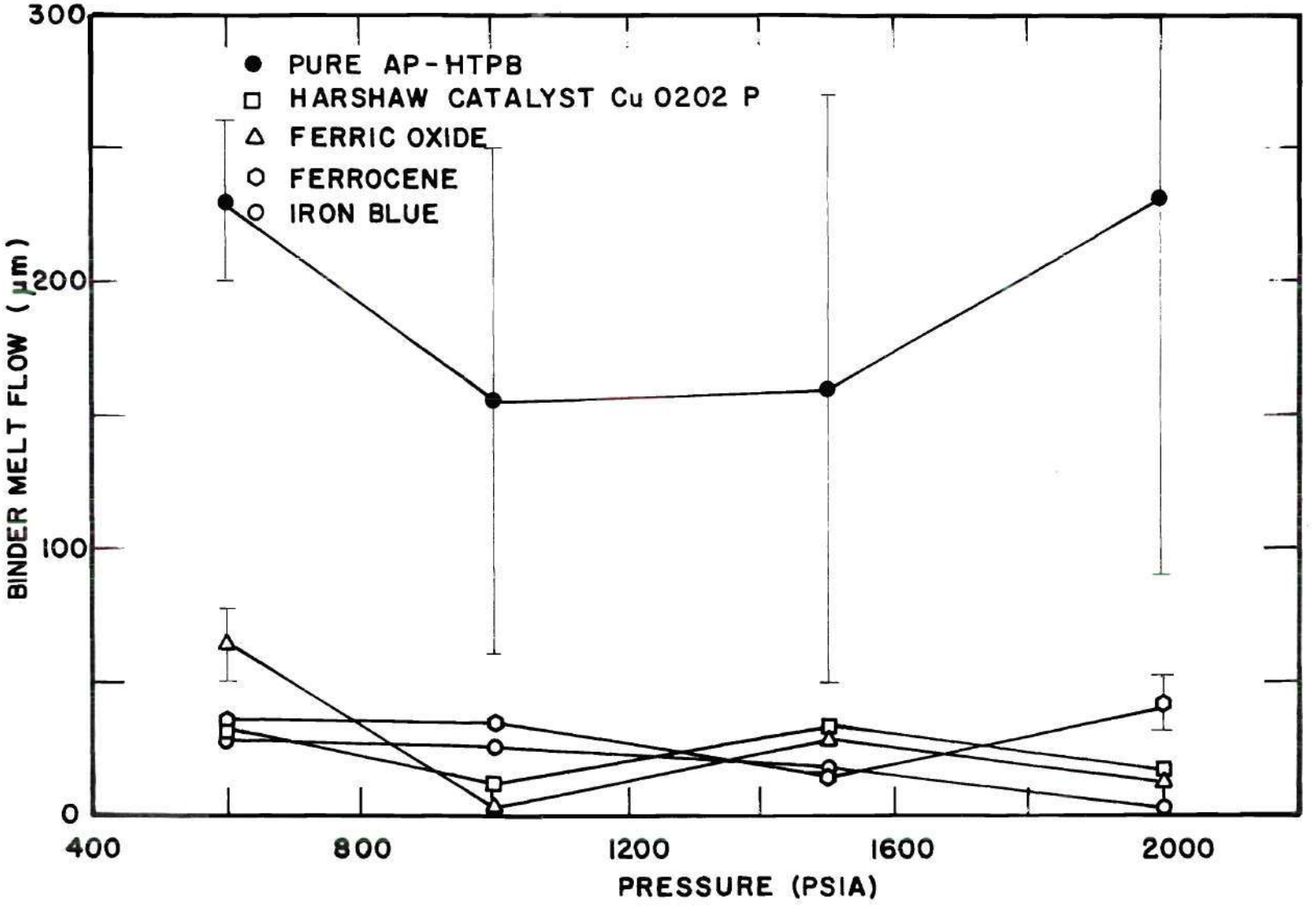

Figure 13. Average Binder Melt Flow for Catalyst Added to the Oxidizer

binder melt flow as pressure increases.

Catalysts in the Binder

A total of eight triple sandwiches of three AP disks and two layers of HTPB binder with different catalysts added to each binder was prepared for this investigation. This allowed two catalysts to be observed in every test. A total of 27 micrographs was obtained for these samples. Only two micrographs are reproduced, in Figure 12c and 12d, as the difference in samples was too small to warrant reproduction of all micrographs. Figure 12c shows the reduction of binder melt flow for iron blue added to the HTPB. There was no obvious change of the AP surface structure of these samples as compared to the pure AP-HTPB sandwiches. A detail of an AP bubble that has occurred near the binder-oxidizer interface is shown in Figure 12d. The partial fracture of this bubble allows the frothy structure of the AP to be observed. The thickness of the solidified layers can also be estimated.

A summary of these tests is given in Table 3. The mean of the maximum and minimum extent of the binder melt flow height is shown in Figure 14 for these samples. The binder melt flows were reduced below those of the pure AP-HTPB results for all samples with the catalysts loaded in the binder. This reduction was not as great as that obtained for the oxidizer loaded samples (Figure 13). Ferrocene consistently reduced the binder melt flow as the pressure increased from 600 to 2000 psia. All four catalysts reduced the binder melt flow extent to zero over regions of the binder-oxidizer interface at 2000 psia.

There were no cusps, double dips or undercutting of the binder

Table 3. Summary of Results from Scanning Electron Microscopy of Composite Solid Propellant Sandwiches with Catalyst in the Binder

Catalyst	Pressure psia	Figure No.	Binder Melt Flow μm	Binder Height μm
Cu 0202 P (CC)	600		19-54	144-164
	1000		44-120	258-328
	1500		27-54	105-645
	2000		0	168-267
Ferric Oxide (IO)	600		41-101	148-174
	1000		44-106	138-215
	1500		45-97	138-518
	2000		0-22	0-396
Ferrocene (F)	600		36-107	164-266
	1000		18-56	165-447
	1500		0-52	340-475
	2000		0-39	195-420
Iron Blue (IB)	600	11c,d	29-126	149-213
	1000		29-54	159-263
	1500		0-28	135-217
	2000		0-75	127-322

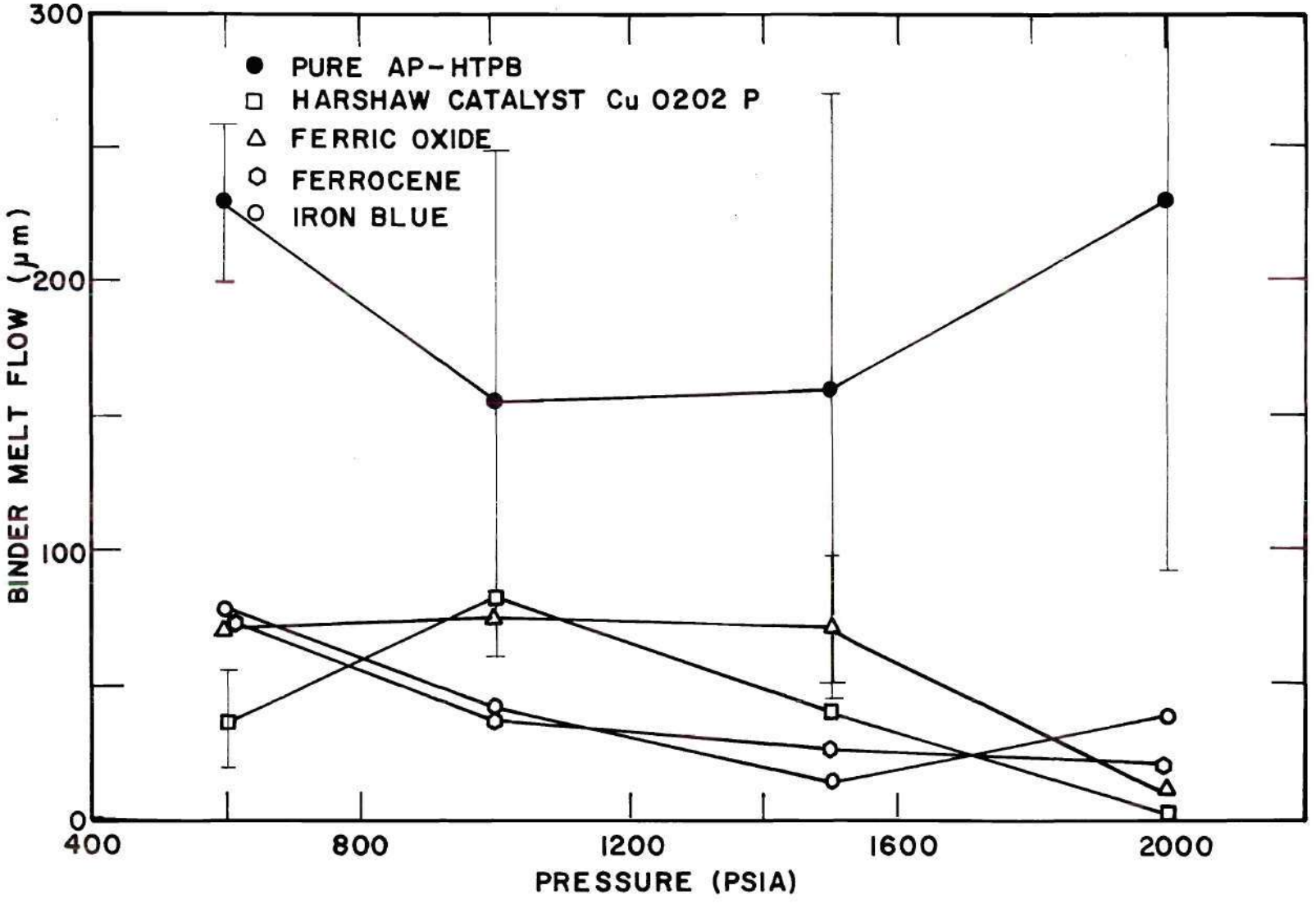

Figure 14. Average Binder Melt Flow for Catalyst Added to the Binder

layer in these samples. There was no solid residue on the vertical solidified binder surfaces. All samples regressed with relatively flat profiles. That is, the surface slope was zero far from the binder-oxidizer interface.

The triple sandwiches were symmetrical about each binder layer. That is, there were pure AP layers on each side of a catalyst loaded binder layer. This allowed residual binder heights to be measured for each sample. These results are plotted in Figure 15. The heights increased for the pressure range 600 to 1500 psia for three of the catalysts and decreased at 2000 psia. Iron blue was the exception and had a nearly constant binder height over the entire pressure range. Both ferrocene and Harshaw catalyst Cu 0202 P samples exceeded the pure sandwich binder heights at 1000 and 1500 psia.

It was difficult to determine a binder height for some samples due to the extensive sagging of the binder. The sagging and wrinkles in the solidified binder with catalyst loading were much more noticeable. These binders appear to have lower viscosity at the time of quench.

Catalysts at the Binder-Oxidizer Interface

A series of seven triple sandwiches, each containing two interface disks with high catalyst loading (two weight percent of total disk weight) at the binder interface and one pure AP disk, were tested. A series of 27 electron micrographs was obtained. A representative micrograph of each catalyst has been reproduced in Figure 16. It must be kept in mind that the samples for this phase of the investigation were not identical to the Harshaw catalyst Cu 0202 P and ferric oxide interface samples used

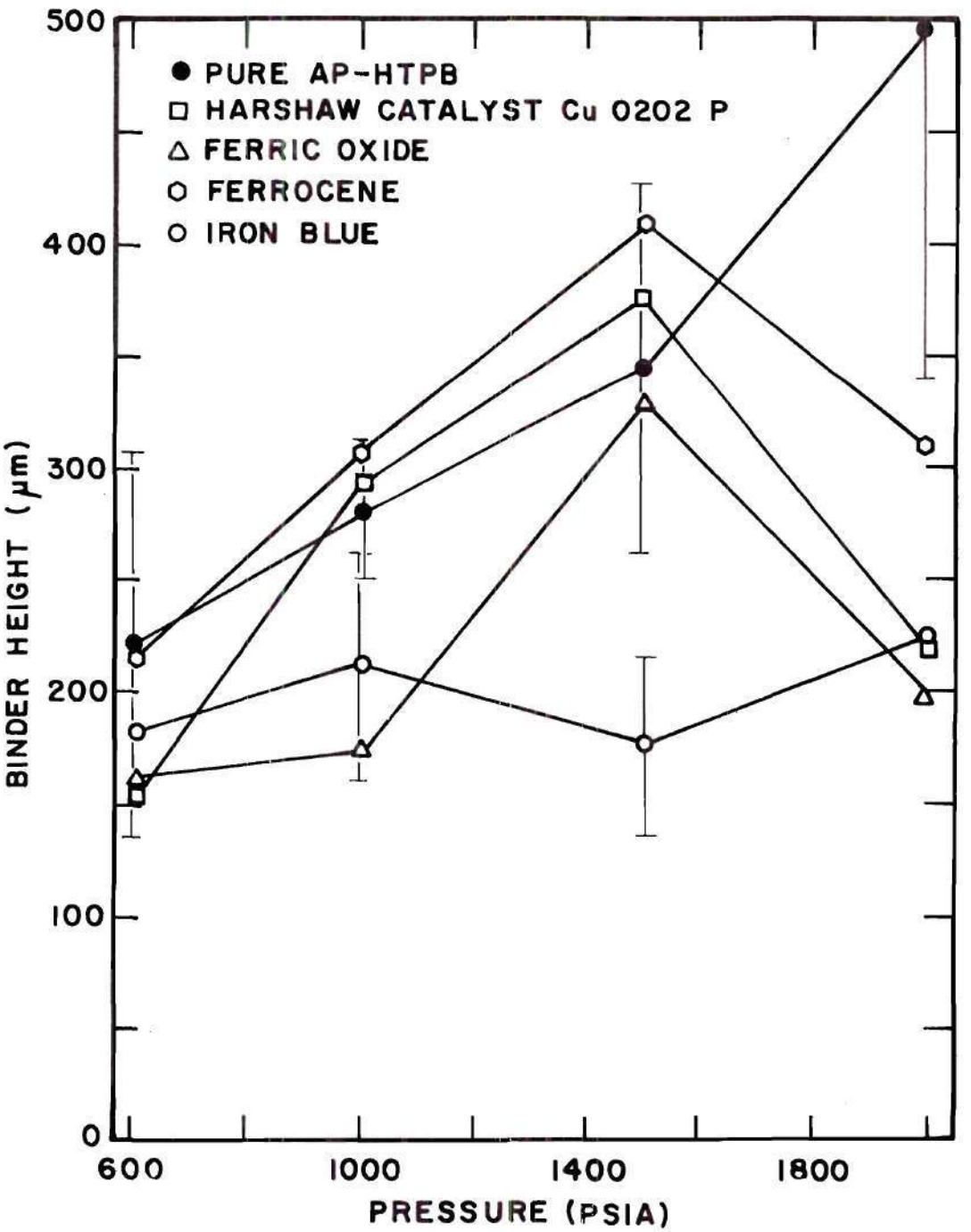

Figure 15. Average Binder Height for Catalyst Added to the Binder

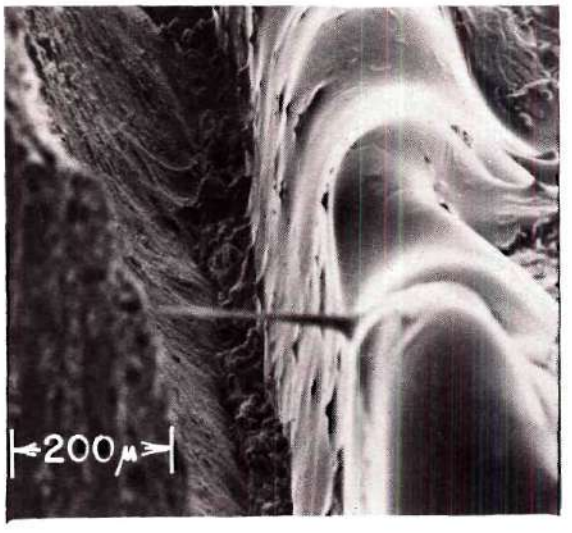

a) Harshaw Catalyst Cu 0202 P
600 psia (x105)

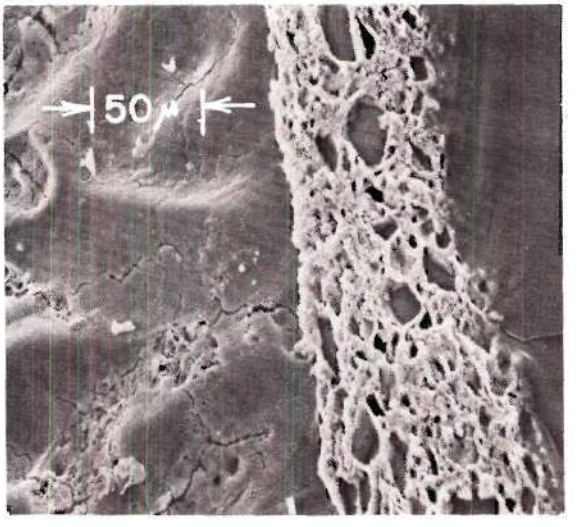

b) Ferric Oxide
1500 psia (x280)

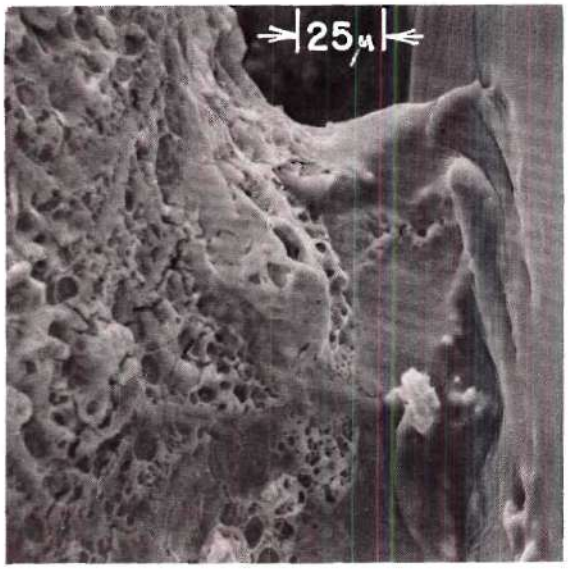

c) Ferrocene
2000 psia (x450)

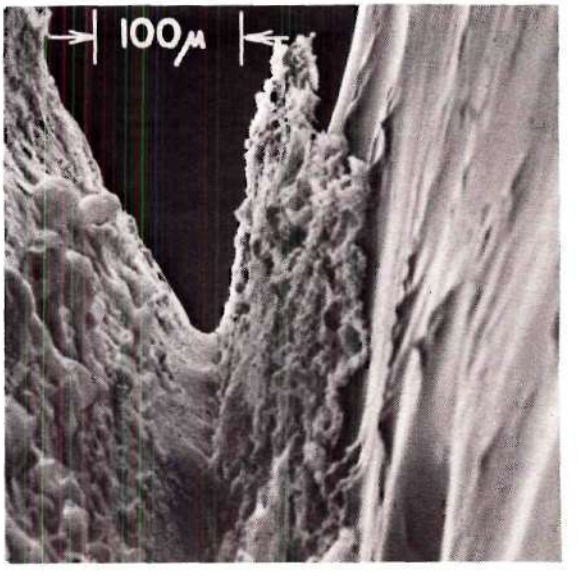

d) Iron Blue
600 psia (x195)

Figure 16. Catalyst Located at the Binder-Oxidizer Interface

in the cinephotomacrographic determination of sample burn rate (Figure 7). Initial interpretation of the interface micrographs did not consider this difference. Discrepancies between the two investigations were difficult to understand. This, together with additional data for higher catalyst loading, has led to a reevaluation of the micrographs. A summary of these tests is given in Table 4.

AP and Cu 0202 P on Interface

600 psia (Figure 16a). Harshaw catalyst Cu 0202 P, when restricted to the interface, catalyzes the sandwich vertical burn rate. There is a slight intermittent binder melt flow of up to 20 μm over the catalyst interface layer which is 42 μm in thickness. There is no binder melt flow out over the pure AP. Excess catalyst material appears to have remained in the interface layer as a frothy material. The presence of the binder appears to have no effect on the maximum regression point of the sandwich. This point lies below the residue layer and at the pure AP-catalyst interface. The oxidizer surface has a high slope of 70 to 75 degrees.

The oxidizer surface of the pure AP layer immediately adjacent to the catalyst layer resembles that of the AP loaded with Cu 0202 P (Figure 10a). This region extends 250 μm from the pure AP-catalyst interface. As one moves farther from this interface up the steep slope of the pure AP surface one finds a surface resembling that of the pure AP (Figure 9a). A single strand of binder has bridged the gap in the foreground of the micrograph in Figure 15a.

1000 psia. Harshaw catalyst Cu 0202 P, when restricted to the interface, catalyzes the sandwich vertical burn rate. The binder has

Table 4. Summary of Results from Scanning Electron Microscopy of Composite Solid Propellant Sandwiches with Catalyst Located at Binder-Oxidizer Interface

Catalyst	Pressure	Figure No.	Binder Melt Flow	Binder Height	Interface Layer Thickness
	psia		μm	μm	μm
Cu 0202 P (CC)	600	16a	0-20		42
	1000		0-10		40-60
	1500		none		41-78
	2000		none		36
Ferric Oxide (IO)	600	16b	23-68	129-169	73
	1000		44-101	120-144	66
	1500		0-19	108-141	70
	2000		none	69-122	76
Ferrocene (F)	600		90-174	323-577	48
	1000		75-145	309-414	52
	2000	16c	34-49		50
Iron Blue (IB)	600	16d	none		80
	1000		none		62
	2000		0-17		50

either flowed or sagged onto the catalyst interface layer for approximately 10 μm in some places. There is no binder melt flow out over the pure AP. The catalyst residue layer has decreased in height as the pressure was increased from 600 to 1000 psia. The thickness of this residue layer appears to vary between 40 and 60 μm. The maximum sandwich regression appears to occur at the pure AP-catalyst interface. It is more difficult to detect due to its irregular variation across the sample. This gives the overall appearance of an uneven sample burn. The oxidizer surface has a slope of 73 degrees with the horizontal.

The oxidizer surface resembles that of the AP loaded with Cu 0202 P sample surface for approximately 250 μm from the pure AP-catalyst interface.

1500 psia. Harshaw catalyst Cu 0202 P, when restricted to the interface, catalyzes the sandwich vertical burn rate. There is no binder melt flow and no indication of binder sag. The catalyst residue layer is less frothy in structure as compared to the 600 psia case. The thickness of this residue layer varies from 41 to 78 μm in width. The maximum regression profile has become more irregular. The point of maximum sandwich regression has definitely undercut the residue layer. It appears to be located at the pure AP-catalyst interface. The binder also appears to have undercut this residue layer at the binder-catalyst interface. The oxidizer surface slope has remained close to 73 degrees with the horizontal.

The oxidizer surface continues to resemble that of the AP loaded with Cu 0202 P sample. The extent of this apparent catalysis of the pure oxidizer deflagration has decreased to 200 μm.

2000 psia. Harshaw catalyst Cu 0202 P, when restricted to the interface, catalyzes the sandwich vertical burn rate. There is no binder melt flow. The catalyst residue layer is approximately 36 μm wide. It appears to bridge the gap between the pure AP and the binder smoothly. That is, the surface slope is continuous as you move across the sample. The maximum regression appears to occur in the binder layer. The oxidizer surface has continued to regress at approximately the same angle, 70 to 75 degrees.

Again the pure AP surface resembles that of AP loaded with Cu 0202 P for 300 μm from the pure AP-catalyst interface. More residue particles appear to be deposited on the residual binder, possibly during the quench process.

Summary of Cu 0202 P

Harshaw catalyst Cu 0202 P, when mixed with an equal amount of ammonium perchlorate and restrained to the binder-oxidizer interface is a very effective catalyst of the sandwich vertical regression rate. There was a residual frothy layer at this binder-oxidizer interface for each partially burned sample. If this layer is excess catalyst, then the same burn rate enhancement could be obtained with less catalyst applied in an equivalent manner. This may be why there was a considerable catalysis of the sandwich burn rate when Harshaw catalyst Cu 0202 P was painted on the AP disks.[20] This could indicate that coating AP particles for cast propellants would be a more effective means of adding the catalyst than adding to the binder mix.

All oxidizer surface slopes for these partially burned samples were between 70 and 75 degrees. There did not appear to be any pressure

dependence. The interface samples with Harshaw catalyst painted on the surface showed an increasing oxidizer surface slope of from 38 to 65 degrees as the pressure increased from 600 to 2000 psia[2] (Figure 7). The high surface slopes obtained for the partially burned samples may be the maximum attainable slope for an excess amount of catalyst located at the binder-oxidizer interface.

The oxidizer surface of the pure AP resembled that of the AP loaded with Cu 0202 P sample for from 200 to 300 μm from the pure AP-catalyst interface. The extent of this surface appearance did not seem to be pressure dependent. This oxidizer surface phenomenon could be explained if the mode of catalysis of Cu 0202 P is attributed to an acceleration of a sub-liquid layer decomposition of AP. The catalyst would have to migrate over the AP surface in the liquid layer, which is highly unlikely. The high sandwich vertical burn rate indicated by the steep slope of the oxidizer is not conducive to a liquid layer mode of catalysis. The diffusion velocities in the liquid layer would have to be very large. A gas phase catalysis of the AP decomposition products with increased heat feedback into the oxidizer would be a more plausible model. The actual alteration of the surface structure would then be a heat transfer phenomenon.

Since this effect has only been noted for samples with high oxidizer surface slope, it may be due to a physical spraying of the pure oxidizer surface with catalyst as the sample burns rapidly. At this time this phenomenon is unexplained.

AP and Ferric Oxide on Interface

600 psia. Ferric oxide, when restricted to the interface, did not catalyze the sandwich vertical burn rate. The binder melt flow extends from 23 to 68 μm from the catalyst-binder interface. This catalyst interface layer is 73 μm wide. There is a frothy residue at this interface. Sections of it have been almost completely covered with the binder melt flow. The sample surface slope is continuous across the pure AP-catalyst-binder interfaces. There was a measurable residual binder height of approximately 150 μm. The maximum sample regression was in the pure AP layer.

Ferric oxide was not as effective as Harshaw catalyst when restrained to the binder-oxidizer interface. The pure AP surface did not resemble that of the catalyst loaded AP sample (Figure 10d). The maximum sample regression was in the pure AP layer. The oxidizer surface slope varied from 30 to 45 degrees for this sample.

1000 psia. Ferric oxide, when restricted to the interface, did not catalyze the sandwich vertical burn rate. The binder melt flow extends from 44 to 101 μm from the catalyst binder interface. This flow has completely covered the frothy interface layer which was approximately 66 μm wide. The surface slope of the oxidizer was less than 600 psia being between 25 to 35 degrees. The maximum sample regression was in the pure AP layer. The solidified average residual binder layer height was 132 μm.

There is an indication on the AP surface near the pure AP-catalyst interface of the flake structure that was detected on the AP with catalyst samples (Figure 11a). The only real indication of the extent of the effect of the catalyst is the porous structure visible on the oxidizer

surface.

1500 psia (Figure 16b). Ferric oxide, when restricted to the interface, did not catalyze the sandwich vertical burn rate. The binder melt flow has only flowed out over the catalyst layer 19 μm in sections. This catalyst layer is approximately 70 μm wide. The oxidizer surface slope was uniform at 30 degrees. The maximum sample regression was in the pure AP layer near the pure AP-catalyst interface. The sample profile is relatively flat over the entire interface layer. The sample surface slope is continuous across the sample. The residual binder height was 125 μm.

The interface region viewed from above is shown in Figure 16b. This structure does not resemble that of earlier catalyst loaded AP samples (Figure 11b).

2000 psia. Ferric oxide, when restricted to the interface, did not catalyze the sandwich vertical burn rate. There was no binder melt flow for this sample. The catalyst interface layer is 76 μm wide. There is a frothy residue at this interface. The point of maximum sample regression occurs 50 to 60 μm from the pure AP-catalyst interface in the pure AP. The oxidizer surface slope is not continuous at the binder-catalyst interface. The pure AP surface slope is 30 degrees. The average residual binder height is approximately 100 μm.

Summary of Ferric Oxide

When ferric oxide is mixed with an equal amount of ammonium perchlorate and restrained to the binder-oxidizer interface, there was no catalysis of the sandwich vertical burn rate, but there was an increase in the binder consumption rate. This is shown by the decrease in both

the residual binder height shown in Figure 17 and the binder melt flow without increasing the oxidizer deflagration rate. This interface layer did not have as much effect on the oxidizer surface as the two percent loading in the AP. Part of its effect when loaded in the oxidizer at the lower percentage may have been due to its dispersion in the liquid layer. This lack of catalysis or inhibition of the AP deflagration rate for the interface samples could be due to an immediate formation of an agglomerated material in this interface layer. This material could not migrate out over the oxidizer surface.

As in the case of Harshaw catalyst Cu 0202 P the slope of the oxidizer surface remained constant with pressure when the ferric oxide was restricted to the binder-oxidizer interface. For ferric oxide this slope was approximately 30 degrees. The cinephotomacrographic techniques for ferric oxide painted on the oxidizer surface showed a different, but constant, slope of 60 degrees at 600, 1500 and 200 psia.

AP and Ferrocene at Interface

600 psia. Ferrocene, when restricted to the interface, did not catalyze the sandwich vertical burn rate. The binder melt flow extends from 90 to 174 μm from the catalyst-binder interface. This flow has covered the catalyst interface layer which appears to be approximately 48 μm wide for this sample. This flow does not appear to be as thick at the catalyst-binder interface. The maximum sandwich regression point is in the pure AP at the edge of the binder melt flow. The surface slope of the sample is discontinuous at the binder-catalyst interface. The surface slope of the sample was between 20 and 30 degrees far away from the pure AP-catalyst interface.

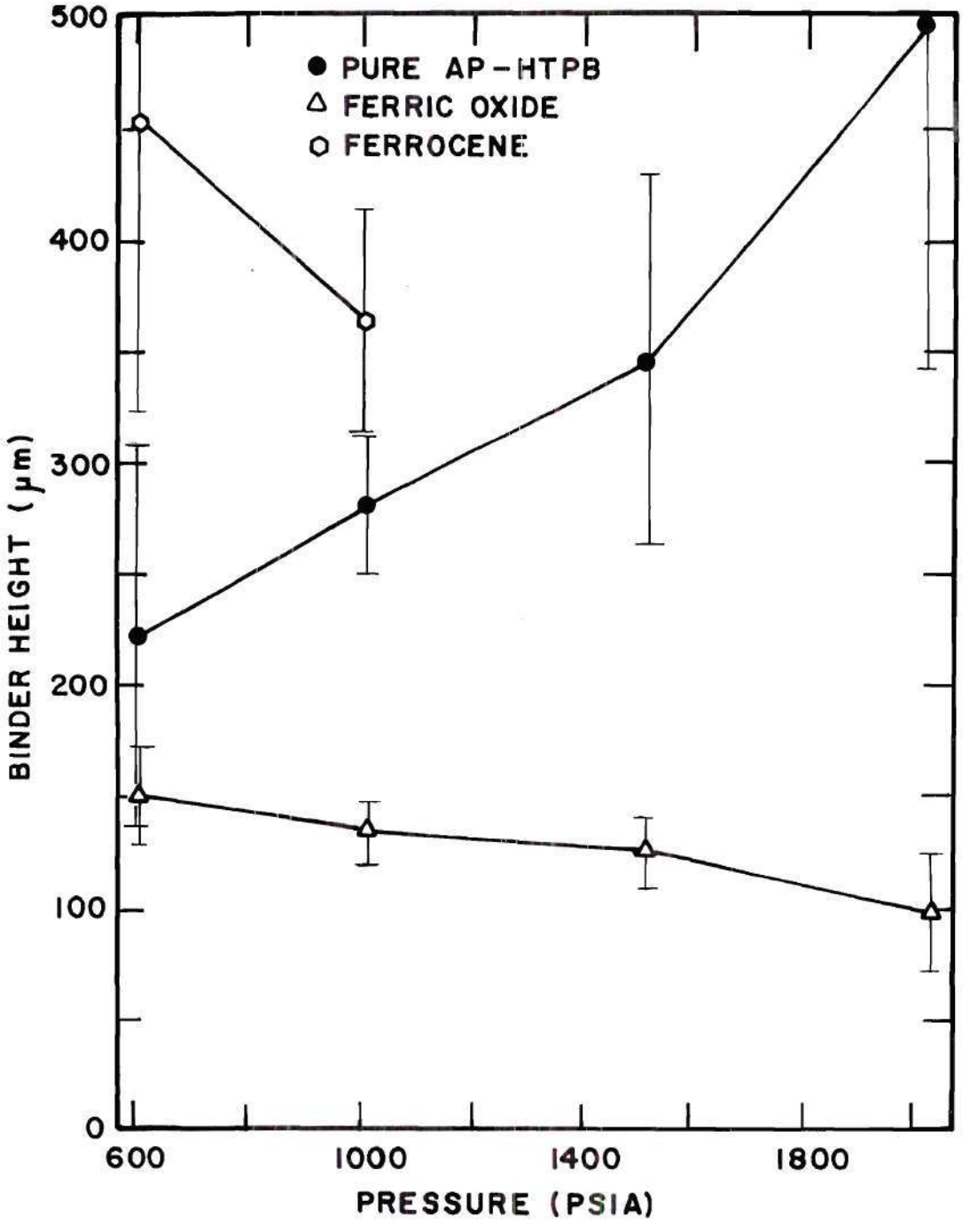

Figure 17. Average Binder Height for Catalyst at the Binder-Oxidizer Interface

There was no evidence of a residual catalyst structure at the interface, but there was an indication of a flake structure within the binder melt flow. There was a residual binder height of 323 to 577 μm. This binder had sagged onto the center pure AP disk. This was greater than the pure AP-HTPB case (Table 1).

1000 psia. Ferrocene, when restricted to the interface, did not catalyze the sandwich vertical burn rate. The binder melt flow extends from 75 to 145 μm from the catalyst-binder interface. The catalyst interface layer was 52 μm wide. The maximum sandwich regression point is in the pure AP beyond the edge of the binder melt flow. The surface slope of the sample is discontinuous at the binder-catalyst interface. The surface slope of the sample was between 15 and 30 degrees far away from the pure AP-catalyst interface.

There was no evidence of a residual catalyst structure at the interface. There was an indication of a flat flake structure suspended in the solidified binder flow at the catalyst layer. The pure AP was more porous near the pure AP-catalyst interface than the pure AP-HTPB sample shown in Figure 9a. Some particles were scattered on the pure AP surface. There was a residual binder height of 309 to 414 μm. This binder did not appear to sag as the 600 psia sample did.

1500 psia. Five attempts were made to obtain a quenched combustion sample at this pressure of 1500 psia. Delay times of from .11 to .022 second from the time of ignition to rupture of the pressure containing diaphragm were used. No partially burned samples were obtained. Either the burn rate was exceedingly high or the sample combustion could not be interrupted by rapidly reducing the pressure.

2000 psia (Figure 16c). Ferrocene, when restricted to the interface, catalyzes the sandwich vertical burn rate. The binder melt flow extends from 34 to 49 μm from the catalyst-binder interface. The catalyst interface layer was 52 μm wide. The maximum sandwich regression point was located in the catalyst layer at the pure AP-catalyst interface. The surface slope is discontinuous at the binder-catalyst interface. The radius of curvature of the surface profile is small at the pure AP-catalyst interface. The surface slope varies from 70 to 80 degrees. There is an indication of undercutting of the binder layer when viewed from above.

There is a flat flake structure visible in the catalyst layer. The surface of the pure AP resembled that of the AP loaded with ferrocene for approximately 200 μm from the pure AP-catalyst interface. There was no comparative residual binder height as measured at 600 and 1000 psia.

Summary of Ferrocene

There was very little indication of augmentation of sample burn rate at 600 and 1000 psia. The slope of the oxidizer surface varied between 15 and 30 degrees. At 2000 psia there was an indication of considerable augmentation of the sample vertical burn rate. A large surface slope angle is generated when the sandwich vertical burn rate is considerably larger than the burn rate normal to the oxidizer surface. This angle was between 70 and 80 degrees for the 2000 psia sample. The oxidizer surface of the pure AP resembled that of the AP loaded with ferrocene for 200 μm from the pure AP-catalyst interface. This was similar to results obtained for Harshaw catalyst Cu 0202 P located at the interface for all pressures. As before this effect has only been noted for

samples with high oxidizer surface slope. At this time this phenomenon is unexplained.

There was no residual frothy material at the interface. There was an indication of flat flaky material suspended in the binder melt flow for all pressures.

The cinephotomacrography results did not indicate any large scale augmentation of binder-oxidizer reactions when ferrocene was loaded in the oxidizer or binder (Figures 4 and 6) for these pressures. The interface samples used for cinephotomacrography observations were prepared in exactly the same way as these partially burned samples. The cinephotomacrography of interface samples (Figure 7) showed little augmentation of sandwich vertical burn rate at 600 and 1000 psia and considerable augmentation at 2000 psia. This was similar to the partially burned samples. The cinephotomacrography results showed a minimum sample burn rate at 1500 psia. No partially burned sample was obtained by venting the combustion vessel at 1500 psia.

AP and Iron Blue at Interface

600 psia (Figure 16d). Iron blue, when restricted to the interface, catalyzes the sandwich vertical burn rate. There is no binder melt flow. There is a porous residue structure 200 to 300 μm in height remaining at the catalyst layer location. This layer is 80 μm in thickness. The point of maximum sandwich regression appears to be located in the pure AP near the pure AP-catalyst interface. The oxidizer surface of the pure AP has a slope of 60 to 70 degrees.

The oxidizer surface of the pure AP layer immediately adjacent to the catalyst layer resembles that of the AP loaded with iron blue (Fig-

ure 12c). This region extends 35 μm from the pure AP-catalyst interface. As one moves farther from this interface the surface slope increases to 60 to 70 degrees. The surface resembles that of the pure AP (Figure 9a). There appears to be an undercutting of the binder at the binder-catalyst interface.

1000 psia. Iron blue, when restricted to the interface, catalyzes the sandwich vertical burn rate. There is no binder melt flow. The volume of the residue structure has increased. The height has remained the same, between 250 and 300 μm. The width of the residue layer has increased to approximately 100 μm. The original catalyst layer was 62 μm thick. The point of maximum sandwich regression appears to be located at the catalyst-binder interface. The slope of the oxidizer surface is discontinuous across the entire catalyst layer. The oxidizer surface far from the pure AP-catalyst interface has a slope of 75 degrees.

The oxidizer surface of the pure AP layer immediately adjacent to the catalyst layer resembles that of the AP loaded with iron blue for approximately 150 μm. The residue layer obscures the point of maximum sandwich regression at both the pure AP-catalyst and catalyst-binder interfaces. There may be binder undercutting at the catalyst binder interface. It was not possible to investigate the extreme penetration of the combustion with the scanning electron microscope.

1500 psia. The iron blue and ferrocene interface samples were combined in one triple sandwich. As was stated above, five attempts were made to obtain a quenched combustion sample at this pressure. No useful samples were obtained.

2000 psia. Iron blue, when restricted to the interface, catalyzes

the sandwich vertical burn rate. There is a binder melt flow of up to 17 μm from the catalyst-binder interface. This melt flow has flowed out over a discontinuous frothy structure. At some sections the surface slope of the sample is continuous across both interfaces. In other sections the frothy structure extends 50 μm in height above the point of maximum sandwich regression. This point is always at the pure AP-catalyst interface. The original catalyst layer was 50 μm thick. The oxidizer surface far from the pure AP-catalyst interface has a slope of 45 to 75 degrees.

The oxidizer surface of the pure AP layer immediately adjacent to the catalyst layer resembles that of the AP loaded with iron blue for approximately 300 μm. This surface effect seems to vary from less than 100 μm for a surface slope of 45 degrees to 300 μm for steeper slopes. The physical makeup of the interface regions for this pressure is considerably different from the 600 and 1000 psia samples. It is much cleaner, i.e. very little residue structure remains from the catalyst layer.

Summary of Iron Blue

Iron blue, when mixed with an equal amount of ammonium perchlorate and restrained to the binder-oxidizer interface, is a very effective catalyst of the sandwich vertical burn rate at all pressures that partially burned samples were obtained. There was a residual frothy layer at this binder-oxidizer interface at 600 and 1000 psia. There was still some indication of the existence of this type of residue, but only fragments, at 2000 psia.

All samples had oxidizer surface slopes of up to 70 degrees. At 2000 psia there was a definite region of 45 degrees surface slope. The surface of the pure AP resembled that of AP loaded with iron blue for

35 μm at 600 psia to 300 μm at 2000 psia. This surface effect increased with pressure, but was only noted for large surface slopes (70 degrees).

The cinephotomacrography results did not indicate any large scale augmentation of binder-oxidizer reactions when iron blue was loaded in the oxidizer or binder (Figures 4 and 6) for these pressures. The interface samples used for cinephotomacrography observations were prepared in exactly the same way as these partially burned samples. The cinephotomacrography of interface samples (Figure 7) showed a consistently increasing augmentation of sandwich vertical burn rate as the pressure increased.

A comparison of the extent of the binder melt flow for catalyst located at the binder-oxidizer interface is shown in Figure 18. The mean of the maximum and minimum extent of the binder melt flow has been plotted, with an indication of the variation where possible. All of the catalysts reduce the binder melt flow over that of the pure AP-HTPB samples. This type of loading was not as effective as the oxidizer loading (Figure 13). Ferrocene samples showed the largest melt flows of any catalyzed samples at 600 and 1000 psia. Iron blue on the other hand, had no melt flow at these pressures, while Harshaw catalyst Cu 0202 P had no melt flow at 1500 psia and 2000 psia. Both of these catalysts had residual frothy layers at the interface at these pressures.

Summary

The observation of quenched samples proved to be an important complement to the high speed combustion photography, giving details of surface quality and profiles not discernible in the movies. In general, the results are consistent between the two methods, showing conditions

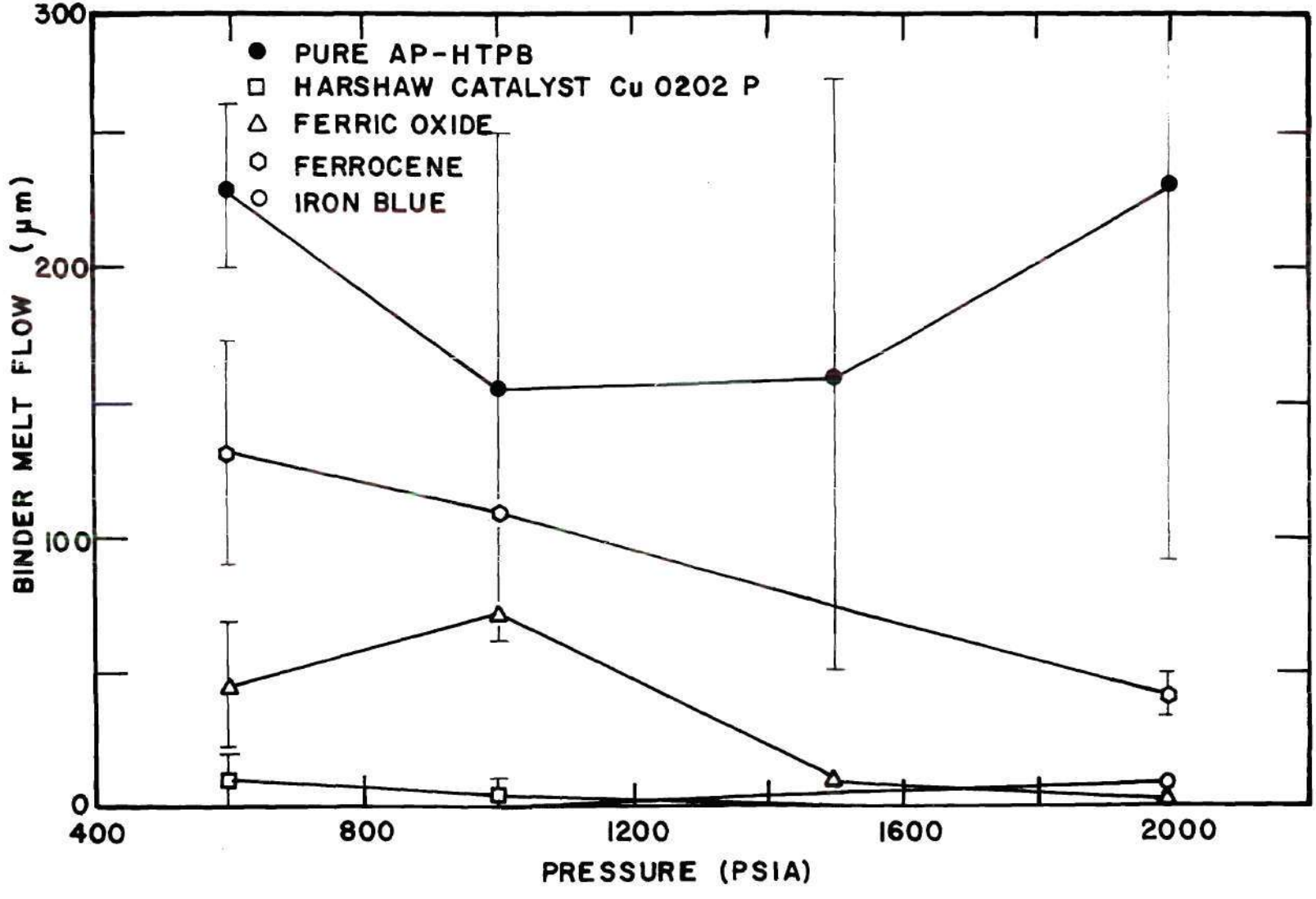

Figure 18. Average Binder Melt Flow for Catalyst at the B-O Interface

under which the catalysts increase sandwich vertical burn rates and alter general surface profiles. However, there were some systematic quantitative differences in variables measured by both methods (notably, the angle of the AP surface slope) and there were some details that were qualitatively different (notably, the flake and froth structure remaining on the oxidizer surface when ferric oxide was added to the oxidizer). Most important, the quench method permitted use of high resolution methods (scanning electron microscopy) that not only added detail to the observation, but also provided electron micrographs that can be included in report form to better communicate results.

All four catalysts, Harshaw catalyst Cu 0202 P, ferric oxide, ferrocene and iron blue, when added to the AP at a concentration of two weight percent, are effective catalysts of the sandwich vertical burn rate over the 600 to 2000 psia range. The only exception was ferric oxide at 600 psia. The cinephotomacrographic results (Figure 4) did not predict a notable catalysis of this burn rate for ferric oxide, ferrocene and iron blue at 600 and 1000 psia.

Harshaw catalyst Cu 0202 P and iron blue, when restricted to the interface, are effective catalysts of the sandwich vertical burn rate over the 600 to 2000 psia range. Ferrocene is an effective catalyst in this configuration at 2000 psia. Ferric oxide is not an effective catalyst over the 600 to 2000 psia range. The cinephotomacrographic results (Figure 7) could only be compared exactly with the quenched samples for iron blue and ferrocene. No quenched combustion sample of iron blue and ferrocene was obtained at 1500 psia.

Binder Melt Flow

A primary observation for all four catalysts at all pressures is that they reduce the binder melt flow from the binder-oxidizer interface out over the adjacent oxidizer surface. This was noted for all three catalyst loading configurations; two weight percent of catalyst added to the polycrystalline AP oxidizer layer (Figure 13), 4.37 weight percent of catalyst added to the HTPB binder (Figure 14) and two weight percent of the AP disk weight of catalyst restricted to the binder-oxidizer interface (Figure 18).

Maximum Regression

For the catalysts added to the oxidizer the leading edge of the sandwich regression was always located at the edge of the binder melt flow, when it existed. When the catalyst was added to the binder, the leading edge was located in the pure AP.

When the catalyst was restricted to the binder-oxidizer interface, the leading edge location varied. For Harshaw catalyst Cu 0202 P, the leading edge was located at the pure AP-catalyst interface for pressures 600 to 1500 psia. At 2000 psia it was located at the catalyst-binder interface. For ferric oxide the leading edge was always in the pure AP layer. For ferrocene the leading edge was located at the edge of an extensive binder melt flow at 600 and 1000 psia. At 2000 psia, the sandwich vertical burn rate was catalyzed very effectively. The leading edge was located in the catalyst layer near the pure AP-catalyst interface. For iron blue the leading edge was either at the pure AP-catalyst interface (600 and 2000 psia) or at the catalyst-binder interface (1000 psia).

Residual Binder Material

The thickness of the binder layer was great enough to cause a protrusion from the quenched samples, a protrusion visible in motion pictures as well, and high enough to be measured in tests on symmetrical sandwiches. Ideally, one would like to make a full tabulation of height and shape of binder protrusion, for four pressures, four catalysts and three different loading conditions, oxidizer, binder or interface. The only symmetrical sandwiches used in this phase of the investigation were the samples with catalyst loaded in the binder. The oxidizer layers on both sides of the binder regressed at the same rate. The protruding binder height increased for three of the catalysts for the 600 to 1500 psia pressure range and decreased at 2000 psia. Iron blue was the exception and yielded a nearly constant binder height over the entire pressure range (Figure 15).

The only other binder height data were obtained for ferric oxide and ferrocene located at the binder-oxidizer interface (Figure 17). These samples were not symmetrical, but the catalysts did not augment the sandwich vertical burn rate over some of the pressure range.

The residual binder layer for the unsymmetrically burning samples was well behaved, for the most part. The binder-oxidizer interface surface slope was almost always continuous for the catalyst added to the oxidizer. Two noticeable exceptions occurred at 1500 and 2000 psia for ferric oxide. There was a definite cusp or double dip of the binder and binder melt flow at the binder-oxidizer interface. This could be formed by the local ejection of molten binder during the quench process. Both of these samples showed evidence of a uniform frothy structure on the quenched sample. Cinephotomacrography showed the growth of a large scale

froth. This could alter the flow of deflagration products and binder decomposition products. Their mixing and subsequent diffusion flame structure and the resultant heat transfer back to the surface could be altered by this frothy growth.

Surface Slope

The slope of the oxidizer surface did not always behave similarly in the cinephotomacrographic tests and the quenched combustion tests.

For Harshaw catalyst Cu 0202 P loaded in the oxidizer, the slope of the oxidizer increased from 44 to 64 degrees as the pressure increased from 600 to 2000 psia for the quenched samples. The high speed movies indicated a decrease of 50 to 20 degrees over the same pressure range increase (600 to 2000 psia). The quenched interface samples all had a slope of between 70 and 75 degrees. The high speed movies were of interface samples with the catalyst painted on the interface. The slope increased from 38 to 65 degrees over the 600 to 2000 psia range.

For ferric oxide loaded in the oxidizer, the slope of the oxidizer varied from 40 degrees at 600 psia to 25 to 30 degrees at 2000 psia. The movies indicated a decrease of from 55 to 60 degrees at 600 psia to 20 degrees at 2000 psia. The quenched interface samples all had a slope of approximately 30 degrees. The movies indicated a slope closer to 60 degrees for all pressures.

For ferrocene loaded in the oxidizer the slope of the oxidizer stayed between 30 and 45 degrees. This was consistent with the movies. The quenched interface samples had a slope of between 15 and 30 degrees at 600 and 1000 psia and a slope of 70 to 80 degrees at 2000 psia. The movies indicated a slope of 40 to 50 degrees at 600 and 1000 psia and 65

degrees at 2000 psia.

For iron blue loaded in the oxidizer the slope of the oxidizer stayed between 30 and 45 degrees. The movies indicated a 45 to 65 degree variation. The quenched interface samples had a slope of up to 75 degrees for all pressures. The movies indicated a variation of 45 to 75 degrees increasing as the pressure varied from 600 to 2000 psia.

The surface slope of the oxidizer remained essentially flat for all samples with catalyst added to the binder.

Oxidizer Surface Details

When Harshaw catalyst Cu 0202 P was added to the AP at a concentration of two weight percent, the surface of the oxidizer had a uniform slope and was relatively smooth, as compared to other catalyzed and pure samples. There was a uniform small scale porosity visible at higher magnifications. These holes were less than four μm in diameter. This surface was obtained at all pressures. The samples with this catalyst restrained to the interface layer had a similar surface appearance for 200 to 300 μm from the pure AP-catalyst interface. This occurred at all pressures. There was a catalyst residue layer at the oxidizer-binder interface for all pressures for these interface loaded samples. At 600 psia the material was porous and frothy, as pressure increased the volume of the frothy material decreased and the material appeared to be solidified from a molten mass.

When ferric oxide was added to the AP at a concentration of two weight percent, the surface of the oxidizer consisted of two distinct formations. There was a smooth sub surface present at all pressures. There were cracks in the surface of four μm width separated by 75 to 100

μm. There was an indication of porosity near these cracks. These holes were not as large and their density was low when compared to the Harshaw catalyst samples. There was a residual structure remaining on this smooth subsurface for all pressures. The high speed motion pictures had showed the formation of a large scale frothy structure for these samples. The majority of this froth was apparently removed during the quench process. At 600 psia all that remained of this froth was a flake structure. These flakes were 50 μm in diameter and appeared to be sprinkled on the surface. At 1000 psia these flakes appeared to coalesce into a petaloid structure composed of layers of flake. The central petal had a diameter of 10 μm. The entire structure was between 100 and 150 μm in diameter. At 1500 and 2000 psia this residual structure consisted of a uniform spongy appearing structure on the smooth subsurface.

The samples with ferric oxide restrained to the interface layer showed very little alteration of the surface due to the presence of this catalyst. It was consumed at the same rate as the pure AP. There was a frothy residue layer at 2000 psia. It was not as extensive as when ferric oxide was loaded in the AP at the same pressure.

When ferrocene was added to the AP at a concentration of two weight percent, the surface of the oxidizer is uneven and frothy. There is a definite resemblance to that of the pure AP. The unevenness of the surface never approaches that of the pure AP at high pressure (2000 psia). There is a scattering of red and black particles sprinkled on the solidified oxidizer surface at 600 psia. Their size decreases and their density increases as the pressure increases from 600 to 2000 psia.

The samples with ferrocene restrained to the interface layer showed

no alteration of the surface at 600 and 1000 psia. The 2000 psia sample surface resembled that of the oxidizer loaded sample for 200 μm from the pure AP-catalyst interface. There was no residue catalyst layer at any pressure when iron blue was added to the AP at a concentration of two weight percent. The surface of the oxidizer was smoother than the pure AP-HTPB surface. It was not as smooth as the Harshaw catalyst case. There were 20 μm diameter red particles visible on the surface at 600 psia. As the pressure increased the particle density increased to a frothy red residue at 1500 psia. It resembled the ferric oxide residue at 2000 psia.

The samples with iron blue restrained to the interface layer had a similar surface appearance for 35 to 300 μm. This extent increased with pressure. There was no flake or froth structure out over the pure AP, just the smooth subsurface. There was a residual frothy layer at the catalyst interface for all pressures. Its volume decreased and its structure deteriorated as the pressure increased. At 2000 psia it only occurred in sections separated by binder melt flow.

There was no change in the oxidizer surface when any of the four catalysts were loaded in the binder alone. The extent of the binder melt was nevertheless reduced for all samples.

CHAPTER V

ELECTRON MICROPROBE EXPLORATORY STUDIES

An electron probe x-ray microanalysis has been performed on two pairs of samples. Both burned and unburned samples of pure AP and AP with two percent iron blue were examined. The analysis was performed in the Physical Sciences Division of the Engineering Experiment Station, Georgia Institute of Technology using an Acton Laboratories Electron Probe X-ray Microanalyzer, Model MS-64. This analyzer is equipped with a light element detection system. It is possible to detect elements from boron, atomic number 5, to uranium, atomic number 92. This system cannot detect the four lightest elements, hydrogen, helium, lithium and beryllium.

The electron probe x-ray microanalyzer is an instrument used for x-ray spectrochemical analysis of surfaces between 0.5 to 200 μm diameter on the surface of a solid specimen. The instrument consists of three basic components, an electron beam similar to the SEM, an x-ray optical system with a suitable detector, and an optical microscope to select the area to be analyzed. The x-ray optical system is arranged to accept x-rays with an effective emergent angle of 18 degrees from the specimen surface for all wavelengths. The optical microscope has a resolution of better than one μm with a magnification of 400x.

An electron beam size of 100 μm was used to investigate the oxidizer samples. This beam size was chosen to minimize damage to the surface

by the electron beam. This would not have been as serious a problem if the sample were an electrical conductor. For a nonconductor, the electrons remain near the irradiation site and create a negative charge which causes the beam to jump back and forth at random on the surface. This is accompanied by sparking which rapidly deteriorates the sample surface. This type of damage was noted for all samples.

The electron micrographs of Chapter IV were obtained by observing the secondary or backscattered electrons emitted by the sample as the electron beam of .01 μm diameter scanned the sample. These electrons are prevented from reaching the x-ray detector by an electron trap consisting of a permanent magnet with a special pole piece designed to deflect any electrons out of the x-ray path before they can enter the spectrometer chamber. These electrons cause a high background noise level if they reach the x-ray detector.

The analyzing electronics of the electron probe result in a strip chart record of the x-ray spectrum of the sample. These are shown in Figures 19 and 20. The ordinate of the spectrum is the variation in intensity of the x-rays, as obtained from a linear ratemeter which displays a signal that has been processed by a pulse-height analyzer system. The abscissa of the trace is the distance from the mica crystal to the sample. The known identification spectra for this microprobe are tabulated in this dimension, which can be converted directly to wavelength by the equation

$$\lambda(\text{Å}) = 0.3978\ L(\text{mm})$$

The pure AP sample spectra are shown in Figure 19. The unburned sample exhibited more damage due to the electron beam than the other three

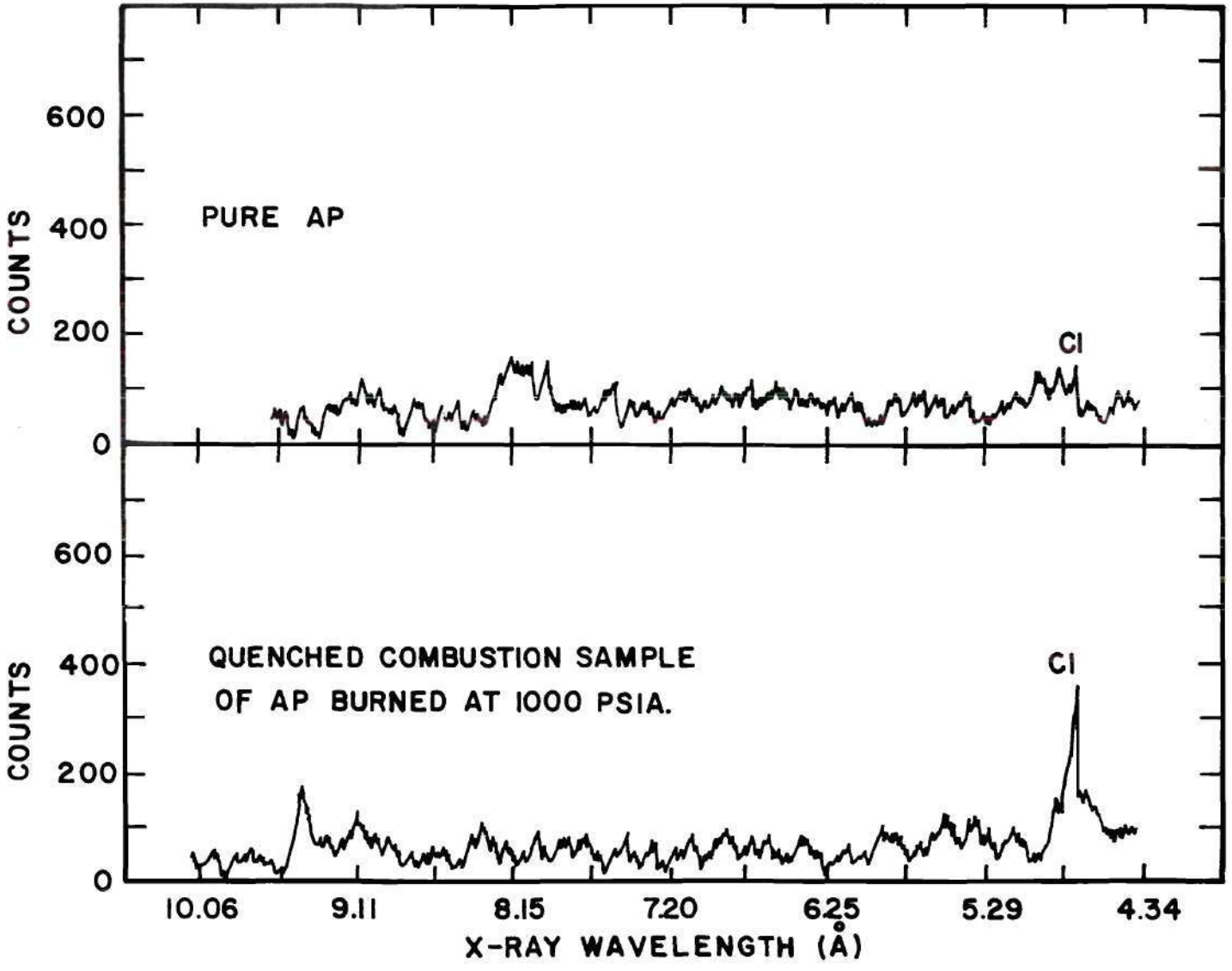

Figure 19. X-ray Spectra from Ammonium Perchlorate Samples

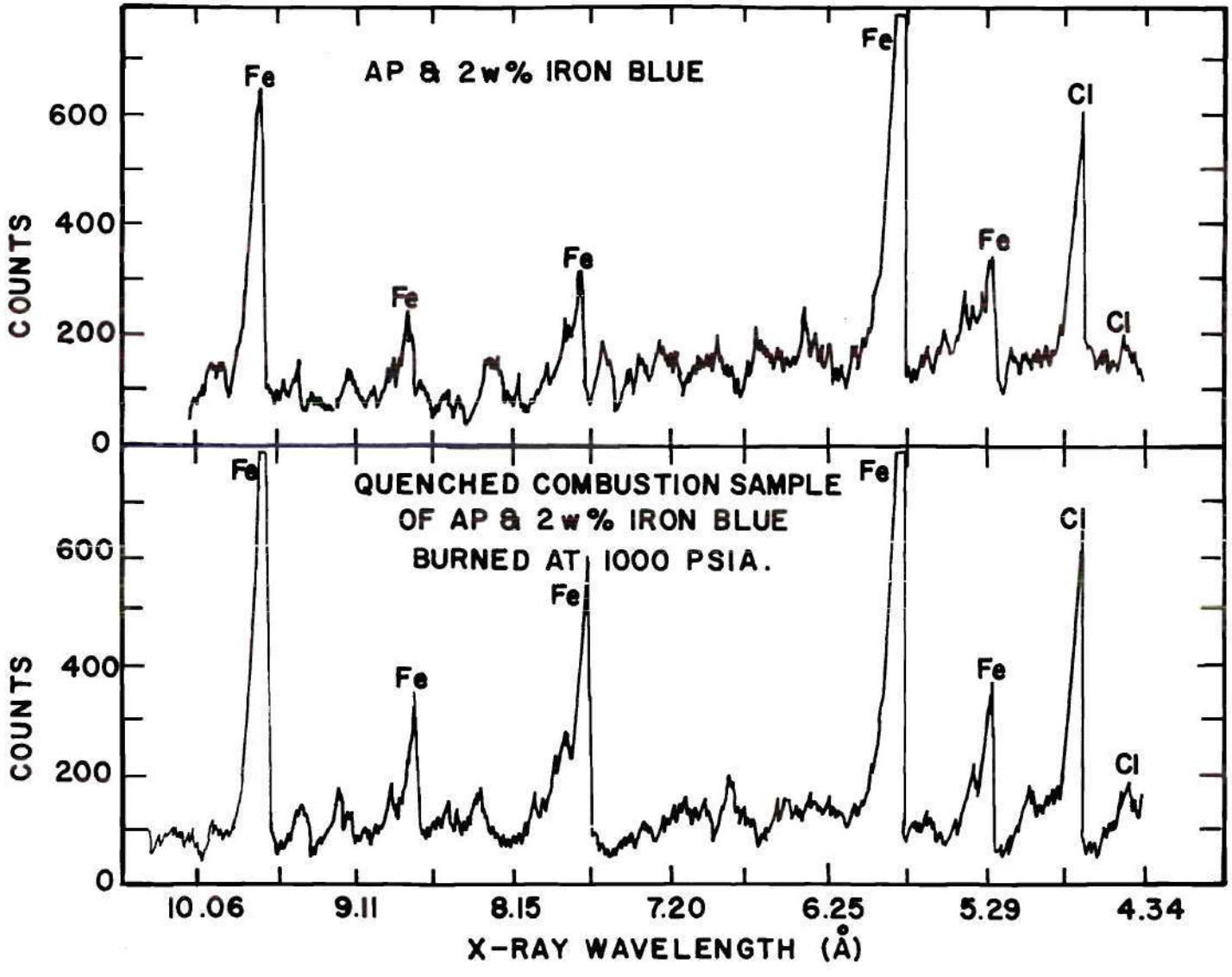

Figure 20. X-ray Spectra from AP and 2 w% Iron Blue Samples

samples. No dominant chlorine peak was detected by the strip chart, but a direct reading of the pulse height analyzer output before beam damage was appreciable showed equal counts for chlorine for both the burned and unburned samples. A small amount of carbon was indicated in the burned sample. The amount was just above the limit of detectability. A slightly higher indication of oxygen was obtained.

The AP with two percent iron blue sample spectra are shown in Figure 20. The beam damaged these samples also. Quick counts were again taken to obtain a quantitative measure of the iron present in the samples. The unburned sample indicated a count equivalent to 3.06 weight percent of a pure iron sample, while the burned sample showed a decrease to 2.60 weight percent. This assumes the iron standard and the iron in the sample are in the same chemical state. This is not true for these samples. The iron in the unburned sample was in the chemical compound, ferric oxide. The pure iron sample was the pure element, Fe. The iron in the burned sample was combined in an unknown chemical compound. The chemical composition of the burned sample was the objective of the microprobe studies. There was an indication of sulfur present on the unburned sample but it was not present on the burned sample. The difference between the quick counts and the intensity of iron x-rays can be attributed to beam damage of the sample.

The results of the microprobe analysis were disappointing. A long delay was encountered in the analysis time due to equipment changes which had to be made with the light element detection system. It was felt that this time delay would result in quantitative measurements of relative concentrations of carbon, iron, nitrogen and oxygen. It is necessary to

use a special vacuum path with a 500 Å collodion window to isolate the detector from the sample for elements below an atomic number of 11. Since the only source of carbon and iron would be the iron blue with the chemical formula, $Fe(NH_4)Fe(CN)_6$, and the only source of oxygen and chlorine would be the ammonium perchlorate, NH_4ClO_4, it was expected that a detailed quantitative chemical analysis of the surface layer of a burned and unburned sample would yield sufficient information to postulate the suitable chemical reactions which had taken place near the oxidizer surface. In some cases concentrations of one part in 10^5 have been reported by this type of microprobe analysis.

As can be seen from Figures 19 and 20 along with the discussion, this was not possible. Because of the extremely long delay in analysis of these samples, a new series of tests was not formulated. It may have been possible to obtain suitable results without sample damage, if the electrically nonconducting samples had been coated as for the scanning electron microscope observations. No sample damage was detected during those observations with a much smaller, more intense beam, i.e., .01 μm as compared to 100 μm in diameter. The quick counts obtained at fixed detector locations would yield more accuracy than the entire spectrum scans. The fixed detector locations would be at known crystal distances for detection of x-ray radiation from specific elements. Further measurements would not be useful unless the light elements (below atomic number 12) could be detected with more accuracy.

CHAPTER VI

SYNERGISTIC EFFECTS IN SOLID PROPELLANTS

Two-Dimensional Composite Solid Propellants

Two-dimensional composite solid propellant sandwiches were used to investigate the optimum location and the extent of the catalytic action of four possible burn rate modifiers in Chapter IV. Both the location and the compounds were varied independently. As a subsequent exploratory test it was determined that if one catalyst was added to the oxidizer prior to compaction of the disk and another effective catalyst was added to the binder, there was a net increase of the burn rate over that of the sum of the independent actions of the catalysts. This combined effect is denoted as a synergistic effect on the burn rate. The results of a systematic investigation of this positive synergism for all combinations of the same four catalysts are presented here.

The two-dimensional composite solid propellant sandwiches were prepared by the method outlined in Chapter II. The samples were prepared with constant volumetric loading of the catalysts based on an addition of two weight percent of the catalyst to the oxidizer. This required the addition of 4.37 percent of the catalyst to the HTPB. The samples prepared with this constant volumetric loading in the oxidizer and binder are referred to as uniformly loaded sandwiches. The samples for this phase of the investigation were prepared using ultra-pure ammonium perchlorate supplied by Boggs. The sandwich vertical burn rate and burn rate

normal to the oxidizer surface as defined in Chapter II and calculated in Appendix D were obtained for all samples prepared for this phase of the investigation. The uniformly loaded catalyst sample was expected to burn at a rate similar to the oxidizer loaded samples of Chapter II (Figure 4) since the binder loaded samples (Figure 6) showed very little catalysis of sample burn rates. Initially all combinations of the four catalysts were tested at 600 psia. The ferrocene samples were dropped from future tests. Harshaw catalyst Cu 0202 P, ferric oxide, and iron blue samples were tested over the 300 to 2000 psia pressure range to provide subsequent comparison test results to evaluate combinations of these catalysts.

The sample burn rates for uniformly loaded sandwiches with Harshaw catalyst Cu 0202 P are shown in Figure 21. Both the sandwich vertical burn rate and the burn rate normal to the oxidizer surface have been normalized by dividing by the sandwich vertical burn rate of AP-HTPB sandwiches prepared from the same lot of ultra-pure (99.99 percent) AP. These AP-HTPB sandwich vertical burn rates were plotted in Figure 5. The burn rates for the oxidizer, binder, and binder-oxidizer interface loading are also shown in Figure 21. These burn rates were normalized by dividing by the sandwich vertical burn rate of AP-HTPB sandwiches prepared from the same lot of AP. These burn rate ratios were plotted in Figures 4, 6, and 7 along with the burn rate ratios for the other three catalysts. The AP for these samples was obtained from the Fischer Scientific Co. and was found by chemical analysis to have a .03 weight percent potassium ion impurity.[15] The sandwich vertical burn rates for these impure AP-HTPB sandwiches were

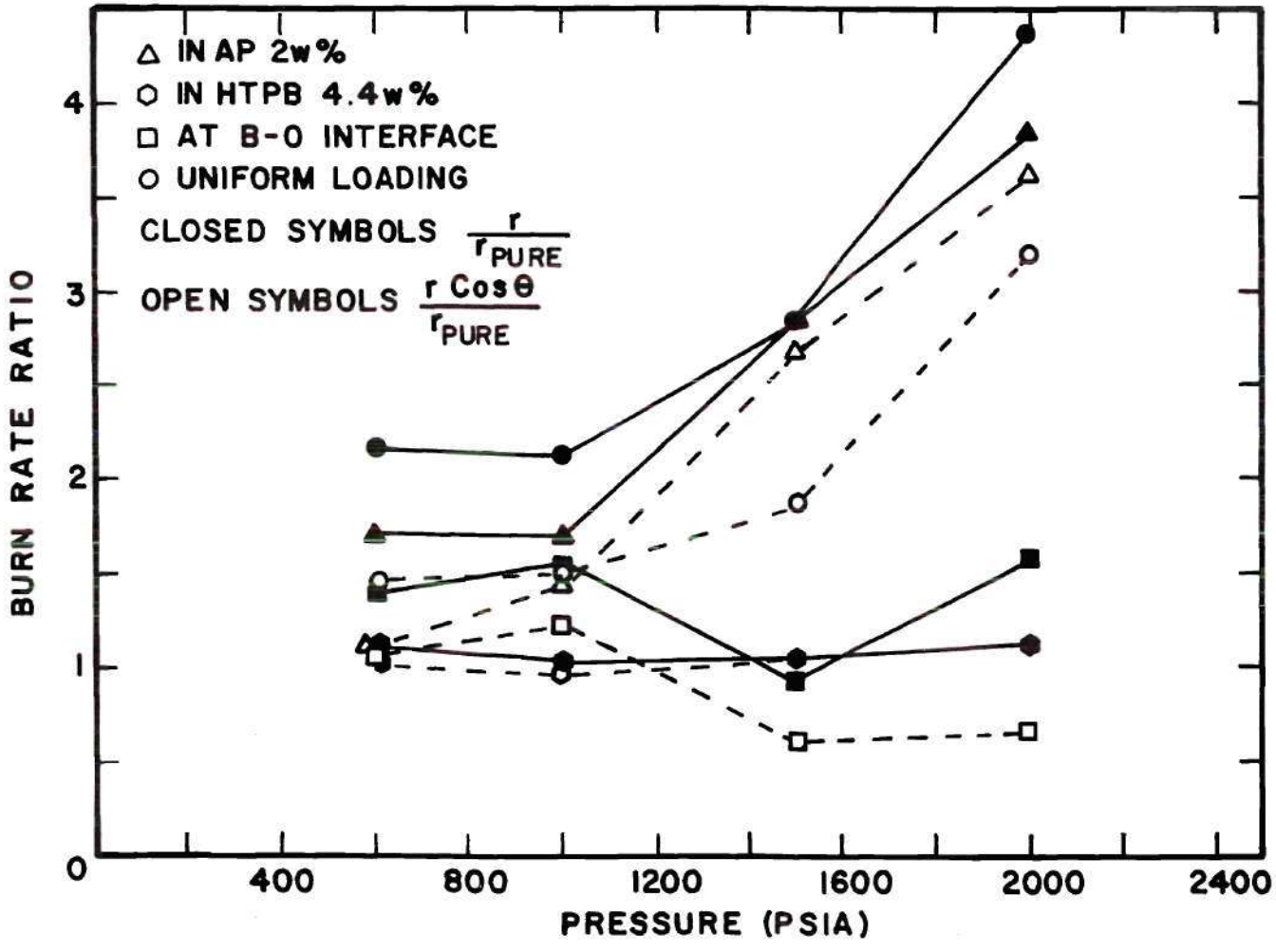

Figure 21. Harshaw Catalyst Cu 0202 P Added to 2-D Sandwiches

also plotted in Figure 5. The burn rates for the impure AP-HTPB samples were from 8 to 28 percent higher than the ultra-pure AP-HTPB burn rates. It must be noted that the amount of catalyst present at the interface is not comparable to either that in the binder or oxidizer. It was painted on with a methyl alcohol solution.

The uniformly loaded sample had a higher sandwich vertical burn rate than the three other types of catalyst loading. It was more effective than would be expected from consideration of separate binder and oxidizer loaded samples.

The normal burn rate of the oxidizer should not be affected when the catalyst is loaded at the binder-oxidizer interface or in the binder. This is shown to a degree by the two lower dashed lines. The burn rate normal to the oxidizer surface for the uniformly loaded sample was considerably less than the oxidizer loaded sample for 1500 and 2000 psia. This increased separation of the sandwich and normal burn rates indicated an increase of the catalysis of the binder-oxidizer reactions for the uniformly loaded sample over the oxidizer loaded sample. This trend is meaningful and related to the catalysis of the gas flame. That is why the effects are larger at low pressures where the kinetics are relatively more important.

The sample burn rates for uniformly loaded sandwiches with ferric oxide are shown in Figure 22 along with the binder, oxidizer and binder-oxidizer interface loaded results. All burn rates have been normalized by dividing by the sandwich vertical burn rates of AP-HTPB sandwiches of the same purity. It must be noted that the amount of catalyst present at the

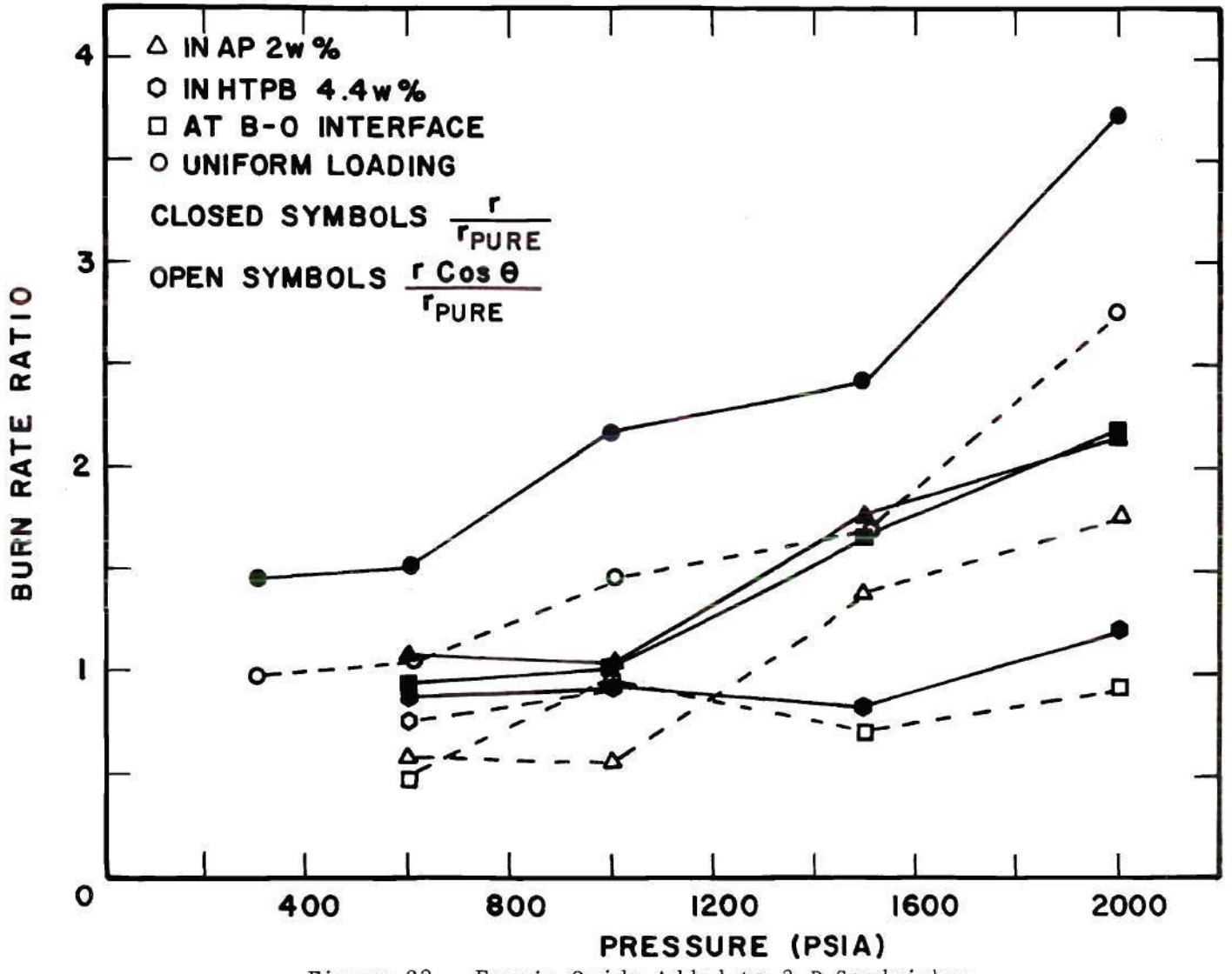

Figure 22. Ferric Oxide Added to 2-D Sandwiches

interface is not comparable to either that in the binder or oxidizer. It was painted on with a methyl alcohol solution. It was still as effective as the oxidizer loading in catalyzing the sandwich vertical burn rate, and had very little effect in catalyzing the normal oxidizer burn rate. There is relatively good agreement between these normal burn rates for the binder and interface loaded samples. They are much closer than for the uniform and oxidizer loaded samples, which should agree if the catalyzed binder products do not migrate over the oxidizer surface.

The uniformly loaded sample had both a higher sandwich vertical burn rate and burn rate normal to the oxidizer surface than the other three types of catalyst addition. The effect could not be expected by considering combining the burn rate augmentation of the separate binder and oxidizer loaded samples. The separation of these two burn rates is greater than all other samples except the binder-oxidizer interface samples at 1500 and 2000 psia.

The sample burn rates for uniformly loaded sandwiches with iron blue are shown in Figure 23 along with the binder, oxidizer, and binder-oxidizer loaded results. All burn rates have been normalized by dividing by the sandwich vertical burn rate of AP-HTPB sandwiches of the same purity. The amount of catalyst present at the interface is the same as that loaded in the oxidizer. It is much more effective at the interface than when loaded in the oxidizer, but not as effective as when loaded uniformly. This uniform loading was more effective for all three catalysts in increasing the sandwich vertical burn rate. There was no agreement between the normal oxidizer burn rate for the uniform and oxidizer loaded samples.

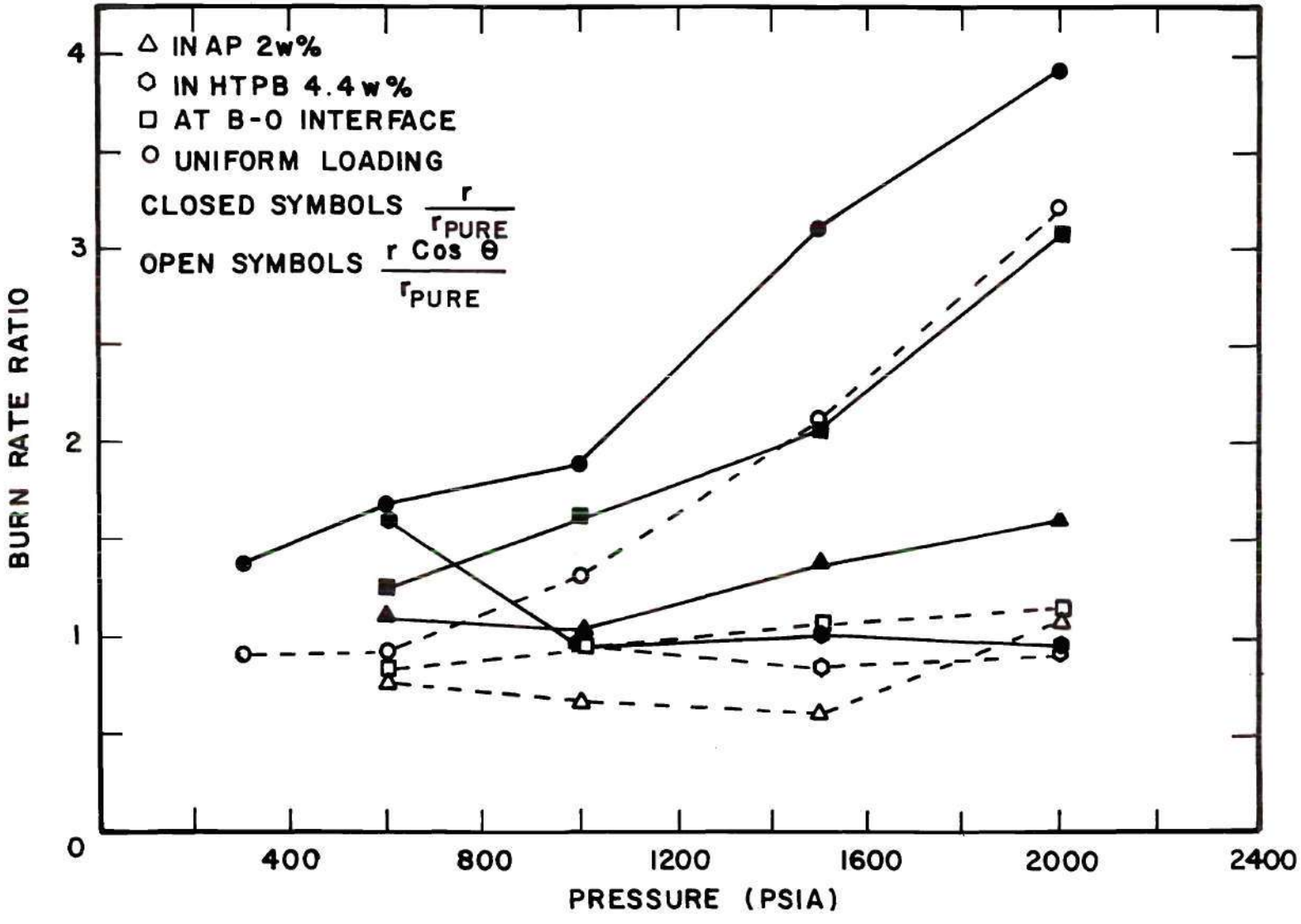

Figure 23. Iron Blue Added to 2-D Sandwiches

Again this would indicate an acceleration of the burn rate due to a reaction of catalyzed binder products with catalyzed AP products, which is deemed impossible. There was good agreement for the oxidizer normal burn rate for the interface and binder loaded samples.

The uniformly loaded sample had both a higher sandwich vertical burn rate and burn rate normal to the oxidizer surface for all three catalysts than the other three types of catalyst addition. This effect could not be expected by considering combining the burn rate augmentation of the separate binder and oxidizer loaded samples. The separation of these two burn rates is again greater than all other samples except the binder-oxidizer interface samples at 1500 and 2000 psia.

Combinations of Catalysts

When two catalysts were uniformly loaded in the two-dimensional composite solid propellant sandwiches, the constant volumetric loading was maintained. One weight percent of one and one weight percent of the other was added to the AP prior to grinding and pressing. For the HTPB, 2.2 weight percent of one and 2.2 weight percent of the other were added prior to curing the binder. All possible combinations of the four catalysts were compared with the uniformly loaded samples with only one catalyst present. The tabulated results are shown in Table 5.

In order to evaluate the existence of a synergistic effect on sample burn rate the following definitions are given. A "positive" synergistic effect or burn rate is obtained when the burn rate of the sample with two catalysts present exceeds the burn rates of both of the corresponding samples with only one catalyst present. A "possible" synergistic effect

Table 5. Burn Rates for Determination of Synergistic Effects for Sandwiches at 600 psia

Catalyst	r/r_{pure}		$r\cos\theta/r_{pure}$	
None	1		1	
Harshaw Catalyst Cu 0202 P (CC)	2.3		1.5	
Ferric Oxide (10)	1.5		1.0	
Iron Blue (IB)	1.7		.91	
Ferrocene (F)	1.4	synergistic	.68	synergistic
CC & 10	2.5	positive	1.6	positive
CC & IB	2.3	possible	2.1	positive
CC & F	2.0	possible	1.3	possible
10 & IB	2.3	positive	1.1	positive
10 & F	2	positive	1.6	positive
IB & F	1.8	positive	1.4	positive

on burn rate is obtained when the burn rate of the sample with two catalysts present is between the burn rates of the corresponding samples with only one catalyst present. A "negative" synergistic effect on burn rate is obtained when the burn rate of the sample with two catalysts present is less than the burn rates of both of the corresponding samples with only one catalyst present.

All combinations of these four catalysts, Harshaw catalyst Cu 0202 P, ferric oxide, iron blue, and ferrocene gave at least an indication of a possible catalysis of the sample burn rates. Only two combinations, Harshaw catalyst with iron blue and with ferrocene, did not give a positive synergistic effect on both sample burn rates. Neither ferric oxide, iron blue, or ferrocene augmented the burn rate normal to the oxidizer surface when used alone at 600 psia. All three combinations of these catalysts exhibited positive synergistic effects on both burn rates.

The maximum sandwich vertical burn rate, .54 inch/sec, was obtained for the combination of Harshaw catalyst and ferric oxide. The largest synergistic effect, burn rate change as compared to both catalysts used alone, for the sandwich vertical burn was obtained for the ferric oxide and iron blue system. This burn rate was .51 inch/sec as compared to .33 inch/sec for ferric oxide alone and .37 inch/sec for iron blue alone.

Considering these screening results, the Harshaw catalyst Cu 0202 P--ferric oxide and the iron blue--ferric oxide systems were chosen for testing over the 300 to 2000 psia pressure range. The results for the Harshaw catalyst Cu 0202 P--ferric oxide system tests are shown in Figure 24. The maximum effect is at 1500 psia. Both catalysts were almost equally

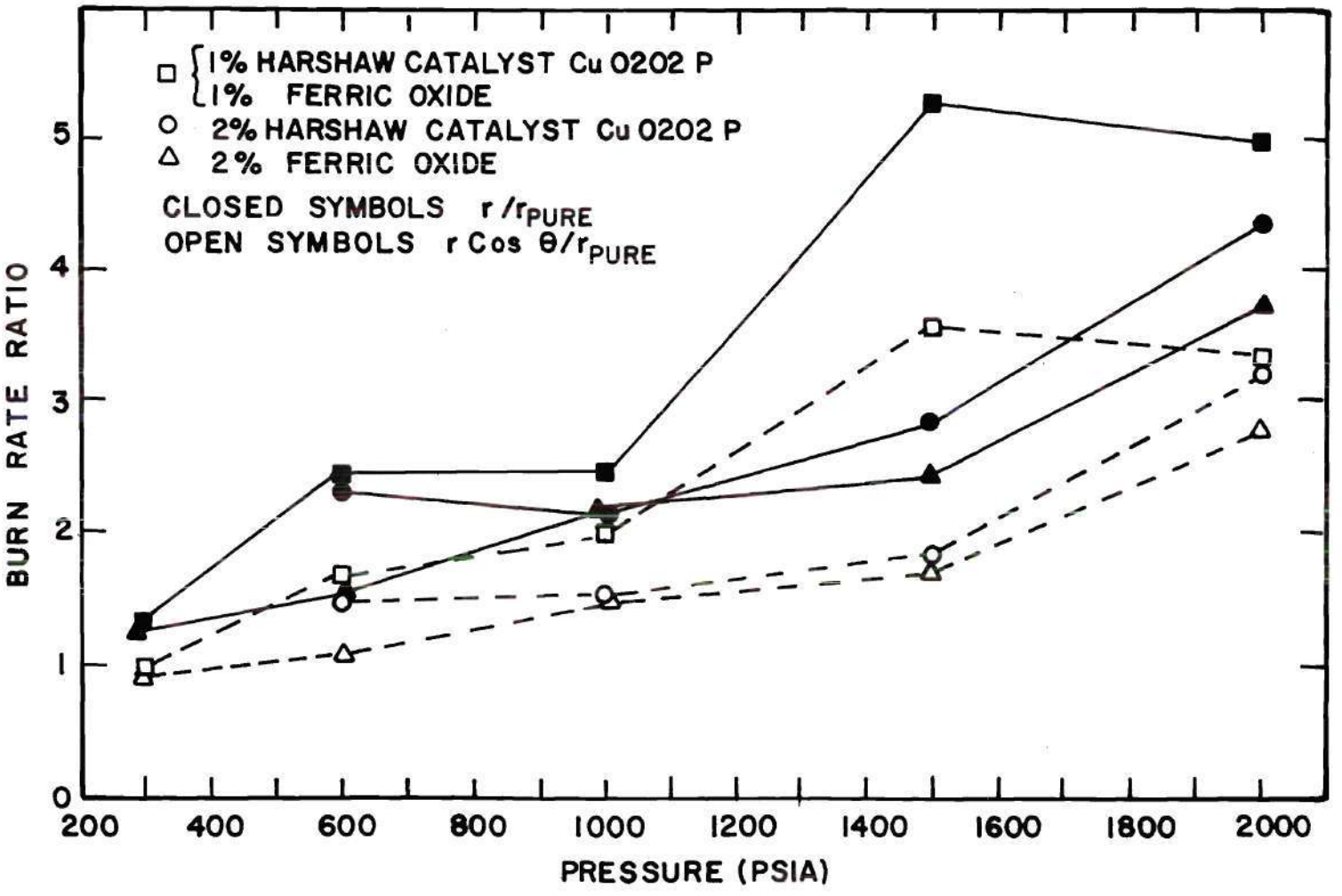

Figure 24. Burn Rate Ratio for Harshaw Catalyst Cu 0202 P and Ferric Oxide

effective in catalyzing the burn rate when used alone. When half of one catalyst was replaced by the same amount of the second catalyst the burn rate doubled. The sandwich vertical burn rate and the burn rate normal to the oxidizer surface both exhibited positive synergism over the 600 to 2000 psia pressure range.

The results for the iron blue--ferric oxide system were not as consistent. They are shown in Figure 25. The maximum positive synergistic effect occurs at 600 psia. There was only a possible synergistic effect indicated at 1000 and 1500 psia. Since the burn rate of the combined catalyst sample is closer to the slower burning single catalyst sample for both 1000 and 1500 psia, this possible synergistic effect is very weak. A negative effect was not obtained at any pressure. The burn rate normal to the oxidizer surface for the combined catalyst loading has followed the single catalyst data for ferric oxide.

The separation of the dashed and the solid curves in Figures 24 and 25 was representative of the amount of catalytic activity taking place on the binder-oxidizer reactions. For the Harshaw catalyst Cu 0202 P--ferric oxide system this separation is greatest at 1500 and 2000 psia when the positive synergistic effect on sandwich vertical burn rate is greatest. For the iron blue--ferric oxide system this separation is greatest at 600 and 2000 psia where the positive synergistic effect on sandwich vertical burn rate exists.

Cast Composite Propellants

Fuse Wire Measurements

2.41 Percent Catalyst. Based on the results of the two-dimensional

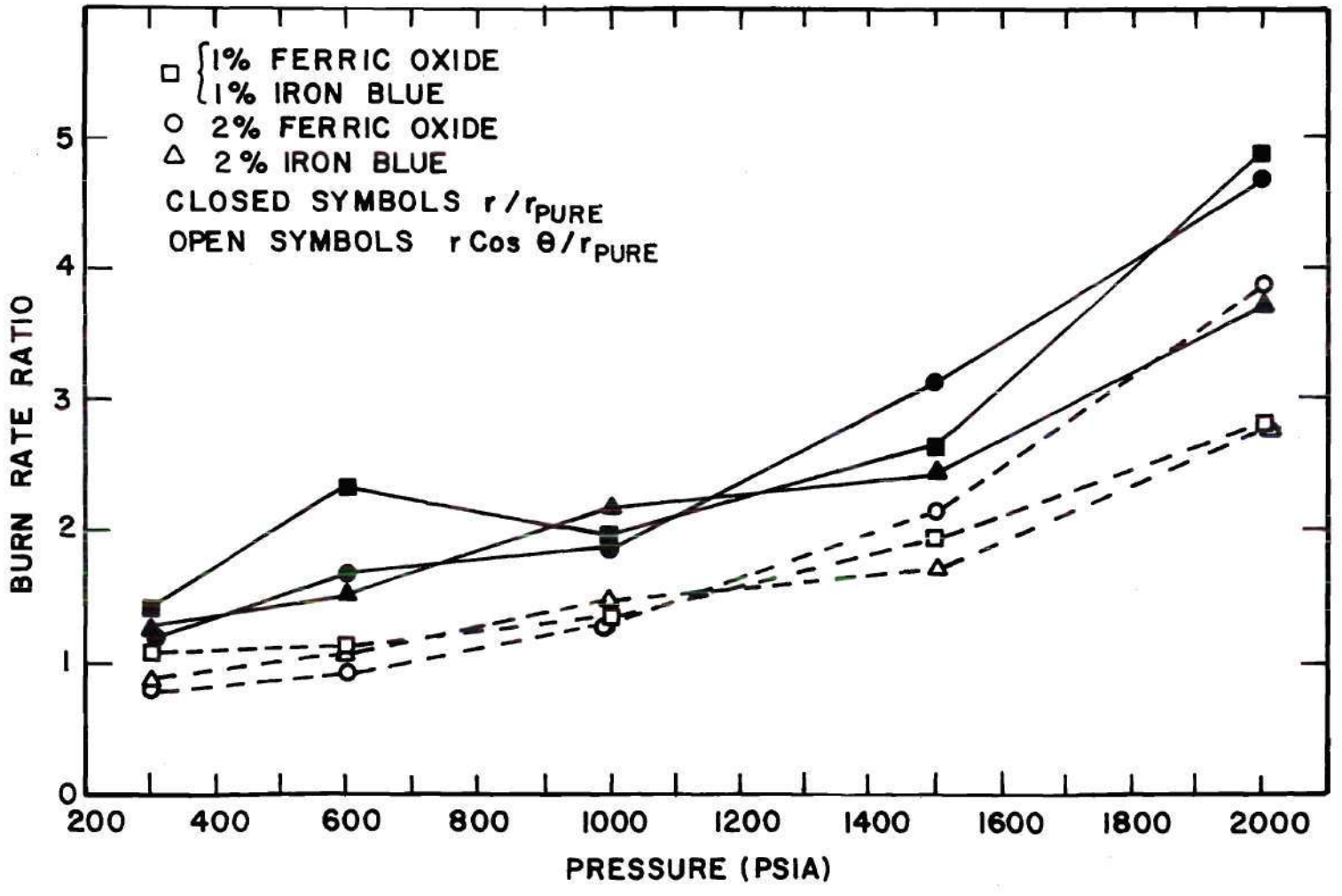

Figure 25. Burn Rate Ratio for Iron Blue and Ferric Oxide

sandwich tests of possible synergistic effects, it was decided to investigate both the Harshaw catalyst Cu 0202 P--ferric oxide and iron blue--ferric oxide systems in real, three-dimensional cast propellants.

Maintaining the same volumetric loading of catalysts as for the two-dimensional sandwiches, three-dimensional cast composite solid propellant strands were prepared to see if this synergistic effect would be carried over to the real cast propellant. These strands were prepared from a common lot of uncured composite propellant, following the procedure outlined in Appendix B. An 82.7 percent solids to 17.3 percent binder loading was used with a bimodal ammonium perchlorate particle distribution of:

$$180\ \mu m < 70\% < 212\ \mu m$$

$$37\ \mu m < 30\% < 45\ \mu m$$

for the oxidizer. Hydroxyl terminated polybutadiene was used as the binder. Burn rate data were available for this uncatalyzed propellant.[28] It was similar to propellant number 78 in the Princeton University test series. The catalyst was added to the uncured propellant at a weight percent of 2.41. This would give the same equivalent total volumetric loading in the cast propellant as in the uniformly loaded sandwiches. All of the catalyst is suspended in the binder matrix. Since the binder only constitutes 17 percent of the total sample weight, then the binder actually contains the equivalent of 14.2 weight percent catalyst loading.

The uncured propellant was cast in Teflon strand molds. All samples were cured for the same length of time. The strand size was .25 inch by .25 inch by 1.7 inches long. The burn rates were obtained by a fuse wire

technique[28] using seven, half ampere wires (approximately .010 inch in diameter). These wires were inserted in predrilled holes which were spaced .2 inch apart. Each fuse wire was connected in series to a 10 K Ω resistor. These seven resistors were connected in parallel with a 57 K Ω resistor across an 18 volt battery power supply. As each fuse wire burns through the equivalent resistance increases and the voltage is recorded on an oscillograph.

The strand with fuse wires is shown in Figure 26. It is mounted on the base of the combustion bomb. A sufficient nitrogen flow is passed over the sample to prevent recirculation of the hot gases that can cause premature melting of the fuse wires. This nitrogen flow was varied from .7 to 1.4 ft/sec. There was less variation in the time between fuse wire burn through when the higher flow velocity was used.

Sample oscillograph traces are shown in Figure 27 for a cast propellant with no catalyst present and with 2.41 weight percent ferric oxide present. These samples were burned at 600 psia. There were variations of the initial ignition time delay along with the time difference between the burn through of the first and second fuse wires. The next five time intervals were more consistent. Because of this, the burn rate was determined over one inch of the sample. The voltage change as each fuse wire melted was not uniform, because all resistors in series with each fuse wire were the same resistance value.

Considering the two-dimensional sandwich screening results, the same two combinations of catalysts, Harshaw catalyst Cu 0202 P--ferric oxide, and iron blue--ferric oxide, were chosen for testing in the cast

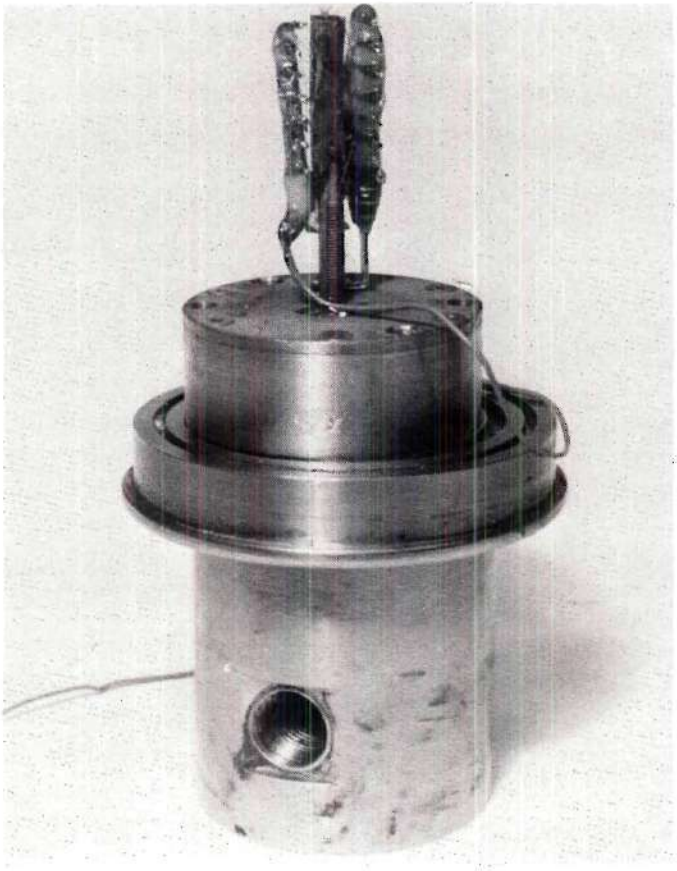

Figure 26. A Strand with Seven Fuse Wires Mounted on the Combustion Bomb Base

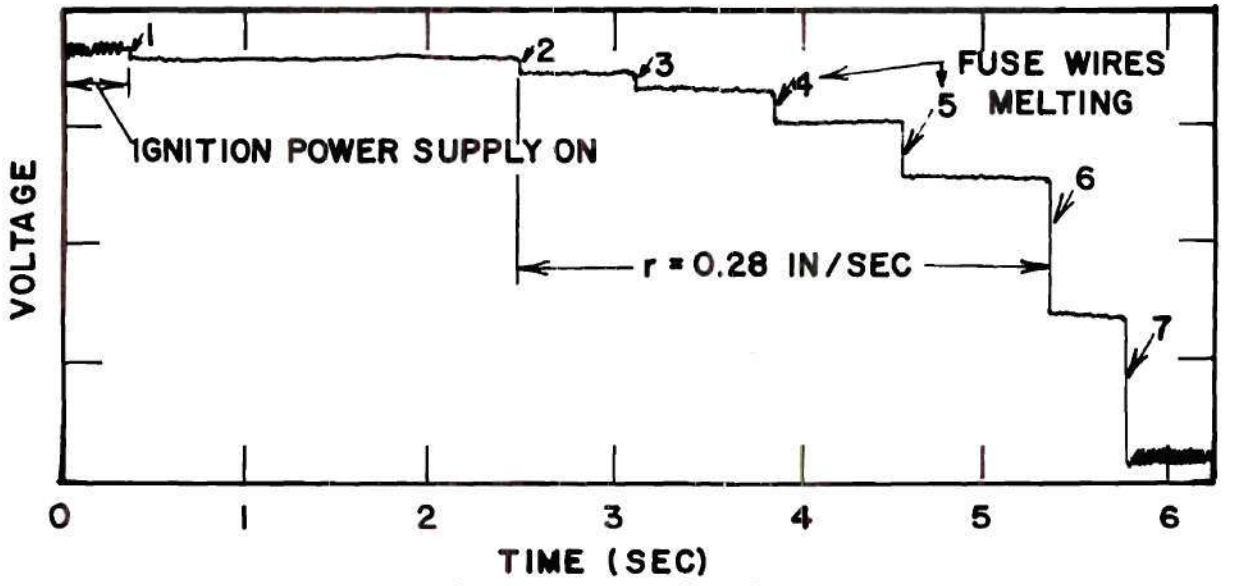

a) AP-HTPB No Catalyst

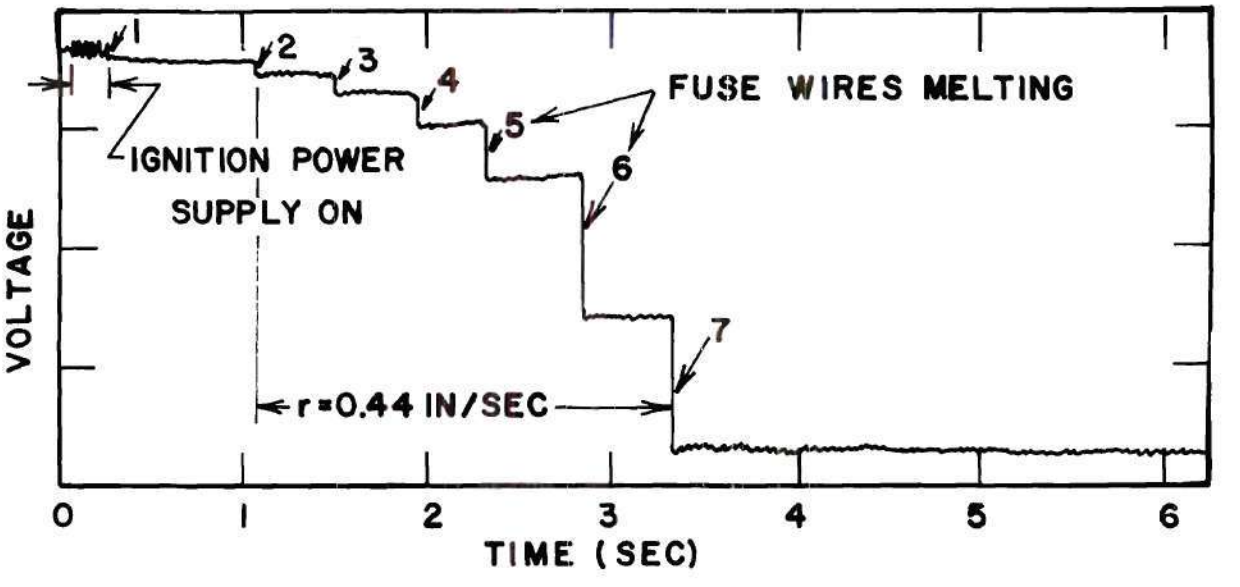

b) AP-HTPB with 2.41 w% Ferric Oxide

Figure 27. Oscillograph Records for Two Strands

composite propellant strands. These strands of combinations of two catalysts and the samples with only one catalyst were burned at 600 psia. The resultant burn rates and their ratio with the uncatalyzed propellant strand burn rate are tabulated in Table 6. A total of 25 tests were necessary to obtain these data. Six tests produced no results. Five tests yielded exceedingly high burn rates that could not be duplicated. The average burn rates of the 14 remaining tests are given in Table 6. Each test resulted in a series of up to six burn rates as each fuse wire burns through. A large amount of data scatter and uncertainty was obtained from these tests. Initially they were proposed to reduce the cost per test and speed the data reduction over that of the cinephotomacrography tests. This was not achieved.

The burn rate augmentation for the combinations of catalysts was not as great as that obtained for the two-dimensional sandwiches in Table 5. The burn rate of the uncatalyzed strands agree with the Princeton data.[28] The sample burn rate of the ferric oxide--iron blue systems indicated a possible synergistic effect. That is, the burn rate of the sample with two catalysts present was between the burn rates of the single catalyst sample. The Harshaw catalyst Cu 0202 P--ferric oxide system had a negative synergistic effect on sample burn rate. That is, the burn rate of the sample with two catalysts present was less than the burn rates of both single catalyst samples.

The structural strength and elasticity of the samples containing Harshaw catalyst Cu 0202 P and iron blue were considerably different from the ferric oxide and pure samples. This may be due to the high equivalent

Table 6. Burn Rates for Cast Composite Propellant Strands with 2.41% Catalyst Addition at 600 psia

Catalyst	r (in/sec)	r/r_p	
None	.28	1.0	
Harshaw Catalyst Cu 0202 P (CC)	.50	1.8	
Ferric Oxide (IO)	.44	1.6	
Iron Blue (IB)	.36	1.3	synergistic
CC & IO	.41	1.5	negative
IO & IB	.43	1.5	possible

loading of catalyst in the binder (14.2 weight percent) for the 2.41 percent overall propellant loading. This could effect the curing properties of the binder. The ferric oxide and uncatalyzed samples were softer and more easily removed from the mold while the samples containing iron blue and Harshaw catalyst Cu 0202 P were brittle and exhibited very rapid burning in several tests. These tests were not considered in the preparation of the results of Table 6 because they could not be duplicated.

Exploratory Tests at One Weight Percent Catalyst Loading

In order to investigate the possibility that the catalyst loading concentration was too high, a new set of samples were prepared using a reduced concentration of one weight percent of catalyst addition. This was not equivalent to the overall uniformly loaded two-dimensional sandwich concentration but it reduced the effective binder concentration to 5.9 weight percent for the cast propellant.

Fuse Wire Tests. Two separate batches of AP and HTPB were prepared for the initial tests of the addition of one weight percent catalyst to the uncured propellant. The ratio of 82.7 percent solids (AP) to 17.3 percent binder (HTPB) was maintained consistent with the earlier tests. The oxidizer particle distribution was maintained at

$$180\ \mu m < 70\% < 212\ \mu m$$

$$37\ \mu m < 30\% < 45\ \mu m$$

Freon TF was mixed with the first batch of propellant. This decreased the viscosity of the mixture and allowed the propellant to be packed much easier in the teflon strand molds. The Freon TF could be removed by vaporization at room temperature or by vacuum in the curing oven. The samples did not have sufficient mass to fill the voids as the freon

vaporized. This yielded porous cast propellants. The second batch of propellant was prepared from oxidizer particles that were premixed. That is the fine and course AP was mixed before the binder and catalyst were added. This propellant was very difficult to mix and pack in the teflon molds. The resultant samples resembled the first batch of samples. They were porous with a grainy appearance.

Thirteen fuse wire tests were conducted using samples from these two batches of propellants. Several variations of sample preparation were used. Different modes of inhibition were tried on the sides of the samples. Coatings of PVC, vacuum grease, and epoxy were used along with water leaching of surface AP and increased inhibiting nitrogen flows. The results for all samples were the same. All wires appeared to break simultaneously Both batches of propellant behaved similarly. This had not been encountered with the 2.41 weight percent catalytic samples. There had been fluctuations of burn rates but not consistently high burn rates as indicated by these samples.

High speed motion pictures were taken of four samples. Based on a frame rate of 1600 frames per second, the pure AP-HTPB sample and the one percent Harshaw catalyst Cu 0202 P sample exploded and burned in .015 second (24 frames). The one percent ferric oxide sample was completely consumed in .009 second (14 frames). The one percent ferric oxide--iron blue sample lasted for .022 second (36 frames).

It is believed that during manufacturing too exact an AP particle size distribution was being employed, preventing binder wetting and good packing. It was decided to broaden the particle size distribution. Based

on the length of time that was necessary to prepare fuse wire samples and the possible areas of uncertainty when the sample burns rapidly, it was decided to return to the cinephotomacrography for determination of sample burn rate and uniformity of burn rate. Poor quality propellant samples can be determined immediately from viewing the motion pictures.

Cinephotomacrography. The samples for these tests were prepared from common lots of uncured propellant. The solids to binder ratio was maintained at 82.7 percent to 17.3 percent. The bimodal AP particle distribution was broadened to

$$\left.\begin{array}{l} 180\ \mu m < 35\% < 212\ \mu m \\ 125\ \mu m < 35\% < 180\ \mu m \end{array}\right\} 125\ \mu m < 70\% < 212\ \mu m$$

$$45\ \mu m < 10\% < 63\ \mu m$$

$$\left.\begin{array}{l} 37\ \mu m < 10\% < 45\ \mu m \\ 10\% < 37\ \mu m \end{array}\right\} 30\% < 63\ \mu m$$

The propellant was mixed following the procedure outlined in Appendix B. When all of the fine AP was mixed in with the rest of the AP and binder, the propellant was divided for catalyst addition. A minimum of 10 grams of propellant was needed for each catalyzed sample. The proper amount of catalyst was added to portion of propellant and the mixing process repeated. This propellant was cast in 22 mm by 22 mm embedding molds and cured for seven days at 60°C.

The physical properties and appearance of the cured propellant was improved by the increased mixing time of the propellant and the broadened AP particle distribution. All of the oxidizer appeared to be wetted with binder.

The cured propellant was cut into 4 by 6 by 19 mm sample sizes for testing in the combustion vessel designed by Varney[1] and Jones.[2] These samples were similar in size to the two-dimensional sandwiches tested previously. This allowed the same cinephotomacrographic techniques to be used to observe the burning samples. The same nitrogen flows that were determined experimentally for the sandwiches were used for smoke control. The latent image magnification was reduced to slightly less than 1:1 (image: actual). The motion picture speed was maintained at 1600 frames per second. The sample was oriented on the sample holder to allow observation of two sides of the sample. This indicated the uniformity of the burn and any effect of the light source on burn rate.

The sample burn rates and their uniformity were determined by recording sample profiles at 100 frame intervals by tracing the projected burning surface. These could be used to determine a burn rate every .0625 second. A sample burn rate data reduction calculation is given in Appendix D.

The same combination of catalysts, Harshaw catalyst Cu 0202 P--ferric oxide and iron blue--ferric oxide, that were found to exhibit positive synergistic effects on sandwich vertical burn rate were tested at one weight percent addition to cast propellants. These two combinations of catalysts were determined by the two-dimensional screening experiment and were tested at 2.41 weight percent catalyst addition at 600 psia in the above mentioned fuse wire tests. The results were shown in Table 6.

Initially six samples with the one weight percent of catalyst addition were tested at 600 psia. These results are tabulated in Table 7.

Table 7. Burn Rate for Determination of Synergistic Effects for 1w% Catalyst Addition to Cast Propellant

Catalyst	Burn Rate					
	600 psia			2000 psia		
	r	r/r_p		r	r/r_p	
None	.34	1		.66	1	
Harshaw Catalyst Cu 0202 P (CC)	.51	1.50		.74	1.12	
Ferric Oxide (IO)	.45	1.32		.83	1.26	
Iron Blue (IB)	.54	1.59		.78	1.18	
			synergistic			synergistic
CC & IO	.48	1.41	possible	.80	1.21	possible
IO & IB	.54	1.59	possible	.88	1.33	positive

No positive synergistic effect was indicated, but both combinations of catalysts did indicate a possible synergistic effect. Because of this further testing was conducted at 2000 psia. These results are also tabulated in Table 7. There was a positive synergistic effect on sample burn rate for the ferric oxide--iron blue system at 2000 psia. Because of this positive result, it was decided to test this combination of catalysts over the 300 to 2000 psia pressure range. The double catalyst samples, single catalyst samples, and uncatalyzed samples were burned at all pressures. The results are shown in Figure 28. There was a positive synergistic effect on sample burn rate at 300 and 2000 psia, a possible synergistic effect at 600 psia and a negative effect at 1000 and 1500 psia.

Summary

The positive synergistic effect of two catalysts on the burn rate of a solid propellant was discovered using the two-dimensional composite solid propellant sandwich. Synergistic effects were noted for all combinations of the four catalysts when tested in the sandwich configuration at 600 psia. The volumetric catalyst loading was maintained constant across the sandwich. The maximum sandwich vertical burn rate was achieved by the Harshaw catalyst Cu 0202 P--ferric oxide system. The maximum synergistic effect was obtained with the ferric oxide--iron blue system. The pressure dependence of these synergistic effects was determined over the 300 to 2000 psia range.

There has been a major experimental effort to extend these two-dimensional synergistic results to the real cast propellant. A fuse wire

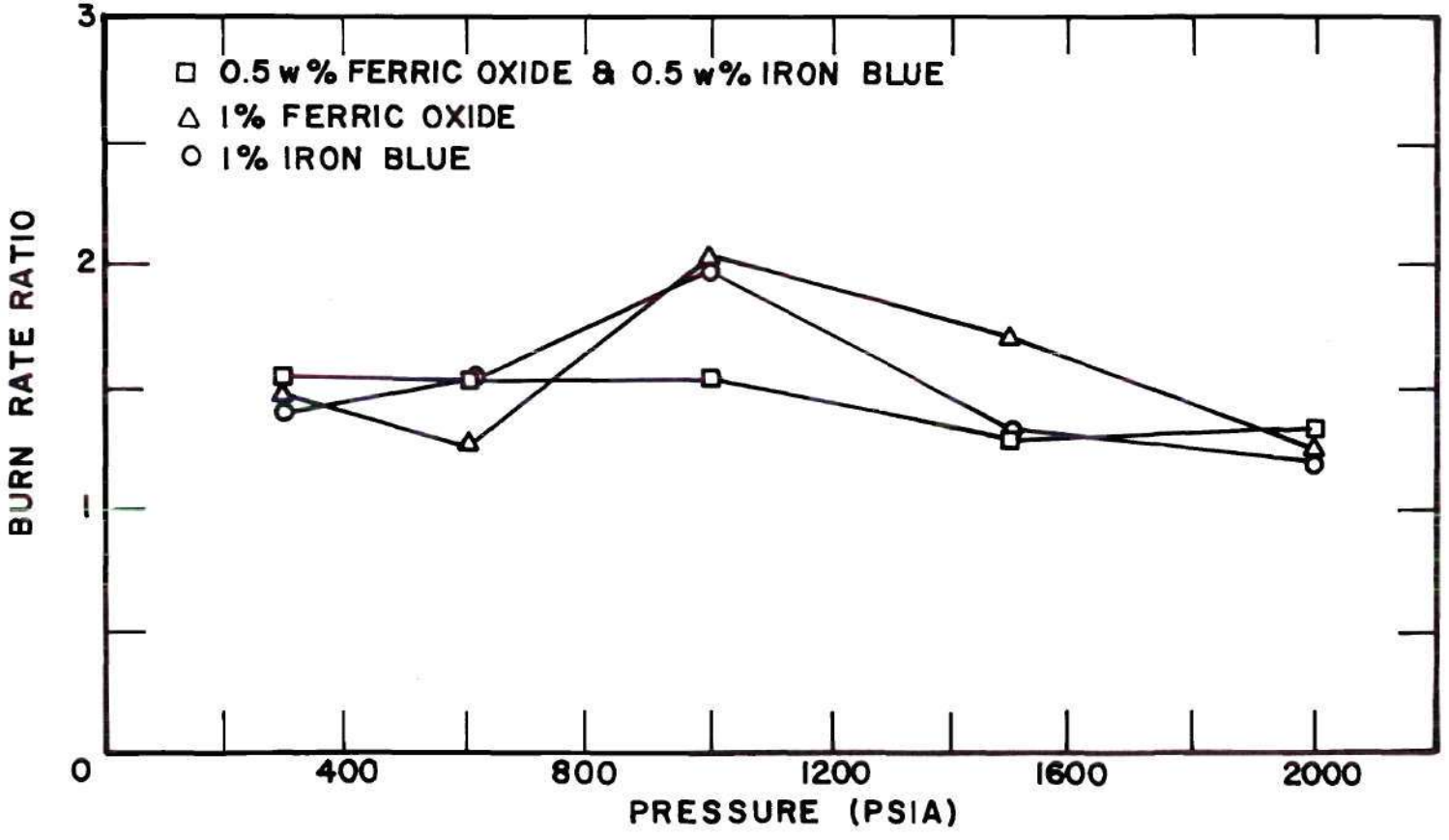

Figure 28. Synergistic Effect for Cast Propellant Samples

technique was developed, but due to propellant formulation problems and sample preparation times, this technique was discarded in favor of the previously developed cinephotomacrography techniques. Initially a 2.41 weight percent catalyst loading, analogous to the two weight percent catalyst loading in the two-dimensional sandwiches, was used. Considering the two-dimensional sandwich screening results, the same two combinations of catalysts, Harshaw catalyst Cu 0202 P--ferric oxide and iron blue--ferric oxide were added to the cast propellant. The initial tests were conducted at 600 psia. No positive synergistic effect was found. There were considerable data scatter and sample structural failure. It was decided to reduce the catalyst loading to one weight percent. The same two combinations of catalysts were tested first at 600 psia and then at 2000 psia. A positive synergistic effect on sample burn rate for the iron blue--ferric oxide was found at 2000 psia. This system was tested over the 300 to 2000 psia range. The only other pressure where a positive synergistic effect was found was at 300 psia.

CHAPTER VII

SUMMARY OF OBSERVATIONS, CONCLUSIONS AND RECOMMENDATIONS

General

An experimental study of the catalysis of four burn rate modifiers in the combustion of composite solid propellants has been made. Harshaw catalyst Cu 0202 P, ferric oxide, iron blue, and ferrocene were used with both two-dimensional oxidizer-binder sandwiches and cast composite propellants. Ammonium perchlorate was used as the oxidizer and hydroxyl terminated polybutadiene was the binder. Cinephotomacrography was used to obtain sample burn rates and observe dynamic changes of the regressing surface. Quenched combustion samples were examined with optical and scanning electron microscopes for binder melt flow, location of the point of maximum regression, and surface details indicating the catalysis mechanisms. The region of action of the various catalysts has been investigated. The existence of a synergistic effect on burn rate due to the addition of two different catalysts has been explored. The feasibility of using an electron microprobe for element identification was investigated.

Summary of Observations

Harshaw Catalyst Cu 0202 P

In the AP.

1) This additive was the most effective catalyst of the oxidizer deflagration process in the sandwich configuration. It also exhibited

the greatest augmentation of the sample vertical burn rate in both the sandwich and cast configurations.

2) The surface of the oxidizer was much smoother than the pure AP surface.

3) There was a porous structure with holes less than four μm in diameter and cracks of the same width occurring in this surface.

4) The binder melt flow was reduced over the pure AP-HTPB binder melt flow.

5) The leading edge of the sandwich regression was at the edge of the slight binder melt flow in the oxidizer.

6) The oxidizer surface slope increased from 44 degrees to 64 degrees for the quenched samples as the pressure increased from 600 to 2000 psia. The high speed movies indicated a decrease of 50 degrees to 20 degrees over the same pressure range.

In the Binder.

1) It had no effect on the sandwich vertical burn rate or the oxidizer normal regression rate when it was added to the binder alone.

2) The binder melt flow was less than for the pure AP-HTPB binder melt for all pressures.

3) The residual binder height was reduced at 2000 psia as compared with the pure AP-HTPB residual binder height.

At the Interface.

1) A thin coating at the binder-oxidizer interface was sufficient to catalyze the sandwich vertical burn rate for all pressures except 1500 psia. The oxidizer normal regression rate was only altered slightly at

600 and 1000 psia and inhibited at 1500 and 2000 psia.

2) No binder melt flow of any extent was observed.

3) There always appeared to be an excess amount of catalyst present in a residual frothy interface layer.

4) The point of maximum regression was always at the pure AP-catalyst interface.

5) The oxidizer surface slopes obtained from the high speed motion pictures and the scanning electron microscope investigation did not agree.

6) The surface of the pure AP resembled that of the AP loaded with catalyst for 200 to 300 μm from the pure AP-catalyst interface for all pressures. The surface slope of these samples were between 70 degrees and 75 degrees.

Uniformly Loaded.

1) This type of catalyst loading produced the maximum sandwich vertical burn rate for this catalyst.

2) It also produced the maximum burn rate normal to the oxidizer surface.

3) It produced the maximum separation of the sandwich vertical burn rate and the oxidizer normal regression rate. This indicated that the binder-oxidizer reactions have been catalyzed.

4) This separation between these two burn rates was constant over the 300 to 2000 psia pressure range. This indicated a constant catalysis of the binder-oxidizer reactions.

Ferric Oxide

In the AP.

1) This catalyst acted as an inhibitor of the oxidizer deflagration

rate below 1200 psia.

2) There was a frothy material above a relatively smooth sub-surface that indicated the possible existence of a liquid layer.

3) The only porous structure was near cracks in the smooth sub-surface layer.

4) Particles of material were visible in the solidified smooth surface. This material could be ferric oxide particles.

5) The binder melt flow was reduced over the pure AP-HTPB binder melt flow.

6) A flake structure remained on the solidified AP surface at 600 and 1000 psia. This structure gave the appearance of being formed in layers parallel to the oxidizer surface.

7) As the pressure increased to 1500 and 2000 psia a more uniform froth was noted in the high speed motion pictures. The residue of this froth adhered to the solidified AP surface. It did not resemble the flake structure.

In the Binder.

1) The additive had no effect on the burn rate when it was added to the binder alone.

2) The residual binder heights were less than the pure AP-HTPB residual binder heights for all pressures.

3) The binder melt flows were reduced below the pure AP-HTPB melt flows for all pressures.

4) There was no visible effect of the presence of the catalyst out over the oxidizer surface.

5) The point of maximum regression was always in the pure AP.

6) The residue of the interface layer of catalyst regressed with the pure oxidizer surface. There was no indication of an extending froth or flake structure above the oxidizer surface.

Uniformly Loaded.

1) This type of catalyst loading produced the maximum sandwich vertical burn rate for this catalyst.

2) This type of catalyst loading produced the maximum burn rate normal to the oxidizer surface for this catalyst.

3) The separation between the sandwich vertical burn rate and the oxidizer normal regression rate was nearly constant over the 300 to 2000 psia pressure range. This indicated a constant catalysis of the binder-oxidizer reactions.

Iron Blue

In the AP.

1) This catalyst acted as an inhibitor of the oxidizer deflagration rate for all pressures.

2) The sandwich vertical burn rate and the burn rate normal to the oxidizer surface differed by an appreciable amount over the entire pressure range. This indicates a catalysis of the binder-oxidizer reactions.

3) There was a residual smooth surface indicating the possible existence of a liquid layer on the oxidizer.

4) There was a porous structure on the residual surface near cracks in the surface. This was similar to the ferric oxide--AP surface.

5) The binder melt flow was reduced over the pure AP-HTPB binder melt flow.

6) A frothy red residue of particles appeared on the surface of the oxidizer at 600 psia. Their density increased until at 2000 psia there was a frothy structure similar to that of the ferric oxide--AP sample.

In the Binder.

1) There was an indication of catalysis of the sandwich vertical burn rate when it was added to the binder at 600 psia.

2) The binder melt flow was less than the pure AP-HTPB melt for all pressures.

3) The residual binder height was always less than any of the other samples tested.

At the Interface.

1) An equal amount of catalyst loaded at the binder-oxidizer interface was much more effective than loading in the oxidizer in catalyzing the sandwich vertical burn rate.

2) This catalyst was consistently effective in catalyzing the sandwich vertical burn rate when restricted to this binder-oxidizer interface.

3) There was essentially no binder melt flow.

4) There always appeared to be an excess amount of catalyst remaining in a residual frothy interface layer.

5) The point of maximum sandwich regression was at the pure AP-catalyst or binder-catalyst interface.

6) The surface of the pure AP resembled that of the AP loaded

with catalyst for 35 to 300 μm from the pure AP-catalyst interface increasing as the pressure increased. All samples had surface slopes of up to 70 degrees.

Uniformly Loaded.

1) This type of catalyst loading produced the maximum sandwich vertical burn rate for this catalyst.

2) This type of catalyst loading produced the maximum burn rate normal to the oxidizer surface for this catalyst.

3) The separation between the two burn rates was constant over the pressure range of 300 to 2000 psia. This indicated a constant catalysis of the binder-oxidizer reactions.

Ferrocene

In the AP.

1) This catalyst acted as an inhibitor of the oxidizer deflagration rate for all pressures.

2) The sandwich vertical burn rate and the burn rate normal to the oxidizer surface differed by an appreciable amount over the entire pressure range. This indicated a catalysis of the binder-oxidizer reactions.

3) The binder melt flow was reduced over the pure AP-HTPB binder melt flow.

4) Red and black particles were visible on the oxidizer surface at all pressures.

5) The sub-surface remained very porous and resembled the pure AP surface. The entire surface remained highly uniform. There were no

ridge and valley formations.

6) The point of maximum sandwich regression was always located very close to the binder-oxidizer interface.

7) The quenched combustion sample regressed faster than the high speed motion pictures indicated.

In the Binder.

1) There was a slight indication of catalysis of the sandwich vertical burn rate when it was added to the binder at 600 psia.

2) The binder melt flow was less than for the pure AP-HTPB melt flow for all pressures.

3) The residual binder height was the largest of any catalyzed samples. It exceeded the pure AP-HTPB heights at 1000 and 1500 psia.

At the Interface.

1) This additive was an effective catalyst of the sandwich vertical burn rate except at 1500 psia.

2) This type of catalyst loading produced larger augmentation of the sandwich vertical burn rate than oxidizer or binder loading.

3) The binder melt flow was less than the pure AP-HTPB melt flow, but greater than the other catalyzed samples.

4) At 2000 psia the sandwich vertical burn rate increased considerably for this sample. There was no residue layer at the interface.

5) The residue binder height exceeded the pure AP-HTPB residue binder heights at 600 and 1000 psia.

6) The surface of the pure AP at 2000 psia resembled that of the AP loaded with catalyst for 200 μm from the pure AP-catalyst interface.

This sample had a surface slope of between 70 and 80 degrees.

Conclusions

1) The extent of the binder melt flow was reduced by all catalysts at all test pressures for the three loading configurations--in the AP, binder, or at the binder-oxidizer interface. The binder melt flow appears to locally retard the deflagration rate of the underlying AP. The point of maximum sandwich regression was located at the edge of the binder melt flow when the catalyst was loaded in the AP. The reduction of the extent of this binder melt flow could be an important mechanism for propellant catalysis.

2) All catalysts at all pressures investigated gave indication of catalyzing the binder-oxidizer reactions that occur in the gas phase for the sandwich configuration with the catalyst loaded in the oxidizer or at the binder-oxidizer interface. Alternatively, when the catalyst was loaded in the binder alone no catalysis of the binder-oxidizer reactions was noted. That is the sandwich vertical burn rate and the oxidizer normal regression rate were the same. This indicates that the catalysts investigated are most effective when introduced hot into the gas phase, as may be expected.

3) The catalyst either suppressed or augmented the AP deflagration rate depending upon catalyst type and pressure level. In all cases, however there is indication of condensed phase activity when the catalyst is loaded into the AP.

4) The positive synergistic effect of two catalysts on the burn rate of a solid propellant was discovered using the two-dimensional

composite solid propellant sandwich. All combinations of the four catalysts exhibited either a positive or a possible synergistic effect on both the sandwich vertical burn rate and the oxidizer normal regression rate when tested at 600 psia. Two catalyst systems were tested over the 300 to 2000 psia pressure range. These results were extended to an investigation of a possible synergistic effect on sample burn rate with cast composite propellants.

5) A positive synergistic effect on sample burn rate was detected for cast composite propellant samples. This effect was not as strong as for the two-dimensional sandwich samples. Further tests at lower effective catalyst loading and a broadened ammonium perchlorate particle distribution were conducted. Again the results were not as conclusive as for the two-dimensional sandwich samples. The results of the extensive investigation of synergistic effects in two-dimensional sandwiches were not reproduced in the bimodal cast propellant samples tested in this investigation.

6) The electron probe x-ray microanalysis did not yield relative concentrations of elements present at the surface of either the burned or unburned oxidizer. There was considerable sample damage due to using uncoated non-conducting samples. In contrast, the electron beam for the scanning electron microscope was much smaller in diameter. This beam could be used with controlled samples coated with different metallic coatings to obtain a consistent test program to determine the chemical composition of residues on the surface of partially burned samples.

7) The oxidizer surface slope and its pressure dependence for the samples obtained for the scanning electron microscopy investigation

did not always agree with the values obtained from the high speed motion pictures. The cinephotomacrography burn rates were used to determine the delay time between sample ignition and depressurization of the combustion chamber for quench tests. This technique did not yield good results for the cases of catalyst loaded at the binder-oxidizer interface. Neither of these results can be explained with the present data. Simultaneous cinephotomacrography of quenched combustion samples would be useful.

8) The sandwich vertical burn rate for uniformly loaded samples was greater than the oxidizer, binder, or binder-oxidizer interface loaded samples. These results can not be explained with the present test procedures or available data.

Recommendations for Future Research

During the course of this investigation new areas of research became apparent. Limitations of present capabilities were also made clear. The techniques that have been developed were used to obtain a better idea of catalytic behavior in composite solid propellants. Both cinephotomacrography and scanning electron microscopy of quenched combustion samples were used. The difficulty encountered in extending the synergistic action of two catalysts on sample burn rate in two-dimensional sandwiches indicates that more experimental and theoretical work must be done in this area. Several topics for future research are listed below.

1) Uniformly loaded two-dimensional sandwiches with two weight percent of ferrocene, or its equivalent, added to the oxidizer should be tested. This would complete the set of uniformly loaded sample data. Test results for cast propellants could be obtained directly by completing

the scan for possible synergistic effects with cast propellants. Based on the data for ferrocene, the evaluation of synergistic effects should be conducted at 2000 psia.

2) Quenched combustion samples of uniformly loaded sandwiches should be obtained for scanning electron microscopy observation. Tests that exhibit non-uniform or inconsistent burn rates and surface slopes should be photographed during the quenching process to determine the dynamic behavior of the sample during the depressurization of the combustion chamber. Relevant binder height data could be obtained for catalytic studies if symmetrically loaded AP sandwiches are used.

3) Based on the apparent success of the uniformly loaded two-dimensional sandwiches an experimental effort should continue to extend this type of loading to cast propellants. The catalysts could either be co-crystallized with the ammonium perchlorate or combined in a polycrystalline structure. The initial AP and catalyst particle sizes will determine the scale of the uniform loading of the resultant particle. The capability to measure the particle size distribution and the amount of catalyst present in AP must be developed.

4) A detailed investigation of quenched combustion samples of cast composite propellants with catalysts loaded in the binder would be helpful in determining the similarities as compared with the two-dimensional samples. A more relevant two-dimensional model might include variable binder and oxidizer thicknesses.

5) A scanning electron microscope could be utilized to measure binder melt flows and binder heights directly from coated quenched samples.

This would eliminate the inaccuracies obtained when scaling dimensions from electron micrographs. Different electrically conducting sample coatings could be investigated. An optimum coating procedure could be developed to allow x-ray spectra to be obtained with the scanning electron microscope electron beam. This would allow a detailed elemental analysis of the quenched combustion sample surface to be obtained. Surface contours of element densities can also be prepared using this same technique. Particle size densities and chemical composition could also be determined from this same contour measurement technique.

6) The gas chromatograph/mass spectrometer system of the fire research program of the School of Aerospace Engineering could be used for chemical analysis of the residue layers of catalysts. A large enough sample would have to be obtained by careful collection of all residue. Binder char layers or oxidizer-catalyst residues can be studied by careful separation or burning separate samples.

APPENDICES

APPENDIX A

THE EFFECT OF CHEMICAL COMPOUNDS ON AMMONIUM PERCHLORATE

The following Table 8 is a compilation of chemical compounds that have been studied by various investigators to determine if they accelerate or inhibit the thermal decomposition or deflagration of ammonium perchlorate or alter the ignition properties of perchloric acid in the presence of fuels. The numbers listed in the various columns correspond to the papers listed in the Bibliography. For the deflagration results the pressure range in atmospheres is listed as a superscript. The majority of the names and empirical chemical formulations have come from the original references. An attempt has been made to supply any missing quantities. When the chemical compound increased the rate of decomposition or deflagration the reference was listed in the accelerate column. The ignition delay is defined as the time from initial exposure to combustion of the chemical compound to perchloric acid vapor in the presence of fuel. If this ignition delay decreases then the compound is listed in the accelerate column. If the rates of decomposition or deflagration have decreased and the ignition delay increased, the chemical compound is listed in the inhibit column. If the compound neither accelerates or inhibits the reaction, the reference is located in between.

Table 8. Chemical Compounds Added to Ammonium Perchlorate

No.	Chemical Compound Name	Formula	AP Thermal Decomposition Accelerate	AP Thermal Decomposition Inhibit	AP Deflagration Accelerate	AP Deflagration Inhibit	Perchloric Acid Ignition Accelerate	Perchloric Acid Ignition Inhibit
1.	Aluminum Acetylacetonate	$Al(C_5H_7O_2)_3$					7	
2.	Aluminum Chloride	$AlCl_3$		29	18^{50-150}	$18^{300-1000}$ 10		
3.	Aluminum Oxide	Al_2O_3	29	15			14,15	6,7
4.	Amid of Salicylic Acid	$C_7H_7NO_2$			18^{300}	18^{150}		
5.	m-aminobenzoic Acid	$C_7H_5NO_4$			$18^{300,600}$	$18^{50,150}$		
6.	Ammonia	NH_3		29,30				
7.	Ammonium Bisulfate	NH_4HSO_4				5		
8.	Ammonium Bromide	NH_4Br			$18^{300-600}$	18^{50-150}		
9.	Ammonium Chlorate	NH_4ClO_3	31					

(Continued)

Table 8. (Continued)

No.	Chemical Compound Name	Formula	AP Thermal Decomposition Accelerate Inhibit	AP Deflagration Accelerate Inhibit	Perchloric Acid Ignition Accelerate Inhibit
10.	Ammonium Chloride	NH_4Cl	10	$18^{300-1000}$ 18^{50-150} 5	
11.	Ammonium Chromate	$(NH_4)_2CrO_4$		5^{20-100}	
12.	Ammonium Dichromate	$(NH_4)_2Cr_2O_7$		5^{20-100}	
13.	Ammonium Fluoborate	NH_4BF_4		18^{1000} 18^{50-300}	
14.	Ammonium Fluoride	NH_4F		18^{600} $5, 18^{100-1000}$	
15.	Ammonium Fluosilicate	$(NH_4)_2SiF_6$		$18^{300-1000}$	
16.	Ammonium Hydrogen Fluoride	NH_4HF_2		5	
17.	Ammonium Iodide	NH_4I	32		

(Continued)

Table 8. (Continued)

No.	Chemical Compound Name	Formula	AP Thermal Decomposition Accelerate	AP Thermal Decomposition Inhibit	AP Deflagration Accelerate	AP Deflagration Inhibit	Perchloric Acid Ignition Accelerate	Perchloric Acid Ignition Inhibit
18.	Ammonium Nitrate	NH_4NO_3	29					
19.	Ammonium Oxalate	$(NH_4)_2C_2O_4$			$18^{600-1000}$	18^{50-300} 5		
20.	Ammonium Ortho Phosphate, di-H	$NH_4H_2H_2PO_4$				5		
21.	Ammonium Ortho Phosphate, mono-H	$(NH_4)_2HPO_4$			18^{600}	$5,18^{50-150}$		
22.	Ammonium Phosphate	$(NH_4)_3PO_4 \cdot 3H_2O$		33				
23.	Ammonium Sulfate	$(NH_4)_2SO_4$		33		5		
24.	Anthracene	$C_{14}H_{10}$			$18^{300,600}$	18^{150}		
25.	Barium Chloride	$BaCl_2$			$18^{300-1000}$	18^{50-150}		

(Continued)

Table 8. (Continued)

No.	Chemical Compound Name	Formula	AP Thermal Decomposition Accelerate Inhibit	AP Deflagration Accelerate Inhibit	Perchloric Acid Ignition Accelerate Inhibit
26.	Barium Fluoride	BaF_2		$18^{300\text{-}600}$ $18^{50\text{-}150}$	
27.	Benzoic Acid	$C_7H_7O_2$		$18^{50,300,600}$ 18^{150}	
28.	Bismuth Fluoride	BiF_3		$18^{300\text{-}1000}$ $18^{50\text{-}150}$	
29.	Bromine-Benzoic Acid	$C_7H_5Br\text{-}O_2$		18^{300} 18^{150}	
30.	Cadmium	Cd	13	5	
31.	Cadmium Chloride	$CdCl_2$		$18^{300\text{-}1000}$ $18^{100,150}$	
32.	Cadmium Fluoborate	$Cd(BF_4)_2$		18^{600} $18^{50\text{-}300}$	
33.	Cadmium Fluoride	CdF_2		18^{600} $18^{50\text{-}300}$	
34.	Cadmium Oxide	CdO	13,15		7 15
35.	Cadmium Perchlorate	$Cd(ClO_4)_2 \cdot 6H_2O$	13	5	

(Continued)

Table 8. (Continued)

No.	Chemical Compound Name	Formula	AP Thermal Decomposition Accelerate	AP Thermal Decomposition Inhibit	AP Deflagration Accelerate	AP Deflagration Inhibit	Perchloric Acid Ignition Accelerate	Perchloric Acid Ignition Inhibit
36.	Cadmium Sulfate	$CdSO_4$		13				
37.	Calcium Carbonate	$CaCO_3$		31	34	$24^{140-340}$		
38.	Calcium Chloride	$CaCl_2$				18^{50-150}		
39.	Calcium Fluoride	CaF_2				$18^{300-600}$ 18^{50-150}		
40.	Calcium Oxide	CaO		15,29		$18^{300,600}$ 18^{50-150} $24^{140-340}$		
41.	Calcium Oxalate	CaC_2O_4				5		
42.	Calcium Perchlorate	$Ca(ClO_4)_2$	33			13		
43.	Carbon	C	35,36		11			
44.	Carbon Tetrachloride	CCl_4		31				
45.	Centralite n.l	--				$18^{300,600}$ 18^{150}		
46.	Cerium Fluoride	CeF_3				$18^{150-1000}$ $18^{50,100}$		

(Continued)

Table 8. (Continued)

No.	Chemical Compound Name	Formula	AP Thermal Decomposition Accelerate	AP Thermal Decomposition Inhibit	AP Deflagration Accelerate	AP Deflagration Inhibit	Perchloric Acid Ignition Accelerate	Perchloric Acid Ignition Inhibit
47.	Chlorine	Cl	31					
48.	Chlorine Dioxide	ClO_2	31					
49.	Chromium Acetylacetonate	$Cr(C_5H_7O_2)_3$					7	
50.	Chromium Oxide	Cr_2O_3	35,37	12,15	$5^{27\text{-}100}$ $24^{200\text{-}400}$		14,15	
51.	"Chromium Oxide"	$CrO_{1.97}$		15				7
52.	Chromium Trioxide	CrO_3						7
53.	Cobalt Oxides	Co_3O_4+ Co_2O_3	15,37				7,15	
54.	Copper Chloride	$CuCl_2$	38	39				
55.	Copper Chromite (Cupurous)	$CuCrO_4 \cdot 2Cu(OH)_2$	40		41		7	

(Continued)

Table 8. (Continued)

No.	Chemical Compound Name	Formula	AP Thermal Decomposition Accelerate	AP Thermal Decomposition Inhibit	AP Deflagration Accelerate	AP Deflagration Inhibit	Perchloric Acid Ignition Accelerate	Perchloric Acid Ignition Inhibit
56.	Copper Chromite Catalyst (Harshaw)	$CuO202$ P	35,40,42,43 39,44		2,5,11,20,21 22,24,27,34	1-400		7
57.	Copper Chromate (Cupric)	$CuCrO_4 \cdot Cu(OH)_2$	40,42		34	13-120		6,7
58.	Copper Oxide (Cupric)	CuO	12,15,33,39,40		5 24	40-100 140-400		7, 14,15
59.	Copper Oxide(Cuprous)	Cu_2O	15,45		5	7-100,46		7
60.	Copper Nitrate	$Cu(NO_3)_2 \cdot 6H_2O$	33					
61.	Copper Oxalate	$CuC_2O_4 \cdot 1/2(H_2O)$	33					
62.	Copper Perchlorate	$Cu(ClO_4)_2$	32,33			5		
63.	Dichromate Ion	$Cr_2O_7^{--}$			19 25	136-340 27-1000	19	20-136

(Continued)

Table 8. (Continued)

No.	Chemical Compound Name	Formula	AP Thermal Decomposition Accelerate	AP Thermal Decomposition Inhibit	AP Deflagration Accelerate	AP Deflagration Inhibit	Perchloric Acid Ignition Accelerate	Perchloric Acid Ignition Inhibit
64.	Dicyandiamide	$C_2H_4N_4$			$18^{300-1000}$	18^{50-150}		
65.	Diphenylamine	$C_{12}H_{11}N$				18^{50-600}		
66.	Ethylester-4-nitro-benzoic Acid	$C_9H_9NO_4$			$18^{50,300,600}$	18^{150}		
67.	Ferrocene	$(C_5H_5)_2$-Fe			21,22 $^{20-136}$		7	
68.	Hexachlorethane	$(CCl_3)_2$			$18^{600-1000}$	18^{50-300}		
69.	Hexamine	$C_6H_{12}N_4$			18^{300}	18^{600}		
70.	Indium Oxide	In_2O_3		13				
71.	Iron Blue	$Fe(NH_4)$-$Fe(CN)_6$			21,22 $^{20-136}$			
72.	Iron Oxide (Ferric)	Fe_2O_3	15,29,35,47		2,5,20,21,22,24 $^{20-400}$	5^{20-100}		

(Continued)

Table 8. (Continued)

No.	Chemical Compound Name	Formula	AP Thermal Decomposition Accelerate	AP Thermal Decomposition Inhibit	AP Deflagration Accelerate	AP Deflagration Inhibit	Perchloric Acid Ignition Accelerate	Perchloric Acid Ignition Inhibit
73.	Iron Oxide (Ferrous)	FeO				5	39	
74.	Iron Oxide(Ferrous-Ferric)	Fe_3O_4					7	
75.	Lanthanum Fluoride	LaF_3			$18^{300-1000}$	18^{50-150}		
76.	Lead Chloride	$PbCl_2$			$18^{300-1000}$	$5,18^{50-150}$		
77.	Lead Fluoride	PbF_2			$18^{300-1000}$	$18^{100-150}$		
78.	Lithium Fluoride	LiF			$18^{50,600}$ 48^{10-100}	$18^{100,150}$ 27^{34}	27	
79.	Lithium Oxide	Li_2O	12,13					
80.	Lithium Perchlorate	$LiClO_4$			5^{20-100}	13		
81.	Magnesium Oxide	MgO	15,37				7	15
82.	Magnesium Perchlorate	$Mg(ClO_4)_2$	13					

(Continued)

Table 8. (Continued)

No.	Chemical Compound Name	Formula	AP Thermal Decomposition Accelerate	AP Thermal Decomposition Inhibit	AP Deflagration Accelerate	AP Deflagration Inhibit	Perchloric Acid Ignition Accelerate	Perchloric Acid Ignition Inhibit
83.	Magnesium Sulfate	$MgSO_4$		13				
84.	Manganese Dioxide	MnO_2	29,37,49		$24^{170-400}$	5^{70-100}	7	
85.	Mercury Chloride	HgCl			$18^{300-1000}$	$18^{100,150}$		
86.	Molybdenum Trioxide	MoO_3						7
87.	β-naphtylester of Salicylic Acid	$C_{17}H_{12}O_3$			$18^{300-600}$	18^{150}		
88.	o-nitrobenzoic Acid	$C_7H_5NO_4$			$18^{300,600}$	18^{50-150}		
89.	Neodymium Fluoride	NdF_3			$18^{300-1000}$	18^{50-150}		
90.	Nickle Oxides	$NiO + Ni_2O_3$	15,37				7,15	
91.	Nitrogen	N_2	30					
92.	Nitric Oxide	NO		30				

(Continued)

Table 8. (Continued)

No.	Chemical Compound Name	Formula	AP Thermal Decomposition Accelerate	AP Thermal Decomposition Inhibit	AP Deflagration Accelerate	AP Deflagration Inhibit	Perchloric Acid Ignition Accelerate	Perchloric Acid Ignition Inhibit
93.	Oxamide	$C_2H_4N_2O_2$			$18^{300-1000}$	18^{50-300}		
94.	8-o-oxychinolin	--			$18^{300-600}$	18^{150}		
95.	Oxygen	O_2	31	30				
96.	Perchloric Acid	HClOH	29,31					
97.	Permangante Ion	MnO_4^-				$19^{100-170}$		
98.	Phenyl-ester of Salicylic Acid	$C_{13}H_{16}O_3$			$18^{300,600}$	18^{150}		
99.	Polyvinylchloride	C_2H_3Cl			$18^{300-1000}$	18^{50-300}		
100.	Potassium Ion	K^+			19^{27-400}			
101.	Potassium Bromide	KBr			$18^{300-1000}$	18^{50-150}		
102.	Potassium Chlorate	$KClO_3$	31					
103.	Potassium Chloride	KCl			5^{20-50} $18^{300,600}$ 36^{10-100}	5^{40-100} 18^{50-150}		

(Continued)

Table 8. (Continued)

No.	Chemical Compound Name	Formula	AP Thermal Decomposition Accelerate Inhibit	AP Deflagration Accelerate Inhibit	Perchloric Acid Ignition Accelerate Inhibit
104.	Potassium Dichromate	$K_2Cr_2O_7$	39		
105.	Potassium Fluoborate	KBF_4		$18^{50,600,1000}$ $18^{100,150}$	
106.	Potassium Fluoride	KF		$18^{600,1000}$ $18^{50,150}$	
107.	Potassium Oxalate	$K_2C_2O_4$		$18^{300\text{-}1000}$ $18^{50\text{-}150}$	
108.	Pyridin Salicylic	--		18^{300} $18^{50,150,600}$	
109.	Pyrocatechin	$C_6H_6O_2$		18^{300} 18^{150}	
110.	Salicylic Acid	$C_7H_6O_3$		18^{300} 18^{150}	
111.	Silicon Carbide	SiC		5	
112.	Silicon Dioxide	SiO_2			6,7
113.	Silver Perchlorate	$AgClO_4$	32		
114.	Sodium Chloride	NaCl		$18^{50,300,600}$ 18^{150}	

(Continued)

Table 8. (Continued)

No.	Chemical Compound Name	Formula	AP Thermal Decomposition Accelerate	AP Thermal Decomposition Inhibit	AP Deflagration Accelerate	AP Deflagration Inhibit	Perchloric Acid Ignition Accelerate	Perchloric Acid Ignition Inhibit
115.	Sodium Fluoride	NaF			[18] 300-1000	[18] 50-150		
116.	Sodium Permanganate-trihydrate	$NaMnO_4 \cdot 3H_2O$			[24] 200-400	[24] 90-200		
117.	Tin Dioxide	SnO_2		15		[5] 70	15	
118.	Titanium Dioxide	TiO_2		15		[5] 50-100	14,15	6,7,14
119.	Tungsten Carbide	WC			5			
120.	Tungsten Trioxide	WO_3						7
121.	Tri-uranium Oct-oxide	U_3O_8					7	
122.	Urea	$(NH_2)_2CO$			[18] 300-1000	[18] 50-300		
123.	Urethane	$C_3H_7NO_2$			[18] 50,300,600	[18] 150		
124.	Vanadium Pentoxide	V_2O_5						7
125.	Zinc Fluoride	ZnF_2			[18] 600	[18] 50-150		

(Continued)

Table 8. (Continued)

No.	Chemical Compound Name	Formula	AP Thermal Decomposition Accelerate	AP Thermal Decomposition Inhibit	AP Deflagration Accelerate	AP Deflagration Inhibit	Perchloric Acid Ignition Accelerate	Perchloric Acid Ignition Inhibit
126.	Zinc Oxide	ZnO	13,15			5	7,14,15	
127.	Zinc Perchlorate	$ZnClO_4$	13			5		
128.	Zinc Sulfate	$ZnSO_4$		13				
129.	Zirconium Carbide	ZrC				[5]55-100		
130.	Zirconium Dioxide	ZrO_2						7
131.	Zirconium Fluoride	ZrF_4				[18]300-1000 [18]50-150		

APPENDIX B

SAMPLE PREPARATION

Hydroxyl Terminated Polybutadiene Binder

The HTPB binder was prepared using the following formulation from materials supplied by T. L. Boggs of the Naval Weapons Center, China Lake, California.

R 45 M lot--001251	90.430%
IPDI	6.450%
CAO--14 (AO 2246)	.978%
MT-4	2.142%
	100.00 %
NCO/OH ratio	.798

R45M lot 001251 is the pre-polymer with an equivalent weight of 1387 gm. IPDI, Isophorene diisocyanate, is the curing agent with an equivalent weight of 114 gm. Both the R45M and IPDI are liquids and must be stored under dry nitrogen.

CAO--14 (AO 2246) is an antioxidant in a powdered form. It has an equivalent weight of 170.2 gm.

MT-4 is a bonding agent dissolved in $CHCl_2/CH_3OH$ solvent at a concentration of 2.78 gm/10 ml of solution. Care must be taken to prevent the solvent from evaporating.

The following mixing procedure should be followed:

a) Weight CAO--14 into a suitable vessel.

b) Weight in R45M.

Mix antioxidant with R45M at 60°C until the antioxidant has dissolved. Allow the mixture to cool then:

c) Weight in IPDI, the diisocyanate curative.

d) Add proper volume of MT-4 solution with pipette.

Mix all ingredients and out-gas in a vacuum oven at 60°C. This should be done several times until no foaming is present. A large enough mixing vessel should be used to allow for considerable foaming. The binder should be carefully poured into the mold and cured for seven days at 60°C.

Ground Ammonium Perchlorate

All ammonium perchlorate for the two-dimensional sandwiches was ground by hand in a pyrex mortar and pestle for ten minutes. This produced a consistent, fine particle distribution for the polycrystalline disks. Approximately 1.3 grams of AP produced a .050 inch thick disk. This mode of oxidizer preparation was ideal for this quantity of material, but could not easily be extended to produce a sufficient quantity of oxidizer for a cast propellant.

A 0.3 gallon porcelain mill jar, a variable speed roller system, and an assortment of 1/2 inch and 1 inch diameter porcelain balls have been used as a ball mill to grind the ammonium perchlorate for the cast propellants. A series of eight inch diameter U.S.A. standard sieves are used to separate the ground AP. These sieves include the following opening sizes: 212, 180, 125, 90, 63, 45, and 37 μm. These sieves are used with

a motor driven portable sieve shaker.

A weighed quantity of AP, usually 50 or 100 grams, was placed in the mill jar along with five one inch porcelain balls and fifteen 1/2 inch porcelain balls. The jar was sealed and placed on the variable speed roller system. The speed was adjusted to give a continuous roller sound rather than a random crashing sound. Both the grinding and sieving procedures should be carried out for definite time intervals. The partially ground AP is removed from the mill jar, along with the balls. As much material as can easily be removed should be placed in the largest sieve. No adequate procedure was developed to reclaim all ground AP from the mill jar and balls, several were attempted. Adequate weight records allow you to estimate various losses, such as mill and sieving losses. Hand agitation is used to separate the AP and the balls. One 1/2 inch diameter ball is placed in each sieve. This is used to provide additional agitation for the AP.

The sieve shaker is used to vibrate the sieves. After a preset time, usually five minutes, the separated AP is removed from the sieves. All unwanted or excess AP is returned to the ball mill for further grinding, and the cycle repeated. Additional drying of ground AP in the vacuum oven at 60-70^{o}C for 24 hours and storage in air tight jars can minimize the tendencies of the fine AP to agglomerate when stored in a humid environment.

Cast Composite Propellants

The following procedure has been developed for mixing small quantities of cast composite propellants by hand using HTPB as the binder.

1. Determine the oxidizer to binder ratio to be used.

2. Determine the oxidizer size distribution.

3. Determine all weights of materials to be used. Be sure that there is a sufficient quantity of ground AP on hand with the proper size distribution.

4. Mark and weigh all mixing cups that will be needed in the preparation of the required samples.

5. Weigh all size distributions of AP needed into marked cups.

6. Place approximately 1/2 of the largest size AP in a marked cup and weigh in the total amount of the pre-polymer, R45M.

7. Weigh in the necessary amount of curing agent, IPDI.

8. Mix thoroughly until all AP has been wetted with binder.

9. Add remaining large size AP and continue mixing. Repeat this mixing until all of the AP sizes have been added, the last being the smallest.

10. The bonding agent MT-4 is added by volume. The antioxidant was eliminated from the cast propellants due to the difficulty in dissolving it.

11. After a uniform mixture has been obtained, the uncured propellant is heated in the vacuum oven for 15 minute periods at 60°C. Upon removal from the oven, the mixing is continued. If no bubbles are visible and a uniform glossy material has been obtained, no further mixing is necessary.

12. If several different catalyst mixtures are to be cast from this common lot of uncured propellant, then the common lot must be divided into marked cups and weighed.

13. The correct amount of each catalyst is added to the proper cup. Care must be taken to keep track of all cup markings and their contents. This care must also be extended to the curing molds.

14. Step 11 is repeated for each catalyst sample.

15. The mixed propellant is placed in the curing mold and the mixing procedure is continued. Care must be taken to be sure that the packed propellant is free of gas bubbles and there is a glossy film of binder at the free surface.

16. The mixed sample is placed in the curing oven at $60^{o}C$ for seven days.

APPENDIX C

RUN PROCEDURES

Cinephotomacrography

1. Turn on timing light generator and frequency counter.
2. Mount sandwich and position ignition wire.
3. Fill out run data sheet (Figure 29).
4. Position sample holder in combustion vessel.
5. Turn on ignition power supply.
6. Check electrical continuity of the ignition system (both lights should glow).
7. Assemble combustion vessel.
8. Tighten all swagelok fittings.
9. Remove lense cap, check for proper lense extension tubes to give desired magnification.
10. Check all camera switches and plugs. Plug camera into the 120 v ac.
11. With ground glass focusing gate in position move camera into position and focus on sample using an auxiliary light source.
12. Put on hard hat and safety glasses.
13. With the "Main Operating Valve -1-," "Emergency Vent Valve," and "Flow Control and Vent Valve" closed, open tank and manifold valve and record tank pressure.

14. Open MOV-1, load dome regulator to 300 psi (Combustion Vessel Pressure). Check for leaks.

15. Set pressure regulator to desired operating pressure.

16. For precise focus it is necessary to refocus the camera at the operating pressure. Close MOV-1, focus camera, replace lower film gate, load film, check camera micro switches, film sprocket holes, timing light, f-stop, and set camera lens focus at infinity.

17. Set camera event switch, close off eye-piece.

18. Remove focusing light source.

19. Check Xenon lamp shutter motion, close the shutter.

20. Enter timing light frequency on the data sheet.

21. Turn on the cooling air fan for the Xenon lamp.

22. Turn on Xenon lamp power supply and strike the arc.

23. Arm the ignition circuit.

24. Open MOV-1.

25. Begin the run:

a. Adjust the "Flow Control Valve" to give the desired nitrogen flow orifice ΔP.

b. Open the Xenon light shutter.

c. Turn on the camera.

d. When the film has been exposed, turn the camera off.

e. Close the Xenon lamp shutter.

f. Close the flow metering valve.

26. Record the final tank pressure and timing light frequency.

27. Close the nitrogen cylinder valve.

28. Depressurize the combustion vessel by venting the nitrogen to the atmosphere through the "Flow Control and Bleed Valve."

29. Unload the dome regulator.

30. Turn off the xenon lamp, ignition power supply, timing light generator, and counter.

31. Remove film from the camera and move camera to end of lath bed.

32. Open combustion vessel.

33. Turn off xenon cooling air fan when the lamp has cooled (Approx. ten minutes).

34. Unplug camera.

Quenched Combustion Testing

1. Cut sample and measure height, width, depth, and binder thickness.

2. Mount sandwich with quick setting epoxy.

3. Position ignition wires and apply a drop of Plio bond cement to top of sandwich.

4. Prepare Mylar disk with rupture wire and install proper number of disks for test pressure. Check rupture delay timer.

5. Fill out run data sheet (Figure 30).

6. Position sample holder in combustion vessel.

7. Assemble combustion vessel.

8. Turn on ignition power supply.

9. Check electrical continuity of the sample ignition system.

10. Tighten all swagelok fittings.

11. Lower steel shield into position.

12. Put on hard hat, safety glasses, and ear protectors.

13. With the "Main Operating Valve -1-," "Emergency Vent Valve," and "Flow Control and Vent Valve" closed, open tank and manifold valve, and record initial tank pressure.

14. Open MOV-1, load dome regulator to 300 psi (Combustion Vessel Pressure). Check leaks.

15. Set pressure regulator to desired operating pressure.

16. Arm the ignition and diaphragm rupturing system.

17. Open MOV-1.

18. Begin run:

a. Adjust the "Flow Control Valve" to give the desired nitrogen flow (negligible).

b. Press "Detonate" button

c. Close Nitrogen Cylinder valve when diaphragm ruptures.

19. Close MOV-1 record final bottle pressure.

20. Close Nitrogen Cylinder Valve.

21. Unload dome regulator.

22. Open combustion vessel.

RUN DATA SHEET FOR THE COMBUSTION OF AP SANDWICHES

RUN NO.													
DATE													
BINDER													
STUDY													
BINDER THICKNESS													
CROSS-SECT. WIDTH													
DEPTH													
ORIENTATION													
PRESSURE													
CAMERA SPEED													
MAGNIFICATION													
EXTENSION													
FILM													
LIGHT SOURCE													
F-STOP													
NITROGEN INIT. PRES.													
FINAL PRES.													
BOTTLES USED													
N_2 FLOW RATE													
ΔP													
TIMING LIGHT													
REMARKS													

Figure 29. Run Data Sheet for Cinephotomacrography of 2-D Sandwiches

RUN DATA SHEET FOR QUENCH TESTING OF AP SANDWICHES

RUN NO.													
DATE													
BINDER													
THICKNESS													
CATALYST													
LOCATION													
SAMPLE WIDTH													
DEPTH													
HEIGHT													
TOP ANGLE													
PRESSURE													
NITROGEN BOTTLES USED													
INIT. PRES.													
FINAL PRES.													
FLOW RATE													
ΔP													
TIME DELAY													
NO. OF DISKS													
RESULTS													

Figure 30. Run Data Sheet for Quench Testing of 2-D Sandwiches

APPENDIX D

SAMPLE DATA REDUCTION

Test No. 7-A

The high speed motion pictures obtained during the cinephotomacrography observation of burning samples were used to obtain accurate burn rates. The motion pictures were projected on a front viewing screen. A detailed tracing of the sandwich profile was made as the sample burns. A tracing of test No. 7-A is shown in Figure 31. This sample was made up of one weight percent ferric oxide and one weight percent iron blue added to the ammonium perchlorate and 2.2 weight percent ferric oxide and 2.2 weight percent iron blue added to the hydroxyl terminated polybutadiene binder. This gave a uniform catalyst loading in the sandwich. This test was one of the initial scanning tests for the determination of the existence of a synergistic effect on sandwich vertical burn rate. The combustion apparatus was pressurized to 600 psia with dry nitrogen for this test. The high speed motion pictures with a latent magnification of two to one (image to actual) were taken at a rate of 1600 frames per second.

The sandwich profiles were traced every 100 frames. The actual measured camera frame rate was 1611.1. This means that a tracing was made every .062 seconds. The regressing surface was covered with an expanding froth that originated on the deflagrating surface and extended over the free edge of the sample. A sample tracing of the extent of this froth is shown in the last tracing at 500 frames. A large bubble of liquid binder

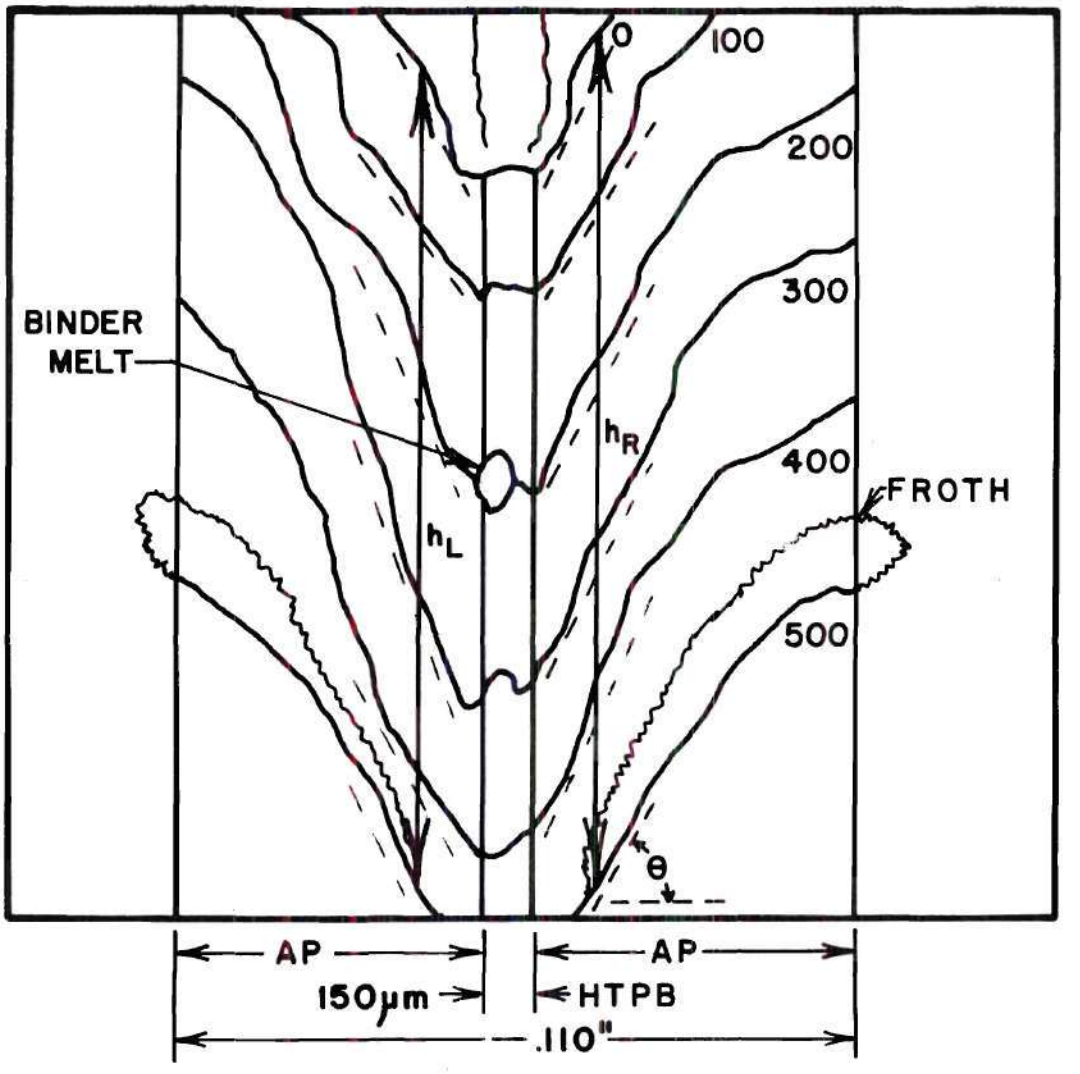

Figure 31. Sample Profiles for Test No. 7-A

was visible at the binder-oxidizer interface on the left hand side of the sample at the 200 frame tracing. This bubble grew in extent and did influence the sandwich vertical burn rate for almost 100 frames. The oxidizer surface slope θ was determined for each side for every tracing. The burn rate data were taken only after a steady profile had been achieved and the surface was clearly visible over a substantial portion of the run. For the steady profile the sandwich vertical burn rate is the same regardless of the perpendicular distance from the binder-oxidizer interface. The burn rate normal to the oxidizer surface must be taken at a distance sufficiently far away from the interface for the oxidizer to have a definable constant slope.

Two possible locations of sandwich vertical burn rate are indicated by h_L and h_R.

The movie analysis sheet for test no. 7-A is shown in Figure 32. The actual data reduction used a larger tracing of the sandwich profiles, but only 315 frames and four tracings. The frame rate is determined by counting the cycles of the timing light generator for a fixed time period. A time period of 10 seconds yielded a frequency of 999.98 hertz. This timing light generator powers a small neon bulb that exposes a .05 inch diameter circle near the edge of the film. To determine the number of frames occurring per flash of the timing light a section of film near the midpoint of the sample burn is used. The edge of the timing light is lined up with a sprocket hole edge. The number of marks occurring before another timing mark lines up with the corresponding sprocket hole edge are recorded. The number of frames occurring in this time period are obtained by counting the number of sprocket holes between these two

MOVIE ANALYSIS

RUN NO. 7-A DATE 11-28-73

150 mm

SAMPLE	AP	HTPB	AP		
DIMENSIONS		.107" .1097"			
STUDY	1% 10 1% 18	2.2% 10 2.2% 18	1% 10 1% 18		

PRESSURE 600 psia.

MOVIE DESCRIPTION COMMENTS: film broke twice, black froth visible with red particles visible. can see oxidizer surface

FOCUS excellent good depth of field

EXPOSURE f / 4 good

SMOKE good

FRAME RATE

CAMERA SETTING 1600 fps 1611.1 actual

TIMING MARKS 999.98 mps $\frac{\text{no. frames}}{\text{no. timing marks}} \frac{29}{18} = 1.611 \frac{f}{t.m}$

BURN RATE

INITIAL CAL $\frac{.1(\text{in}) \times CS\,(\text{fps})}{PR(\text{fps})\ PT(s)} = .437$ in./sec. $\frac{.1 \times 1600}{16 \times 22.9}$

LENTH OF BURN	3.257		3.740		
FRAME COUNT	315		315		
sc.in./frame					

MAGNIFICATION $\frac{\text{screen}}{\text{actual}} \frac{4.233}{.107} = 39.56$ sc.in./in.

BURN RATE $= 999.98 \frac{m}{sec} \frac{29}{18} \frac{f}{fm} \frac{h}{315} \frac{sc.in.}{f} \frac{in}{sc.in.} \left(\frac{4.233}{.107}\right)^{-1} = h \times .12928$

r (in./sec.)	.421		.484		average .452
θ	62°		60°		61°
cos θ	.469		.500		
r·cos θ "	.198		.242		.220

Figure 32. Movie Analysis Sheet for Test No. 7-A

timing marks. These two integer numbers can be determined accurately.

All samples were scribed with two contrasting marks spaced approximately .1 inch apart. The time to burn between these two marks yielded an initial burn rate based on the camera film speed setting (CS = 1600 frames per second), projector speed (PR = 16 frames per second), and the projector time (PT = 22.9 seconds).

$$(\text{Burn rate})_{\text{initial}} = r_i = \frac{0.1 \times CS}{PR \times PT} \tag{D-1}$$

$$r_i = \frac{.1 \text{ inch} \times 1600 \text{ f/sec}}{16 \text{ f/sec } 22.9 \text{ sec}} \tag{D-2}$$

$$r_i = .437 \text{ inch/sec}$$

The final burn rate calculations based on the actual frame rate, the sample magnification and the sandwich profiles are obtained using the relation

$$r = f_{tl} \frac{f}{m} \frac{h}{F} \frac{w}{W} \tag{D-3}$$

where r is the sandwich vertical burn rate and f_{tl} is the timing light generator frequency. The number of 16 mm frames occurring between two corresponding timing marks is f. The number of timing marks occurring between corresponding timing marks is m. The projected and magnified sandwich vertical burn distance is h. The total number of frames for this sandwich vertical burn distance is F. The actual sample width is w and

projected and magnified width is W. For test no. 7-A the following values and an estimate of their accuracy were obtained for these quantities.

f_{t1}	(timing light frequency)	= 999.98	±	.01	hertz
f	(frames)	= 29.000	±	.001	frames
m	(timing marks)	= 18.00	±	.01	marks
h_L	(left side screen burn distance)	= 3.257	±	.02	inches
h_R	(right side screen burn distance)	= 3.740	±	.02	inches
F	(total number of frames)	= 315	±	1	frames
w	(sample width)	= .107	±	.001	inch
W	(screen width)	= 4.233	±	.02	inches

Substituting back into Equation D-3 gives the sandwich vertical burn rate as

$$r_L = 999.98 \times \frac{29}{18} \times \frac{3.257}{315} \times \frac{.107}{4.233} \frac{\text{inches}}{\text{sec}}$$

$$r_L = .421 \frac{\text{inch}}{\text{sec}} \quad \text{and} \quad r_R = .484 \frac{\text{inch}}{\text{sec}}$$

The average value of the surface slope was

$$\theta_L = 62 \pm 5^o \text{ and } \theta_R = 60 \pm 5^o .$$

The burn rate normal to the oxidizer surface is defined as $r_n = r \cos \theta$. For the left and right side this is

$$r_{n_L} = r_L \cos \theta_L = .198 \frac{\text{inch}}{\text{sec}} \qquad \text{(D-4)}$$

$$r_{n_R} = r_R \cos \theta_R = .242 \frac{\text{inch}}{\text{sec}}$$

The values that have been tabulated in Appendix E, Table 10 are the average of the left and right values. For test no. 7-A this is:

$$\text{sandwich vertical burn rate} = r = .452 \frac{\text{inch}}{\text{sec}}$$

$$\text{burn rate normal to the oxidizer surface} = r_n$$

$$= r \cos \theta = .220 \frac{\text{inch}}{\text{sec}}$$

Experimental indications of the accuracy of the various tests have been discussed in the main sections of the dissertation. A calculation of the accumulation of the various errors associated with these burn rate calculations can be made by expanding all quantities on the right side of Equation D-3 in a Taylor series and neglect the squares, products and higher powers of the error terms Δf_{t1}, Δf, Δm, Δh_L, ΔF, Δw, and ΔW.

The relative error of the sandwich vertical burn rate is:

$$\frac{\Delta r}{r} = \frac{\Delta f_{t1}}{f_{t1}} + \frac{\Delta f}{f} - \frac{\Delta m}{m} + \frac{\Delta h}{h} - \frac{\Delta F}{F} + \frac{\Delta w}{w} + \frac{\Delta W}{W} \qquad \text{(D-5)}$$

Since these error terms can be positive or negative the maximum error will be obtained for a summation of the absolute values.

$$\left(\frac{\Delta r}{r}\right)_{max} = \frac{\Delta f_{t1}}{f_{t1}} + \frac{\Delta f}{f} + \frac{\Delta m}{m} + \frac{\Delta h}{h} + \frac{\Delta F}{F} + \frac{\Delta w}{w} + \frac{\Delta W}{W} \qquad \text{(D-6)}$$

Substituting in Equation D-6 for test No. 7-A gives

$$\left(\frac{\Delta r}{r}\right)_{max} = \frac{.01}{999.98} + \frac{.001}{29} + \frac{.01}{18} + \frac{.02}{3.257} + \frac{1}{315} + \frac{.04}{.107} + \frac{.02}{4.233}$$

$$\left(\frac{\Delta r}{r}\right)_{max} = .024$$

$$(\Delta r)_{max} = .452 \times .024$$

$$(\Delta r)_{max} = .011 \text{ inch}$$

therefore

$$r = .452 \pm .011 \text{ inch}$$

This is indicative of the magnitude of the maximum error obtained in this data reduction technique. Making this same type of calculation for the burn rate normal to the oxidizer surface

$$\frac{\Delta r_n}{r_n} = \frac{\Delta r}{r} - \tan \theta \Delta\theta \qquad \text{(D-7)}$$

$$\left(\frac{\Delta r_n}{r_n}\right)_{max} = \frac{\Delta r}{r} + \Delta\theta \tan \theta \qquad \text{(D-8)}$$

$$\left(\frac{\Delta r_n}{r_n}\right)_{max} = .024 + \frac{5 \times}{180} \tan 62$$

$$\left(\frac{\Delta r_n}{r_n}\right)_{max} = .188$$

$$(\Delta r_n)_{max} = .085 \text{ inch}$$

$$r_n = r \cos \theta = .220 \pm .085 \text{ inch}$$

This text exhibited a steady regressing profile but there was still enough fluctuation of the surface profile slope to give a considerable uncertainty in the burn rate normal to the oxidizer surface.

Test No. 42-A

As this series of tests progressed several changes were made to obtain more information from the high speed motion pictures. The camera was elevated and tilted to give a possible view of the oxidizer surface. The sample was rotated with respect to the camera so that both the front and side of the sandwich could be viewed. This allowed us to determine if we were measuring the regression of a trailing edge of a burning surface and if the sample profile along the depth of the sample was regressing uniformly. A tracing of test no. 42-A is shown in Figure 33. This sample was made up of two weight percent Harshaw catalyst Cu 0202 P added to the ammonium perchlorate and 4.37 percent added to the hydroxyl terminated polybutadiene. The tracings in Figure 33 include the entire 16 mm frame. The data reduction shown on the Movie Analysis sheet of Figure 34 was taken from a larger tracing. The camera was tilted $4.8^{\circ} \pm .1^{\circ}$ for this test. No initial burn rate calculation was made. The following quantities and an estimate of their accuracy for this test are:

f_{t1}	(timing light frequency)	= 999.3	±	.1	hertz
f	(frames)	= 17	±	.001	frames
m	(timing marks)	= 11	±	.01	marks
h_L	(left side screen burn distance	= 5.784	±	.020	inches
h_R	(right side screen burn distance)	= 5.794	±	.020	inches
F	(total no. of frames)	= 250	±	1	frames

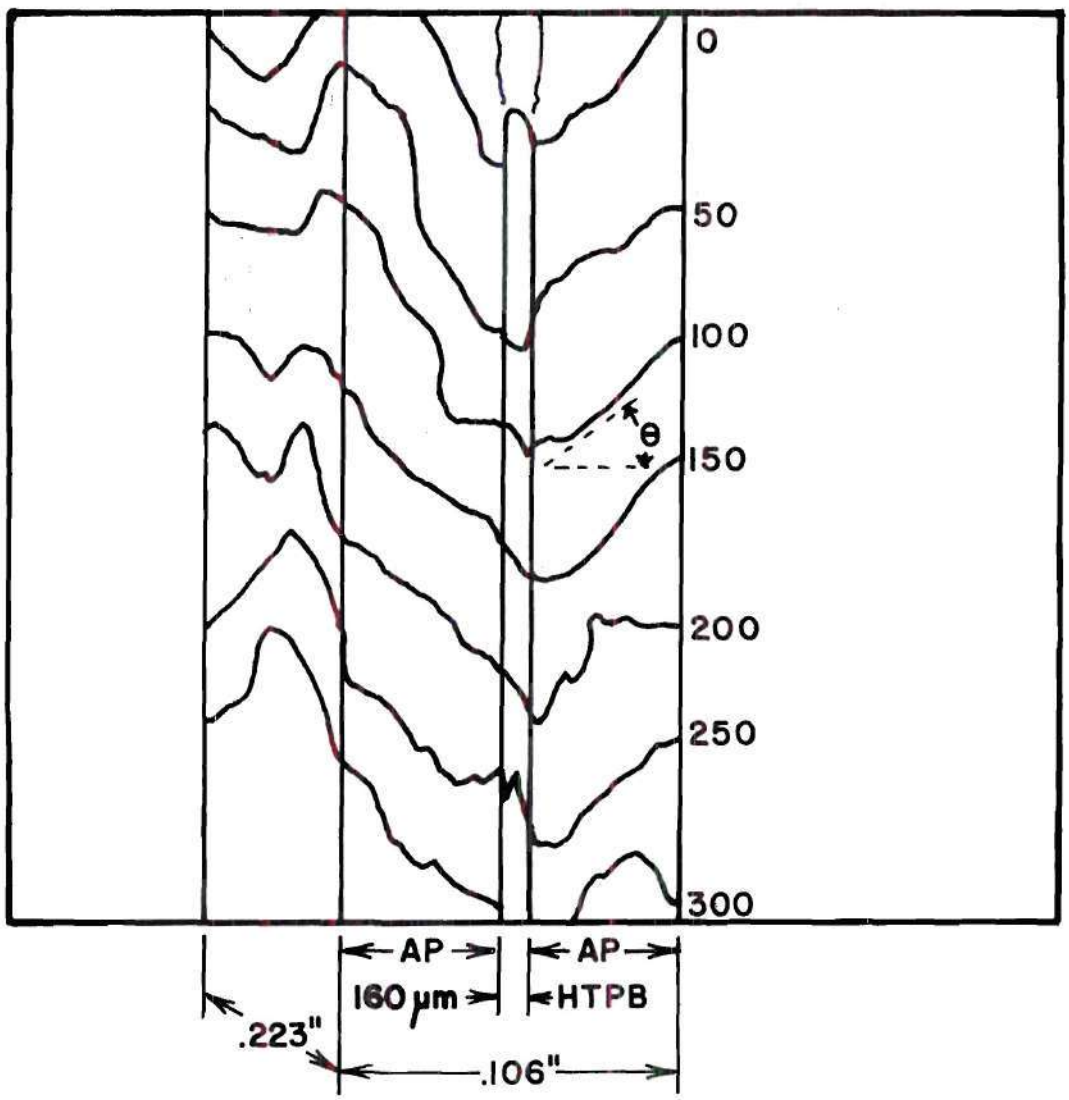

Figure 33. Sample Profiles for Test No. 42-A

MOVIE ANALYSIS

RUN NO. 42-A DATE 6-4-74

160 Mm

SAMPLE	AP	HTPB	AP		
DIMENSIONS	2.63mm .106"				
STUDY	2% CC	4.4% CC	2% CC		

PRESSURE 2000 psia. Depth = .2228"

MOVIE DESCRIPTION
FOCUS good
EXPOSURE f/2.8
SMOKE good

COMMENTS: Side close to light appears to burn faster. Lense was found to be defective on 5-31-74. White flame at binder layer, white smoke, pink glow from LHS, white vapor from RHS. (light from right)

FRAME RATE
CAMERA SETTING 1600 fps 1544.37 actual
TIMING MARKS 999.3 mps $\frac{\text{no. frames}}{\text{no. timing marks}} \frac{17}{11} = 1.5455 \frac{f}{t.m}$

$\beta = 4.8°$
$\alpha = 7.956°$
$\Delta h' = \frac{\Delta h}{\cos 4.8°}$

BURN RATE
INITIAL CAL $\frac{.1(\text{in}) \times CS(\text{fps})}{PR(\text{fps})\ PT(s)} =$ in./sec.

LENTH OF BURN	5.784 = h			5.795 = h	
FRAME COUNT	250 h' = 5.8044			250 h' = 5.8154	
sc.in./frame					

MAGNIFICATION $\frac{\text{screen}}{\text{actual}} \frac{2.925}{.1035} = 28.26$ sc.in./in.

BURN RATE = $999.3 \frac{m}{sec} \frac{17}{11} \frac{f}{fm} \frac{\Delta h' \text{ sc.in.}}{250 f} \frac{in}{sc.in.} \frac{.1035}{2.925} = \Delta h' \times .21859$

					average
r (in./sec.)	1.269		1.271		1.27
θ	50.248°		30.313°		41.3°
cos θ	.6395		.8633		
r·cos θ "	.811		1.097		.954

Figure 34. Movie Analysis Sheet for Test No. 42-A

f	(screen width)	=	.106 ± .003 inch
W	(screen width)	=	2.966 ± .02 inches
d	(sample depth)	=	.223 ± .001 inch
D	(screen depth	=	.880 ± .02 inch

The angle of the sample rotation, α, was determined geometrically using the following relationship

$$\tan \alpha = \frac{D}{W} \frac{w}{d} \tag{D-9}$$

Substituting in Equation D-9 for test No. 42-A

$$\tan \alpha = \frac{.880 \times .106}{2.966 \times .223} = .141^{o}$$

$$\alpha = 8.03^{o}$$

The maximum error associated with this determination of the rotation angle is given by

$$\frac{\Delta\alpha}{\cos \alpha \sin \alpha} = \frac{D}{D} + \frac{w}{w} + \frac{W}{W} + \frac{d}{d} \tag{D-10}$$

$$\Delta\alpha = .0086 \times \frac{180^{o}}{\pi} = 0.49^{o}$$

$$\alpha = 8.03 \pm .49^{o}$$

The average surface slope for the left and right sides of the sample from the tracings are $\theta_l = 47.05 + 5^{o}$ and $\theta_r = 36.13 + 5^{o}$. These angles are

distorted by the rotation of the sample. The correct angles can be found by using the following equations

$$\tan \theta_L' = \cos \alpha \tan \theta_L + \sin \alpha \qquad \text{(D-11)}$$

$$\tan \theta_R' = \cos \alpha \tan \theta_R - \sin \alpha \qquad \text{(D-12)}$$

Substituting into these equations gives

$$\theta_L = 50.3°$$

$$\theta_R = 30.3°$$

These angles are still accurate to $\pm 5^o$. The burn distance must be corrected for the tilt of the camera. The actual burn distance is given by

$$h' = \frac{h}{\cos B} = \frac{h}{\cos 4.8^o} \qquad \text{(D-13)}$$

$$h_L' = 5.804 \pm 0.020" \text{ and } h_R' = 5.814 \pm 0.020"$$

Substituting into Equation D-3 yields the sandwich vertical burn rate

$$r_L = 999.3 \times \frac{17}{11} \times \frac{5.804}{250} \times \frac{0.106 \times \cos 8.1}{2.966} = 1.269 \frac{\text{inches}}{\text{sec}}$$

$$r_R = 1.271 \text{ inches/sec}$$

The burn rate normal to the oxidizer surface is found by substituting

into Equation D-4.

$$r_{n_L} = r_L \cos \theta$$

$$r_{n_L} = 1.269 \cos 50.3^{o}$$

$$r_{n_L} = .811 \text{ inch/sec and } r_{n_R} = 1.097 \text{ inches/sec}$$

The average values of these quantities have been tabulated in Appendix E, Table 10.

$$\bar{r} = 1.270 \text{ inches/sec} \qquad \bar{r}_n = .954 \text{ inch/sec} \qquad \bar{\theta} = 41.3^{o}$$

The accumulation of possible errors for the sandwich vertical burn rate is found by substituting into the following equation:

$$\left(\frac{\Delta r}{r}\right)_{max} = \frac{\Delta f_{t1}}{f_{t1}} + \frac{\Delta f}{f} + \frac{\Delta m}{m} + \frac{\Delta h}{h} + \frac{\Delta F}{F} + \frac{\Delta w}{w} + \frac{\Delta W}{W} + \tan \qquad \text{(D-14)}$$

$$\left(\frac{\Delta r}{r}\right)_{max} = \frac{.1}{999.3} + \frac{.001}{17} + \frac{.01}{11} + \frac{.02}{5.804} + \frac{1}{250} + \frac{.003}{.106}$$

$$+ \frac{.02}{2.966} + \frac{.49}{180} \tan 8.03^{o}$$

$$\left(\frac{\Delta r}{r}\right)_{max} = .0447$$

$$\Delta r = .057 \text{ inch/sec}$$

The possible accumulation of error for the burn rate normal to the oxidizer

surface is found by substituting into Equation D-8:

$$\left(\frac{\Delta r_n}{r_n}\right)_{max} = 0.0447 + \frac{5}{180} \tan 41.3^{o}$$

$$\left(\frac{\Delta r_n}{r_n}\right)_{max} = .121$$

$$\Delta r_n = .116 \text{ inch/sec}$$

therefore:

$r = 1.27 \pm .06$ inches/sec and $r_n = .95 \pm .12$ inches/sec.

Test No. 8-B

The cinephotomacrography technique was used on the cast propellants also. A tracing of test no. 8-B is shown in Figure 35. This sample contained one weight percent of ferric oxide added to a bimodal ammonium perchlorate distribution (37 μm < 30% < 63 μm and 125 μm < 70% < 212 μm) with a 83/17 solids to binder loading. The entire 16 mm frame is shown in Figure 35. The data reduction shown on the Movie Analysis sheet of Figure 36 was taken from a larger tracing. The following quantities and an estimate of their accuracy for this test are:

f_{t1}	(timing light frequency)	= 999.4	± .1	hertz
f	(frames)	= 9	± .001	frames
m	(timing marks)	= 6	± .01	marks
h_l	(left side screen burn distance)	= 5.629	±	inches
h_R	(right side screen burn distance)	= 5.733	±	inches

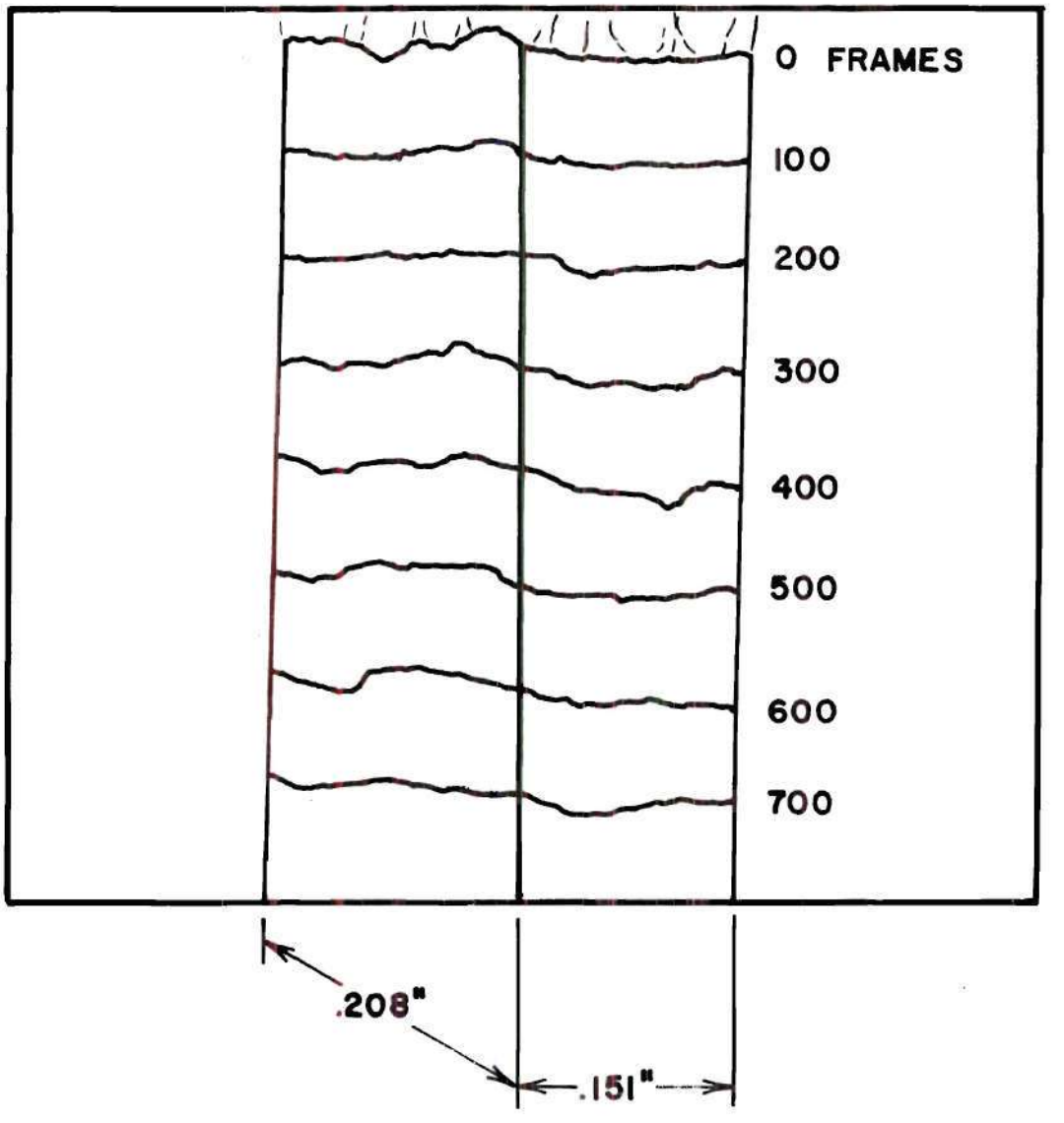

Figure 35. Sample Profiles for Test No. 8-B

MOVIE ANALYSIS

RUN NO. 8-B DATE 12-11-74

SAMPLE DIMENSIONS h = .8125" w = .151" d = .208"

STUDY PRESSURE 2000 composite cast propellant 1% Fe_2O_3 psia.

MOVIE DESCRIPTION
FOCUS good
EXPOSURE f/2.8 slightly overexposed for flame
SMOKE control good except at 600psia

COMMENTS: Orange flame, white flame froth comes off in flimsy sheets every 20-40 frames

FRAME RATE
CAMERA SETTING 1600 fps 1499.1
TIMING MARKS 9994 mps $\frac{\text{no. frames}}{\text{no. timing marks}} \frac{9}{6} = 15 \frac{f}{t.m}$

BURN RATE
INITIAL CAL $\frac{.1(\text{in}) \times CS\,(\text{fps})}{PR(\text{fps})\ PT(s)} = \quad \text{in./sec.}$

LENTH OF BURN	5.629	5.733			
FRAME COUNT	700	700			
sc.in./frame					

MAGNIFICATION $\frac{\text{screen}}{\text{actual}} \frac{1.770}{.151 \cos\alpha} = 14.697$ sc.in./in.

$.120$

BURN RATE = $999.4 \frac{m}{sec} \frac{9}{6} \frac{f}{fm} \frac{\Delta h}{700 f} \frac{sc.in.}{in} \frac{in}{sc.in.} (14.697)^{-1} = \Delta h \times .1457$ average

r (in./sec.)	.820	.835			.828
θ					
cos θ					
r·cos θ "					

Figure 36. Movie Analysis Sheet for Test No. 8-B

F	(total number of frames)	=	700	±	frames
w	(sample width)	=	.151	± .002	inch
W	(screen width)	=	1.770	± .01	inches
d	(sample depth)	=	.208	± .002	inch
D	(screen depth)	=	1.844	± .01	inches

The angle of the sample rotation, α, was determined using Equation D-9. Substituting in for test no. 8-B gives

$$\tan \alpha = \frac{1.844}{1.770} \quad \frac{.151}{.208}$$

$$\alpha = 37.10^{o}$$

Substituting into Equation D-10 yields an indication of the accuracy.

$$\frac{\Delta\alpha}{\cos \alpha \sin \alpha} = \frac{.01}{1.844} + \frac{.002}{.151} + \frac{.01}{1.770} + \frac{.002}{.208}$$

$$\Delta\alpha = .016 \times \frac{180}{} = .94^{o}$$

therefore,

$$\alpha = 37.10 \pm .94^{o}$$

The sample vertical burn rate is found by substituting into Equation D-3.

$$r_1 = 999.4 \times \frac{9}{6} \times \frac{5.629}{700} \times \frac{.551}{1.770} \cos 37.1$$

$$r_1 = .820 \frac{\text{inch}}{\text{sec}} \qquad \text{and} \qquad r_R = .835 \frac{\text{inch}}{\text{sec}}$$

$$\bar{r} = .828 \text{ inch/sec}$$

The accumulation of possible maximum error for the sample burn rate is found by substituting into Equation

$$\left(\frac{\Delta r}{r}\right)_{max} = \frac{.1}{999.4} + \frac{.001}{9} + \frac{.01}{6} + \frac{.02}{5.629} + \frac{1}{700} + \frac{.002}{.151}$$

$$+ \frac{.01}{1.770} + .016 \tan 37.1$$

$$\left(\frac{\Delta r}{r}\right)_{max} = .038 \quad \text{and} \quad \Delta r = .031$$

therefore,

$$r = .828 \pm .031 \text{ inch/sec.}$$

APPENDIX E

RUN DATA RECORDS

Quenched Combustion Samples

Tests 133 through 220 were quenched combustion tests to obtain partially burned samples for scanning electron microscope observations. The four catalysts, Harshaw catalyst Cu 0202 P (CC), ferric oxide (IO), iron blue (IB), and ferrocene (F) were loaded in the oxidizer, binder or at the binder-oxidizer interface. Tests were conducted at 600, 1000, 1500 and 2000 psia. Double sandwiches of two layers of polycrystalline ammonium perchlorate separated by one layer of binder and triple sandwiches of three layers of polycrystalline ammonium perchlorate separated by two layers of binder were used for this series of tests. A slight nitrogen flow was maintained to prevent a pressure build up during the combustion process. A variable electronic time delay was used to allow a definite period of time from combustion of the sample until quenching of the combustion process by rapid depressurization of the combustion chamber. This time delay varied from .75 to .022 second. An experimentally determined number of .005 inch thick Mylar disks was used to contain the pressure. These disks were ruptured by a heated nichron wire inserted between the two outer Mylar disks.

All of these samples were cut with no slope on the top surface. The physical size and results of these tests are tabulated in Table 9.

Table 9. Run Data Records for Quenched Combustion Samples

Run No.	133	134	135	136	137	138	139	140	141	142
Sandwich	double	double	double	double	double	double	double	double	double	triple
Catalyst and Amount	none	none	none	none	none	none	none	2% CC	2% IO	2% IB 2% F
Location								in AP	in AP	in AP
Binder Thickness	150μm	150μm	150μm	145μm	150μm	150μm	150μm	130μm	125μm	IB110μm F 130μm
Width	.101"	.102"	.100"	.100"	.103"	.102"	.102"	.104"	.107"	.156"
Depth	.201"	.168"	.195"	.166"	.177"	.143"	.168"	.195"	.193"	.201"
Top Angle	0°	0°	0°	0°	0°	0°	0°	0°	0°	0°
Pressure	600	600	1000	1500	2000	1500	600	1000	1000	1000
No. of Disks	4	3	5	7	9	7	3	5	5	5
Time Delay	.5	.5	.5	.5	.5	.5	.75	.3	.5	.5
Comments	no quench	poor ignition	SEM	only half sample burnt	SEM	SEM	SEM	SEM	delay time too long	no sample left

(Continued)

Table 9. (Continued)

Run No.	143	144	145	146	147	148	149	150	151	152
Sandwich	double	triple	triple	triple	double	double	triple	triple	double	double
Catalyst and Amount	2% IO	2% F 2% IB	2% F 2% IB	2% F 2% IB	2% CC	2% IO	2% F 2% IB	2% F 2% IB	2% CC	2% CC
Location	in AP	in AP	in AP	in AP	in AP	in AP	in AP	in AP	in AP	in AP
Binder Thickness	100μm	F 125μm IB 100μm	F 125μm IB 125μm	F 125μm IB 120μm	150μm	100μm	F 125μm IB 125μm	F 125μm IB 125μm	100μm	100μm
Width	.108"	.163"	.158"	.163"	.106"	.106"	. -	.162"	.106"	.107"
Depth	.148"	.194"	.204"	.187"	.202"	.161"	-	.175"	.205"	.184"
Top Angle	0°	0°	0°	0°	0°	0°	0°	0 0°	0°	0°
Pressure	1000	1000	1500	600	600	600	1000	1000	1000	1500
No. of Disks	5	5	7	3	3	3	5	5	5	7
Time Delay	.3	.3	.2	.2	.3	.4	.30	.30	.2	.15
Comments	SEM	SEM	no sample left	SEM	SEM	unsym. burn	no sample left	unsym. burn	insuf. ignition	SEM

(Continued)

Table 9. (Continued)

Run No.	153	154	155	156	157	158	159	160	161	162
Sandwich	double	triple	double	double	double	double	double	double	double	double
Catalyst and Amount	2% CC	2% CC 2% IO	2% CC	2% CC	2% IO	2% IO	2% IO	2% IO	2% IO	2% IO
Location	in AP	inter-face	in AP	in AP	in AP	in AP	in AP	in AP	in AP	in AP
Binder Thickness	100μm	100μm	125μm	125μm	150μm	125μm	125μm	125μm	125μm	150μm
Width	.106"	-	.106"	.106"	.105"	.108"	.108"	.102"	.103"	.106"
Depth	.205"	-	.199"	.185"	.211"	.209"	.209"	.193"	.191"	.211"
Top Angle	0°	0°	0°	0°	0°	0°	0°	0°	0°	0°
Pressure	1000	1000	2000	2000	2000	1500	1000	600	1500	1000
No. of Disks	5	5	9	9	9	7	5	3	7	5
Time Delay	.3	.3	.1	.7	.3	.28	.15	.25	.16	.15
Comments	SEM	no sample left	no sample left	sample broken	reject-ed	no ignition	reject-ed	-	reject-ed	-

(Continued)

Table 9. (Continued)

Run No.	163	164	165	166	167	168	169	170	171	172
Sandwich	double	triple	triple	triple	triple	triple	triple	triple	triple	triple
Catalyst and Amount	2% IO	4.4% CC 4.4% IO	4.4% IB 4.4% F	4.4% CC 4.4% IO	4.4% IB 4.4% F	4.4% CC 4.4% IO	4.4% IB 4.4% F	4.4% CC 4.4% IO	4.4% IB 4.4% F	2% IB 2% F
Location	in AP	binder	binder	binder	binder	binder	binder	binder	binder	inter-face
Binder Thickness	150 μm	CC 150 μm IO 125 μm	IB 120 μm F 125 μm	CC 150 μm IO 125 μm	IB 125 μm F 125 μm	CC 150 μm IO 125 μm	IB 125 μm F 125 μm	CC 150 μm IO 125 μm	IB 125 μm F 125 μm	IB 100 μm F 175 μm
Width	.108"	.159"	.160"	.159"	.160"	.160"	.158"	.158"	.160"	.160"
Depth	.210"	.172"	.169"	.173"	.206"	.172"	.206"	.180"	.172"	.169"
Top Angle	0°	0°	0°	0°	0°	0°	0°	0°	0°	0°
Pressure	600	1000	1000	600	600	2000	2000	1500	1500	600
No. of Disks	3	5	5	3	3	9	9	7	7	3
Time Delay	.25	.41	.40	.51	.52	.48	.40	.35	.34	.51
Comments	-	SEM	SEM	SEM	-	SEM	SEM	SEM	no sample left	IB burnt to base

(Continued)

Table 9. (Continued)

Run No.	173	174	175	176	177	178	179	180	181	182
Sandwich	triple	triple	triple	triple	triple	triple	double	double	triple	triple
Catalyst and Amount	2% IB 2% F	2% IB 2% F	2% IB 2% F	2% IB 2% F	2% CC 2% IO	2% CC 2% IO	2% CC	2% IO	2% IB 2% F	2% IB 2% F
Location	inter-face	inter-face	inter-face	inter-face	inter-face	inter-face	in AP	in AP	in AP	in AP
Binder Thickness	IB 150 μm F 150 μm	IB 130 μm F 150 μm	IB 150 μm F 170 μm	IB 150 μm F 150 μm	CC 150 μm IO 150 μm	CC 150 μm IO 125 μm	CC 130 μm	IO 125 μm	IB 150 μm F 150 μm	IB 150 μm F 150 μm
Width	.158"	.163"	.166"	.170"	.165"	.166"	.109"	.104"	.164"	.161"
Depth	.156"	.198"	.171"	.190"	.194"	.170"	.189"	.276"	.164"	-
Top Angle	0°	0°	0°	0°	0°	0°	0°	0°	0°	0°
Pressure	600	600	2000	1000	600	1000	2000	2000	2000	2000
No. of Disks	3	3	9	5	3	5	9	9	9	9
Time Delay	-	.26	.09	.13	.27	.28	.10	.20	.23	-
Comments	dia-phragm wire shorted	SEM	burnt to base	SEM	SEM	-	SEM	SEM	delay time too long	apparent self-ignition

(Continued)

Table 9. (Continued)

Run No.	183	184	185	186	187	188	189	190	191	192
Sandwich	triple	double	double	double	double	triple	double	triple	triple	triple
Catalyst and Amount	2% IB 2% F	2% IO	2% IO	2% IO	2% IO	2% IB 2% F	2% IO	2% IB 2% F	2% CC 2% IO	2% CC 2% IO
Location	in AP	in AP	in AP	in AP	in AP	in AP	in AP	in AP	inter-face	inter-face
Binder Thickness	150μm	125μm	150μm	150μm	150μm	IB 125μm F 125μm	125μm	125μm	125μm	125μm
Width	.157"	.101"	.101"	.105"	.105"	.163"	.103"	.162"	.158"	.160"
Depth	.153"	.172"	.155"	.194"	.174"	.177"	.193"	.182"	.133"	.234"
Top Angle	0°	0°	0°	0°	0°	0°	0°	0°	0°	0°
Pressure	2000	1500	1000	1000	1500	1500	1500	1500	2000	1000
No. of Disks	9	7	5	5	7	7	7	7	9	5
Time Delay	.15	.21	.15	.15	.11	.19	.08	.11	.14	.19
Comments	apparent self ignition	burnt to base	no ignition	SEM	burnt to base	F burnt to base	burnt to base	SEM	CC burnt to base	SEM

(Continued)

Table 9. (Continued)

Run No.	193	194	195	196	197	198	199	200	201	202
Sandwich	triple	triple	triple	triple	triple	triple	triple	triple	triple	triple
Catalyst and Amount	2% CC 2% IO	2% CC 2% IO	4.4% IB 4.4% F	2% IB 2% F	2% IB 2% F	2% CC 2% IO	2% CC 2% IO	2% IB 2% F	2% IB 2% F	2% IB 2% F
Location Binder	interface	interface	binder	interface	interface	interface	interface	interface	interface	interface
Thickness	125 μm	125 μm	150 μm	150 μm	IB 140 μm F 150 μm	150 μm	150 μm	150 μm	IB 200 μm F 150 μm	150 μm
Width	.160"	.160"	.166"	.163"	.172"	.161"	.161"	.164"	.161"	.162"
Depth	.206"	.206"	.196"	.226"	.228"	.228"	.228"	.199"	.190"	.219"
Top Angle	0°	0°	0°	0°	0°	0°	0°	0°	0°	0°
Pressure	1500	2000	1500	1500	1500	2000	2000	2000	1500	1500
No. of Disks	7	9	7	7	7	9	9	9	7	7
Time Delay	.17	.11	.34	.11	.06	.14	.15	.024	.047	.022
Comments	SEM	-	SEM	F burnt to base	F burnt to base	diaphragm ruptured early	SEM	SEM	burnt to base	burnt to base

(Continued)

Table 9. (Continued)

Run No.	203	204	205	206	207	208	209	210	211	212
Sandwich	triple	double	double	triple	double	triple	double	triple	triple	double
Catalyst and Amount	2% IB 2% F	2% IO	2% CC	2% IB 2% F	2% CC	2% IB 2% F	2% CC	2% IB 2% F	2% IB 2% F	2% CC
Location	inter-face	in AP	in AP	in AP	in AP	in AP	in AP	in AP	in AP	in AP
Binder Thickness	150 μm	150 μm	150 μm	150 μm	150 μm	150 μm	150 μm	150 μm	150 μm	150 μm
Width	.163"	.104"	.111"	.160	.107"	.160"	.107"	.159"	.156"	.104"
Depth	.222"	.210"	.239"	.215"	.182"	.220"	.180"	.221"	.192"	.225"
Top Angle	0°	0°	0°	0°	0°	0°	0°	0°	0°	0°
Pressure	1500	1500	2000	2000	2000	2000	2000	2000	2000	2000
No. of Disks	7	7	9	9	9	9	9	9	9	9
Time Delay	.032	.029	.074	.058	.023	.032	.025	.022	.032	.026
Comments	-	SEM	-	SEM	burnt to base	SEM	-	ignition wire dropped onto AP	SEM red and white residue on IB	burnt to base

(Continued)

Table 9. (Continued)

Run No.	213	214	215	216	217	218	219	220		
Sandwich	double	double	single	single	double	double	double	double		
Catalyst and Amount	new F	2% CC	none	2% IB	new F	new F	new F	new F		
Location	binder	in AP	-	in AP	binder	binder	binder	binder		
Binder Thickness	150μm	150μm	-	-	125μm	125μm	150μm	125μm		
Width	.103"	.103"	.049"	.051"	.106"	.103"	.106"	.106"		
Depth	.205"	.244"	.186"	.206"	.205"	.210"	.207"	.218"		
Top Angle	0°	0°	0°	0°	0°	0°	0°	0°		
Pressure	1000	2000	1000	1000	1000	1000	1000	1000		
No. of Disks	5	9	5	5	5	5	5	5		
Time Delay	.40	.031	.23	.22	.30	.18	.11	.22		
Comments	-	SEM	for micro-probe	for micro-probe	burnt down edges	burnt to base	--	SEM		

Cinephotomacrography of Sandwiches for Synergistic Effects

Tests 1-A through 46-A were used to determine the existence of a synergistic effect on sandwich vertical burn rate of various combinations of catalysts. All combinations of Harshaw catalyst Cu 0202 P (CC), ferric oxide (IO), iron blue (IB) and ferrocene (F) were tested at 600 psia. The Cu 0202 P--ferric oxide and iron blue--ferric oxide systems were chosen for testing over the 300 to 2000 psia range. The volumetric loading of catalyst was maintained constant in the sandwich. For a two weight percent of catalyst added to the ammonium perchlorate 4.37 weight percent was added hydroxyl terminated polybutadiene binder. The binder thickness was maintained at a nominal value of 150 μm by use of a .005 inch Teflon shim.

The camera speed was set at 1600 frames per second. The latent image magnification (object to image size) was maintained at two for the first 12 tests and one for the rest of these tests. The light source was a 2500 watt xenon lamp maintained at its minimum current of 60 amperes. The film was Kodak Ektachrome EF 7241 (daylight) with a specification number 430. It was designated as 16 mm film for High Speed Cameras. One bottle of high pressure nitrogen was connected to the gas manifold for each test.

The physical size and the results of these tests are tabulated in Table 10. The top surface was sloped to insure a view of the leading edge of the regressing surface. The nitrogen flow was adjusted to give a velocity of one foot per second in the test section. The actual nitrogen orifice ΔP is listed in pounds per square inch (psia). The camera was tilted to obtain a possible view of the regressing surface.

Table 10. Run Data Records for Cinephotomacrography of Sandwiches for Synergistic Effects

Run No.	1-A	2-A	3-A	4-A	5-A	6-A	7-A	8-A	9-A	10-A
Catalyst and Amount	2% CC	2% CC	1% CC 1% IO	1% CC 1% F	1% CC 1% IB	1% IO 1% F	1% IO 1% IB	2% F	1% F 1% IB	2% IB
Binder Thickness	190 μm	190 μm	220 μm	280 μm	240 μm	220 μm	150 μm	160 μm	150 μm	180 μm
Width	.112"	.112"	.108"	.113"	.103"	.114"	.110"	.106"	.106"	.109"
Depth	.212"	.212"	.202"	.181"	.218"	.205"	.211"	.181"	.198"	.207"
Top Angle	10°	10°	10°	10°	10°	10°	10°	10°	10°	10°
Pressure	600	600	600	600	600	600	600	600	600	600
Orifice ΔP	2.2	2.2	2.2	2.2	2.2	2.2	2.2	2.2	2.2	2.2
Camera Tilt	-	-	-	-	-	-	-	-	-	-
Camera f-stop	4	4	4	4	1.8	5.6	4	5.6	4	4
Frame Rate	-	1646.8	1541.7	1579.2	1687.8	1611.2	1611.1	1600.0	1618.9	1587.9
θ	-	50.8°	56.1°	48.3°	19.9°	34.8°	60.9°	61.3°	39.1°	56.5°
r	-	.558	.645	.432	.501	.436	.452	.275	.397	.370
r cosθ	-	.353	.360	.288	.471	.358	.220	.132	.308	.204
	no burn									

(Continued)

Table 10. (Continued)

Run No.	11-A	12-A	13-A	14-A	15-A	16-A	17-A	18-A	19-A	20-A
Catalyst and Amount	none	2% IO	none	2% CC	2% IO	2% IB	2% F	1% CC 1% F	2% CC	1% IB 1% IO
Binder Thickness	150 μm	160 μm	190 μm	190 μm	160 μm	200 μm	200 μm	200 μm	200 μm	160 μm
Width	.112"	.110"	.114"	.112"	.108"	.113"	.112"	.114"	.110"	.111"
Depth	.195"	.185"	.215"	.265"	.186"	.214"	.156"	.190"	.180"	.184"
Top Angle	10°	10°	5°	5°	25°	10°	10°	10°	10°	5°
Pressure	600	600	600	600	600	600	600	600	600	2000
Orifice ΔP	2.2	2.2	2.2	2.2	2.2	2.2	2.2	2.2	2.2	7.1
Camera Tilt	-	-	4°	5°	5.5°	4.4°	4.5°	4.4°	4.2°	4.2°
Camera f-stop	5.6	4	5.6	4	4	4	4	4	4	4
Frame Rate	1631.5	1624.7	1681.6	1832.9	1666.3	2052.2	1839.6	1706.7	1721.0	1709.4
θ	16.0°	49.7°	18.2°	44.0°	42.0°	57.7°	61.4°	51.5°	49.4°	54.6°
r	.231	.314	.209	.730	.354	.518	.332	.400	.506	1.428
r cosθ	.222	.203	.198	.525	.262	.277	.159	.248	.329	.828

(Continued)

Table 10. (Continued)

Run No.	21-A	22-A	23-A	24-A	25-A	26-A	27-A	28-A	29-A	30-A
Catalyst and Amount	1% IO 1% IB	1% IO 1% IB	1% IO 1% IB	1% CC 1% IO	1% CC 1% IO	1% CC 1% IO	1% CC 1% IO	none	2% IB	2% IB
Binder Thickness	200μm	100μm	200μm	250μm	170μm	160μm	190μm	210μm	210μm	160μm
Width	.111"	.109"	.111"	.112"	.109"	.113"	.110"	.112"	.114"	.112"
Depth	.238"	.252"	.182"	.216"	.195"	.183"	.186"	.199"	.174"	.183"
Top Angle	5°	5°	5°	5°	5°	5°	5°	10°	5°	10°
Pressure	1500	1000	300	2000	1500	1000	300	2000	2000	2000
Orifice ΔP	5.4	3.6	1.1	7.1	5.4	3.6	1.1	7.1	7.1	7.1
Camera Tilt	4.5°	5°	5.5°	4°	4°	4.8°	3.8°	4°	4.5°	4.4°
Camera f-stop	4	4	4	4	4	4	4	4	1.8	1.8
Frame Rate	1642.7	1642.9	1614.4	1615.7	1636.7	1643.2	1636.7	1882.0	1550.2	1733.5
θ	42.5°	46.1°	40.7°	47.6°	47.2°	36.5°	41.0°	-4.2°	34.7°	42.0°
r	.922	.550	.254	1.450	1.839	.689	.236	.295	1.379	1.096
r cosθ	.680	.382	.192	.978	1.248	.554	.178	.294	1.133	.814

(Continued)

Table 10. (Continued)

Run No.	31-A	32-A	33-A	34-A	35-A	36-A	37-A	38-A	39-A	40-A
Catalyst and Amount	none	2% IB	none	2% IB	2% IO	none	2% IB	2% IO	2% IO	none
Binder Thickness	240μm	200μm	190μm	200μm	180μm	210μm	200μm	150μm	220μm	220μm
Width	.113"	.109"	.112"	.110"	.108"	.110"	.114"	.107"	.115"	.112"
Depth	.213"	.200"	.288"	.206"	.208"	.208"	.184"	.211"	.292"	.274"
Top Angle	10°	5°	10°	10°	10°	10°	10°	5°	5°	10°
Pressure	1500	1500	1000	1000	1000	300	300	300	1500	1500
Orifice ΔP	5.4	5.4	3.6	3.6	3.6	1.1	1.1	1.1	5.4	5.4
Camera Tilt	4.2°	4.5°	5.0°	5.2°	5.1°	5.0°	4.8°	5.0°	5.0°	5.5°
Camera f-stop	4	1.8	4	1.8	1.8	4	1.8	1.8	1.8	1.8
Frame Rate		1769.6	1692.6		1500.4	1667.0	1667.0	1667.0	1714.6	1787.3
θ		46.9°	27.3°		47.7°	41.8°	48.7°	47.6°	45.3°	0
r		1.094	.661		.614	.180	.218	.230	.851	.352
r cosθ		.748	.588		.413	.134	.144	.155	.598	.352
	no burn			flash down LHS						

(Continued)

Table 10. (Continued)

Run No.	41-A	42-A	43-A	44-A	45-A	46-A				
Catalyst and Amount	none	2% CC	2% CC	2% CC	2% IB	2% CC				
Binder Thickness	150μm	160μm	200μm	200μm	250μm	180μm				
Width	.112"	.106"	.108"	.108"	.117"	.108"				
Depth	.206"	.223"	.218"	.212"	.192"	.217"				
Top Angle	10°	10°	10°	10°	10°	10°				
Pressure	1000	2000	1500	1000	1000	1000				
Orifice ΔP	3.6	7.1	5.4	3.6	3.6	3.6				
Camera Tilt	4.8°	4.8°	5.0°	4.4°	4.9°	5.2°				
Camera f-stop	4	2.8	2.8	2.8	2.8	2.8				
Frame Rate	1638.0	1544.4	1538.3	1428.6	1533.3	1478.3				
θ	14.9°	41.3°	48.4°	43.9°	45.9°	46.2°				
r	.282	1.270	.986	.586	.534	.622				
r cosθ	.272	.954	.655	.422	.372	.430				

The frame rate was determined from the timing light marks at the edge of the film and an accurate measurement of the timing light generator frequency. The slope of the deflagrating surface with respect to horizontal, θ, is given in degrees. The sandwich vertical burn rate, r, and the oxidizer normal regression rate, r cos θ, are given in inches per second.

Cinephotomacrography of Cast Propellants

Tests 1-B through 26-B were used to determine the combined effect of two catalysts on the sandwich vertical burn rate. Two systems were suggested by the two-dimensional sandwich testing. Harshaw catalyst Cu 0202 P (CC)--ferric oxide (IO) and iron blue (IB)--ferric oxide (IO) have been evaluated at 600 and 2000 psia. The iron blue--ferric oxide system was tested over the 300 to 2000 psia range. The total catalyst loading was maintained at one weight percent. The binder was hydroxyl terminated polybutadiene. The oxidizer was ammonium perchlorate. The binder to oxidizer ratio was maintained at 17/83. The oxidizer size distribution was

$$37\ \mu m < 15\% < 45\ \mu m \text{ and } 45\ \mu m < 15\% < 63\ \mu m$$

$$125\ \mu m < 35\% < 180\ \mu m \text{ and } 180\ \mu m < 35\% < 212\ \mu m$$

The camera speed was set at 1600 frames per second for all tests. The latent image magnification (object to image size) was maintained at .64 for all tests. The light source was a 2500 watt xenon lamp maintained at its minimum current of 60 amperes. The film was Kodak Ektachrome EF 7241 (daylight) with a specification number 430. It was designated as 16 mm film for High Speed Cameras. One bottle of high pressure nitrogen

was connected to the gas manifold for each test.

The physical size and the results of these tests are tabulated in Table 11. The initial nitrogen flows were higher than previous cinephotomacrography tests. This was because of the difficulty encountered with the fuse wire tests of the cast propellants. This flow was reduced as the test series continued. The tabulated rotation refers to orientation of the sample so that the camera can view the burn rate of both the sample width and depth. The burn rate, r, is given in inches per second and is an average value of both sides.

Table 11. Run Data Records for Cinephotomacrography of Cast Propellants

Run No.	1-B	2-B	3-B	4-B	5-B	6-B	7-B	8-B	9-B	10-B
Catalyst and Amount	none	1% IO	1% IB	.5% IO .5% IB	1% CC	.5% CC .5% IO	none	1% IO	1% IB	.5% IO .5% IB
Height	.781"	.812"	.766"	.766"	.812"	.812"	.812"	.812"	.828"	.797"
Width	.129"	.142"	.153"	.162"	.160"	.174"	.132"	.151"	.123"	.158"
Depth	.219"	.219"	.234"	.250"	.230"	.250"	.183"	.208"	.200"	.162"
Pressure	600	600	600	600	600	600	2000	2000	2000	2000
Orifice ΔP	10	10	10	10	10	10	8	8	16	16
Camera f-stop	4	2.8	1.8	1.8	1.8	1.8	4	2.8	2.8	2.8
Frame Rate	1600.8	1583.0	1571.0	1600.0	1599.4	1573.8	1501.0	1499.1	1499.1	1514.4
Rotation	12.5°	6.8°	42.7°	35.6°	36.3°	49.0°	33.1°	37.1°	32.0°	33.9°
r	.359	.452	.544	.539	.511	.483	.663	.828	.783	.879

(Continued)

Table 11. (Continued)

Run No.	11-B	12-B	13-B	14-B	15-B	16-B	17-B	18-B	19-B	20-B
Catalyst and Amount	1% CC	.5% CC .5% IO	none	none	none	none	1% IO	1% IC	1% IOL	1% IB
Height	.812"	.812"	.771"	.762"	.772"	.762"	.781"	.800"	.758"	.750"
Width	.139"	.128"	.116"	.098"	.099"	.110"	.120"	.125"	.111"	.087"
Depth	.213"	.156"	.185"	.185"	.186"	.169"	.206"	.216"	.214"	.216"
Pressure	2000	2000	1500	1000	600	300	1500	1000	300	1000
Orifice ΔP	16	16	5.4	3.6	3.6	3.6	5.4	3.6	3.6	3.6
Camera f-stop	2.8	2.8	1.8	4	4	4	4	4	4	4
Frame Rate	1544.8	1587.7	1297.8	1633.9	1627.4	-	1659.2	1637.8	1653.5	1609.7
Rotation	34.8°	40.1°	38.0°	31.9°	27.6°	-	38.7°	35.1°	34.6°	42.6°
r	.738	.794	.581	.406	.318	- no film end of 400' reel	.985	.822	.489	.800

(Continued)

Table 11. (Continued)

Run No.	21-B	22-B	23-B	24-B	25-B	26-B				
Catalyst and Amount	1% IB	1% IB	.5% IB .5% IO	.5% IB .5% IO	.5% IB .5% IO	none				
Height	.750"	.800"	.760"	.750"	.750"	.750"				
Width	.101"	.086"	.099"	.099"	.105"	.117"				
Depth	.212"	.194"	.190"	.190"	.192"	.173"				
Pressure	300	1500	1500	1000	300	300				
Orifice ΔP	3.6	5.4	5.4	3.6	3.6	3.6				
Camera f-stop	2.8	2.8	2.8	2.8	2.8	4				
Frame Rate	1609.7	1603.8	1575.4	1574.6	1574.6	1565.6				
Rotation	38.9°	44.1°	35.1°	40.1°	36.8°	41.0°				
r	.465	.759	.747	.622	.515	.335				

BIBLIOGRAPHY

1. Varney, A. M., "An Experimental Investigation of the Burning Mechanisms of Ammonium Perchlorate Composite Solid Propellants," Ph.D. Dissertation, Georgia Institute of Technology (1970).

2. Jones, H. E., "An Experimental Investigation Relating to the Combustion Mechanism of Ammonium Perchlorate Composite Propellants," Ph.D. Dissertation, Georgia Institute of Technology, 1971.

3. Varney, A. M. and Strahle, W. C., "Experimental Combustion Studies of Two-Dimensional Ammonium Perchlorate-Binder Sandwiches," Combustion Science and Technology, 4, 197-208 (1972).

4. Ashmore, P. G., Catalysis and Inhibition of Chemical Reactions; Butterworth & Co., London, 1963.

5. Boggs, T. L., Zurn, D. E., and Cordes, H. F., "The Combustion of Ammonium Perchlorate and Various Inorganic Additives," AIAA Paper No. 75-233 (1975).

6. Pearson, G. S. and Sutton, D., "Composite Solid Propellant Ignition: Ignition of Ammonia and Other Fuels by Perchloric Acid Vapor," AIAA Journal, 5, 344-346 (1967).

7. Pearson, G. S. and Sutton, D., "Catalyzed Ignition of Composite Propellant Fuels by Perchloric Acid Vapor," AIAA Journal, 5(11), 2101-2103 (1967).

8. Thomas, C. L., Catalytic Processes and Proven Catalysts; Academic Press, New York, 1970.

9. Levy, J. B. and Friedman, R., "Further Studies of Pure Ammonium Perchlorate Deflagration," in Eighth Symposium (International) on Combustion; Williams and Wilkins, Baltimore, 1962, pp. 663-672.

10. Arden, E. A., Powling, J., and Smith, W. A. W., "Observations on the Burning of Ammonium Perchloric," Combustion and Flame, 6, 21-33 (1962).

11. Evans, M. W., Beyer, R. B., and McCulley, L., "Initiation of Deflagration Waves at Surfaces of Ammonium Perchlorate-Copper Chromite-Carbon Pellets," Journal of Chemical Physics, 40(9), 2431-2438 (1964).

BIBLIOGRAPHY (Continued)

12. Solymosi, R. and Krix, E., "Catalysis of Solid Phase Reactions: Effect of Doping of Cupric Oxide Catalyst on the Thermal Decomposition and Explosion of Ammonium Perchlorate," Journal of Catalysis, 1, 468-480 (1962).

13. Solymosi, F. and Fonagy, K., "Effect of Cadmium Oxide and Cadmium Perchlorate on the Decomposition and Ignition of Ammonium Perchlorate," in Eleventh Symposium (International) on Combustion; The Combustion Institute, Pittsburgh, 1967, pp. 429-437.

14. Solymosi, F., Börcsök, S., and Lázár, E., "Catalytic Decomposition of Perchloric Acid in the Vapor Phase," Combustion and Flame, 12, 398-400 (1968).

15. Solymosi, F., Gera, L., and Börcsök, S., "Catalytic Pyrolysis of $HClO_4$ and Its Relation to the Decomposition and Combustion of NH_4ClO_4," in Thirteenth Symposium (International) on Combustion; The Combustion Institute, Pittsburgh, 1971, pp. 1009-1017.

16. Glaskova, A. P., "On Deceleration of Chemical Reactions in Deflagration," Combustion and Flame, 13, 55-62 (1969).

17. Glaskova, A. P., "Mechanism of the Synergistic Effect During Combustion of Ammonium Perchlorate with Inhibitors of Various Classes," Doklady Adademii Nauk SSSR, 213, 622-625 (1973), (UDC 541.126).

18. Glaskowa, A. P., "Three Possible Ways of Inhibition of the Ammonium Perchlorate Combustion Process," AIAA Paper No. 74-120 (1974).

19. Boggs, T. L., Price, E. W., and Zurn, D. E., "The Deflagration of Pure and Isomorphously Doped Ammonium Perchlorate," in Thirteenth Symposium (International) on Combustion; The Combustion Institute, Pittsburgh, 1971, pp. 995-1008.

20. Boggs, T. L., Zurn, D. E., Strahle, W. C., Handley, J. C., and Milkie, T. T., "Mechanisms of Combustion," Naval Weapons Center, NWC TP 5514, July, 1973.

21. Strahle, W. C., Handley, J. C., and Milkie, T. T., "Catalytic Effects in the Combustion of AP-HTPB Sandwiches to 3200 psia," Combustion Science and Technology, 8, 297-304 (1974).

22. Strahle, W. C., Handley, J. C., and Kumar, N., "Catalytic Behavior in Solid Propellant Combustion," Annual Summary Report for the Office of Naval Research Contract No. N0014-67-A-0159-0016, November 1, 1973.

BIBLIOGRAPHY (Continued)

23. Harshaw Catalysts for Industry; Harshaw Chemical Co., Cleveland,

24. Friedman, R., Nugent, R. G., Rumbel, K. E., and Scurlock, A. C., "Deflagration of Ammonium Perchlorate," in Sixth Symposium (International) on Combustion; Reinhold, New York, 1957, pp. 612-618.

25. Boggs, T. L. and Zurn, D. E., "The Temperature Sensitivity of the Deflagration Rates of Pure and Doped Ammonium Perchlorate," Combustion Science and Technology, 4, 221-232 (1972).

26. Boggs, T. L. and Zurn, T. E., "The Deflagration of Ammonium Perchlorate-Polymeric Binder Sandwich Models," Combustion Science and Technology, 4, 279-292 (1972).

27. Hightower, J. D. and Price, E. W., "Experimental Studies Relating to the Combustion Mechanism of Composite Propellants," Astronautica Acta, 14, 11-21 (1968).

28. Steinz, J. A., Stang, P. L. and Summerfield, M., "The Burning Mechanism of Ammonium Perchlorate-Based Composite Solid Propellants," Aerospace and Mechanical Sciences Report No. 830; Princeton University (February, 1969).

29. Bircumshaw, L. L. and Newman, B. H., "The Thermal Decomposition of Ammonium Perchlorate I. Introduction, Experimental, Analysis of Gaseous Products, and Thermal Decomposition Experiments," Proceedings of the Royal Society, A 227, 115-132 (1954).

30. Majer, J. R. and Smith, M., "Gas Phase Thermal Decomposition of Ammonium Perchlorate," Combustion and Flame, 13, 635-644 (1969).

31. Suetlov, B. S. and Koroban, V. A., "Thermal Decomposition Mechanism of Ammonium Perchlorate," Combustion, Explosion, and Shock Wave, pp. 9-14; Fizika Goreniya i Vzryva, 6, 12-18 (1970).

32. Freeman, E. S., Anderson, D. A., and Campisi, J. J., "The Effects of X-ray and Gamma Ray Irradiation on the Thermal Decomposition of Ammonium Perchlorate in the Solid State," The Journal of Physical Chemistry, 64, 1727-1732 (1960).

33. Boldyrev, V. V., Alexandrov, V. V., Boldyreva, A. V., Gritsan, V. I., Karpenko, Yu. Ya., Korobeinitchev, O. P., Panfilov, V. N., and Khairetdinov, E. F., "On the Mechanism of the Thermal Decomposition of Ammonium Perchlorate," Combustion and Flame, 15, 71-77 (1970).

BIBLIOGRAPHY (Continued)

34. Powling, J., "Experiments Relating to the Combustion of Ammonium Perchlorate-Based Propellants," in Eleventh Symposium (International) on Combustion; The Combustion Institute, Pittsburgh, 1967, pp. 447-456.

35. Inami, S. H., Rosser, W. A., and Wise, H., "Heat-Release Kinetics of Ammonium Perchlorate in the Presence of Catalysts and Fuel," Combustion and Flame, 12, 41-44 (1968).

36. Galwey, A. K. and Jacobs, P. W. M., "The Thermal Decomposition of AP in the Presence of Carbon," Transactions of the Faraday Society, 56, 581-590 (1959).

37. Hermoni, A. and Salmon, A., "The Catalytic Decomposition of Ammonium Perchlorate," in Ninth Symposium (International) on Combustion; Academic Press, New York, 1963, pp. 656-662.

38. Ward, J. R., "On the Copper (II)-Catalyzed Low Temperature Decomposition of Ammonium Perchlorate," U.S.A. Ballistic Research Laboratories, BRL MR 2390 (1974).

39. Jacobs, P. W. M. and Russell-Jones, A., "The Thermal Decomposition and Ignition of Mixtures of Ammonium Perchlorate + Copper Chromite," in Eleventh Symposium (International) on Combustion; The Combustion Institute, Pittsburgh, 1967, pp. 457-462.

40. Pearson, G. S., "Composite Propellant Catalysts: Copper Chromate and Chromite," Combustion and Flame, 14, 73-83 (1970).

41. Nadaud, L., "Models Used at ONERA to Interpret Combustion Phenomena in Heterogeneous Solid Propellants," Combustion and Flame, 12, 177-195 (1968).

42. Pearson, G. S. and Sutton, D., "The Mechanism of Thermal Decomposition in Ammonium Perchlorate-Copper Chromite Mixtures," Combustion and Flame, 13, 330-332 (1969).

43. Rosser, W. A., Inami, S. H., and Wise, H., "Thermal Decomposition of Ammonium Perchlorate," Combustion and Flame, 12, 427-435 (1968).

44. Inami, S. H. and Wise, H., "Catalytic Reactions of Dissociation Products of Ammonium Perchlorate," Combustion and Flame, 13, 555-557 (1969).

45. Jacobs, P. W. M. and Kureishy, A. R. T., "The Effect of Additives on the Thermal Decomposition of Ammonium Perchlorate," in Eighth Symposium (International) on Combustion; Williams and Wilkins, Baltimore, 1962, pp. 672-677.

BIBLIOGRAPHY (Concluded)

46. Cohen Nir, E., "Combustion of Powdered Metals in Contact with a Solid Oxidizer (Ammonium Perchlorate)," in Thirteenth Symposium (International) on Combustion; The Combustion Institute, Pittsburgh, 1971, pp. 1019-1029.

47. Inami, S. H., McCulley, L., and Wise, H., "Ignition Response of Solid Propellants to Radiation and Conduction," Combustion and Flame, 13, 531-536 (1969).

48. Bakman, N. N., Tsyganov, S. A., and Zakharov, V. B., "Acceleration of Burning Rate by Means of Additives That Form a Molten Layer on the Surface of the Change," Combustion, Explosion and Shock Waves, 6(1), 98-102 (1970).

49. Galwey, A. K. and Jacobs, P. W. M., "The Thermal Decomposition of Ammonium Perchlorate in the Presence of Manganese Dioxide," Transactions of the Faraday Society, 55, 1165-1172 (1959).

VITA

John Charles Handley was born in Ironton, Ohio, on February 19, 1938. He was the second child of Mr. and Mrs. John F. Handley. Three sisters, Carol Ann Handley, Mrs. Margaret Orlando and Mrs. Mary Sue Michael completed the family. Mr. Handley attended Sacred Heart Grade School in Pomeroy, Ohio. He graduated from Pomeroy High School in May, 1956, as the class valedictorian. He entered Case Institute of Technology in September, 1956 and graduated with scholastic honors with the degree of Bachelor of Science in Engineering Science in June, 1960.

Mr. Handley began his engineering career with the B. F. Goodrich Chemical Company in Avon Lake, Ohio. He returned to Case Institute of Technology in September, 1960 as a graduate teaching assistant in the School of Mechanical Engineering. He completed his graduate studies at Case in November, 1962, as a research assistant in the Plasma Research Group. He received the degree of Master of Science in Aeronautical Engineering in June, 1963.

Mr. Handley accepted employment with the Douglas Aircraft Company in Santa Monica, California in November, 1962. While at Douglas, he worked in the Aerothermo, Solid Mechanics and Physics Groups. He was employed as an Engineer/Scientist Specialist in charge of the Plasma Diagnostics Laboratory at Douglas when he resigned to accept employment as a Research Engineer in the School of Aerospace Engineering of the Georgia Institute of Technology in November, 1967. Mr. Handley began his

graduate studies at Georgia Institute of Technology in the summer quarter of 1969.

Mr. Handley was married to the former Phyllis Virgene Blackwood of Pomeroy, Ohio on December 28, 1959. They have five children, Deborah Lynne, John Charles, Jr., Stephen Gregory, Melinda Jayne, and Daniel Everett.